Dissertation for the degree of

Doctor of Philosophy

Evaluation of energy release rate related to crack kink and simulation of surface crack shape change of round bar

The Graduate School

of the University of Ulsan

Department of Mechanical and Automotive Engineering

Ya Li Yang

Evaluation of energy release rate related to crack kink and simulation of surface crack shape change of round bar

Supervisor : **Seok Jae Chu**

A Dissertation

Submitted to

the Graduate School of the University of Ulsan

In partial Fulfillment of the Requirements

for the Degree of

Doctor of Philosophy

by

Ya Li Yang

Department of Mechanical and Automotive Engineering

University of Ulsan, Korea

February 2021

Evaluation of energy release rate related to crack kink and simulation of surface crack shape change of round bar

This certifies that the dissertation of Ya Li Yang is approved.

위원장	교수 염영진
Committee Chair	**Prof. Young-Jin Yum**
위원	교수 여태인
Committee Member	**Prof. Tae-In Yeo**
위원	교수 김동규
Committee Member	**Prof. Dong-Kyu Kim**
위원	교수 박재학
Committee Member	**Prof. Jae-Hak Park**
위원	교수 주석재
Committee Member	**Prof. Seok-Jae Chu**

Department of Mechanical and Automotive Engineering

University of Ulsan, Korea

February 2021

Acknowledgments

First and foremost, I would like to express my deep and sincere gratitude to my supervisor Prof. Seok-Jae Chu. He has not only provided me invaluable guidance but also meticulous care in life. I am deeply inspired by his patience, motivation, vision, sincerity, and immense knowledge. It's going to have a profound impact on my future work and study.

Special thanks to the thesis committee members, Prof. Young-Jin Yum, Prof. Tae-In Yeo, Prof. Dong-Kyu Kim and Prof. Jae-Hak Park, for the precious time on my thesis.

Thank you to all the professors who have given lectures to me. I learned a lot of valuable knowledge from them.

Sincerely thanks to the professors in China, Prof. Li Hua Chen and Prof. Yan Song Wang for giving me the opportunity and encouragement to complete this learning experience.

Thanks to all my friends who accompany me in Korea, the precious friendship is something I will never forget in my whole life.

Finally, heartfelt thanks to my parents, my husband Hao Chen, my daughter and my sister, all my strength comes from you, you are so priceless to me and I am proud of you.

Abstract

Evaluation of energy release rate related to crack kink and simulation of surface crack shape change of round bar

Ya Li Yang

The Graduate School of the University of Ulsan

Department of Mechanical and Automotive Engineering

Fracture damage usually occurs from pre-existing defects or small cracks in service. These cracks influence the stress distribution in the component and can result in significant reduction in its strength and service life. As an important impact on the safety of engineering components, the crack problem is an interesting research area.

In this paper, two topics are studied about the crack problem. One is the evaluation of the energy release rate related to crack kink under mixed-mode loading. The other one is the prediction of shape change of surface crack subjected to tension based on the three-parameter model.

Most of the researches on crack kink are focused on the crack under two kinds of loading situation, the mixed-mode I-II-III loading situation is rarely mentioned, and the validity of conclusions reached cannot be evaluated yet. The energy release rate related to crack kink under mixed-mode loading for aluminum alloy material has been investigated using both numerical methods and theoretical derivation. A relatively simple and precise numerical method was established to evaluate the energy release

rate associated with stress intensity factors under mixed mode loading, based on the concept that the energy release rate is equal to the change rate of the energy difference before and after crack kink. Based on the numerical method, a series of spatial inclined ellipses in Mode I-II and ellipsoids in Mode I-II-III with different propagation angles computed from the non-dimensional value ($K/\sqrt{EG}$) were fitted by MATLAB, and the expression of energy release rate with crack propagation angle was obtained. A theoretical expression of energy release rate at any propagation angle for a crack tip under I-II-III mixed-mode crack was deduced based on the propagation mechanism of the crack tip under the influence of a stress field. It is confirmed that the deduced theoretical expression could provide results as accurate as of the present numerical method.

The results of the proposed method are consistent with experimental data. The error, which is lower than 5%, can be accepted considering that the specimens are not manufactured using an ideal elastic material. Consequently, the proposed method can achieve an accurate evaluation of the energy release rate with concise calculation.

Meanwhile, the initiating and propagation analysis of surface crack is critical for structural integrity prediction of cylindrical metallic components with a circular cross-section, since these components have been applied widely in engineering.

Most attempts to predict fatigue growth of a surface crack in an un-notched or very mild notched bar have focused on the ‘almond’ crack employing a certain shape with a fixed center, which reduced the fatigue calculations to one-or two-dimensional problems. Few efforts have been made utilizing a three-parameter model.

The fatigue propagation of a surface crack in a round bar subjected to tension loads has been investigated. The crack growth circles method is developed for the surface cracks of a round bar, and the circles are tangent to both current and new crack fronts. A three-parameter model with fewer shape restraints whose center is allowed to move along the vertical axis is built, and the shape change of a fatigue crack is predicted more precisely. The nominal aspect ratio of an ellipse, which is the ratio of the maximum crack depth to the chord length, is considered, instead of the actual aspect ratio of an ellipse semi-axis. A relatively large crack growth increment can be used by adopting the equivalent stress intensity factor ΔK_e based on the stress intensity factors along the current and new crack fronts.

The crack propagation process is described accurately based on the ratio of vertical growth toward the horizontal surface. It can be seen that the crack propagation paths differ with different initial flaws, but will converge asymptotically.

The present results demonstrate good convergence speed and accurate prediction of crack shape patterns. Comparisons have been done to verify the proposed solutions, it is illustrated that the proposed solutions agree well with experimental data and is better than other numerical solutions.

Table of Contents

List of Figures

List of Tables

Chapter 1 Introduction

1.1 Background and overview

Fracture damage usually occurs from pre-existing defects or small cracks in service. Cracks are generated in many engineering structures and components during service lives. These cracks influence the stress distribution in the component and can result in significant reduction in its strength and service life. As an important impact on the safety of engineering components, the crack problem is an interesting research area.

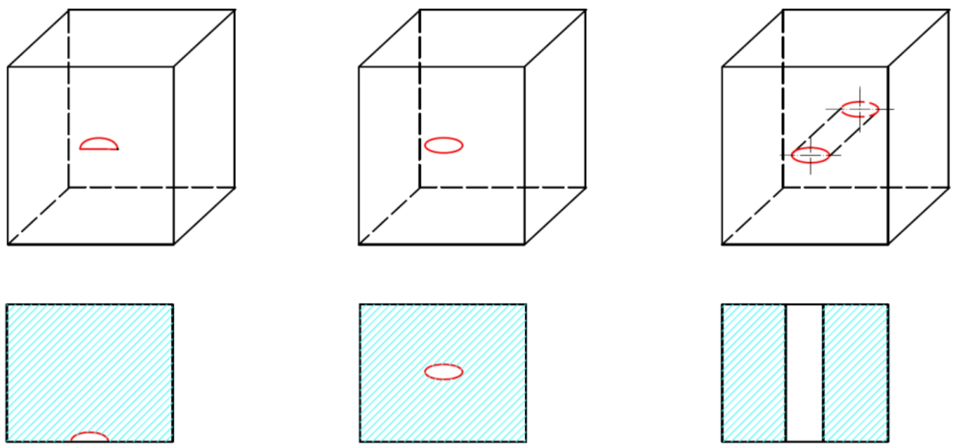

(a) Surface crack (b) Embedded crack (c) Through crack

Figure 1-1 Cracks at different locations

According to the position of the crack, there are three kinds of crack defects within structures: through crack, surface crack, and embedded crack, as shown in Figure 1-1. The depth of surface crack is smaller than the thickness of the structure, and the shape of a surface crack is often reduced to elliptic, and the same to the embedded crack. Usually, the through crack would penetrate over half the thickness of the structure member, called edge crack (Figure 1-2), the radius of curvature of the crack tip for the through crack approaches zero, it is easy to accept in engineering as the conservative of a design concept. Generally, the problem of through crack is classified into two-dimensional fracture mechanics, and non-through crack problems are in the field of three-dimensional.

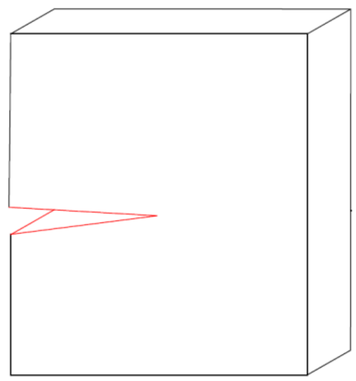

Figure 1-2 An edge crack

1.1.1 Overview for crack analysis with fracture mechanics

The presence of a crack in a part magnifies the stress in the vicinity of the crack and may fail before that predicted using traditional strength-of-materials methods. Fracture mechanics is a common methodology that is used to predict and diagnose the failure of a part with an existing crack or flaw, which is concerned with predicting the response of a system to external disturbances.

Most analyses of crack propagation involve planar crack under normal loading conditions (Mode I loading) for some special problem that the crack tends to extend in its plane are certainly important since it provides many design-relevant concepts for the prediction of structural failures. Meanwhile, the understanding of mixed-mode fracture is also an important subject in Fracture Mechanics, as material flaws or pre-cracks may inevitably occur in the manufacturing process. To describe crack propagation under mixed-mode loading, the classical formula of energy release rate G was expanded in this hypothesis that crack extends collinearly with initial crack.

While many kinds of research show that the actual expanding direction is not collinear with its initial path under the combined loading condition, the crack branch is produced and it should also be mentioned that energy release rate in the limit as the propagation kink goes to zero is not same as the one without kink [1-6].

Analytical and approximate solutions have been studied for the SIF of kinked and branched cracks. Chatterjee, S.N. [7] discussed the nature of the stress singularity at the re-entrant corner considering a branched crack with two straight arms in an infinite sheet. Amestoy, M. and Leblond J.B. [8] calculated precisely the various functions of the expansion of the stress intensity factors. Kishen, J.M.C. [9] showed the application of the contour integral method for the determination of SIFs. Meggiolaro, M.A. et al [10] studied the stress intensity factors of kinked and bifurcated cracks through the specialized finite element. Berto, F. and Lazzarin, P. [11] presented higher-order terms on the stress field of a cracked plate under plane loading. Sih, G.C. [12] proposed a critical value of the strain-energy-density factor governing the direction of crack growth and fracture toughness for the mixed problem. Cornetti, P. et al [13] exploiting expressions for the asymptotic stress field and T-stress in mixed-mode brittle fracture of cracked structures.

The kink angle of a crack in mixed-mode fracture has been widely investigated. Li, X.F. et al [14] determined the kink angle of a plate with an angled crack subjected to far-field compressive loading by analysis of T-stresses. Fajdiga, G. [15] defined the direction in which the crack kinks at different load modes using maximum energy release rate (MER), minimum strain energy density (SED), and maximum tangential stress (MTS) criterion. Guo, B. K. et al [16] calculated the initial cracking angle of a crack with an arbitrary oriented direction in a strip material through dislocation density functions based on the numerical method. However, it is generally recognized that it is very difficult to develop accurate solutions due to their complex propagation behavior.

For I-II mixed-mode crack, the analytic method is widely used in the early development of Fracture Mechanics. Hussian’s [17] work as a founder is worthy to be mentioned, which simplified the star-shaped crack to an L-shaped crack and used a mapping function [18] to obtain a specific expression of energy release rate in terms of a Cauchy integral equation [19] by iteration based on the new path independent integrals [20]. However, some inaccuracy of Hussain's equation will be pointed out through the comparison with the present method in this paper later, as the derivatives of two stress functions in the mapping function during the "simultaneous expansion" procedure are incorrect. Meanwhile, complex numerical calculations were used. Another way to obtain the complete energy release rate for crack kink is started with the stress distribution function by Williams, M.L. [21], then maximum hoop stress criterion was proposed by Erdogan, F. and Sih, G. C. [22], which presented polar stress state in the neighborhood of the crack tip, and the work was verified and supplemented by Williams, J.G. and Ewing, P.D. [23]. Cotterell, B. et al. [24] gave specific stress intensity factors for crack kink with the concept of surface tractions base on the prior research. Finally, Anderson, T.L. [25] proposed an approximate evaluation of energy release rate as a function of propagation direction in mixed-mode 2D problems.

Wu, C.H [26] gave the numerical relationship of $K-G$ for non-crack-parallel propagations by using the explicit asymptotic analysis. Hayashi, K. and Nemat-Nasser, S. [27] obtained energy release rate in the form of a quadratic of stress intensity factors with the coefficients tabulated for various kink angles by the method that models a kink as a continuous distribution of edge dislocations. Chambolle, A. [28] revisited the energy release rate using the expansion of Amestoy, M and Leblond, J.B [8]. Also, the validity of Irwin's formula for the energy release rate for any kink angle, material anisotropy, and loading condition was proved by Azhdari, A. and Nemat-Nasser, S. [29]. Sih, G.C. and Paris, P. C. [30] used a complex variable method to evaluate the strength of stress singularities at crack tips in plane problems and plate bending problems, which can extend the Griffth-Irwin fracture theory to an arbitrary crack extension.

Although the phenomenon of crack branching is interesting and of great importance in fracture mechanics, and many achievements have been made for energy release rate, because of the mathematical complexity of the problem, the validity of conclusions reached through a complex process cannot be evaluated. Most of the researches are aimed at the crack under two kinds of loading situation. The mixed-mode I-II-III loading situation was rarely mentioned, and the methods used were either analytical or numerical methods, therefore, it is difficult to be generalized to other crack problems.

1.1.2 Literature review for shape change with fatigue damage

The initiating and propagation analysis of surface crack is critical for structural integrity prediction of cylindrical metallic components (bolts, screws, shafts, etc.) with a circular cross-section since these components have been applied widely in engineering.

Part-through flaws appear on the free surface of a smooth round bar and the front of a growing crack can be classified as a so-called ‘sickle’ crack and ‘almond’ crack by extensive experimental works [31–33], as shown in Figure 1-3.

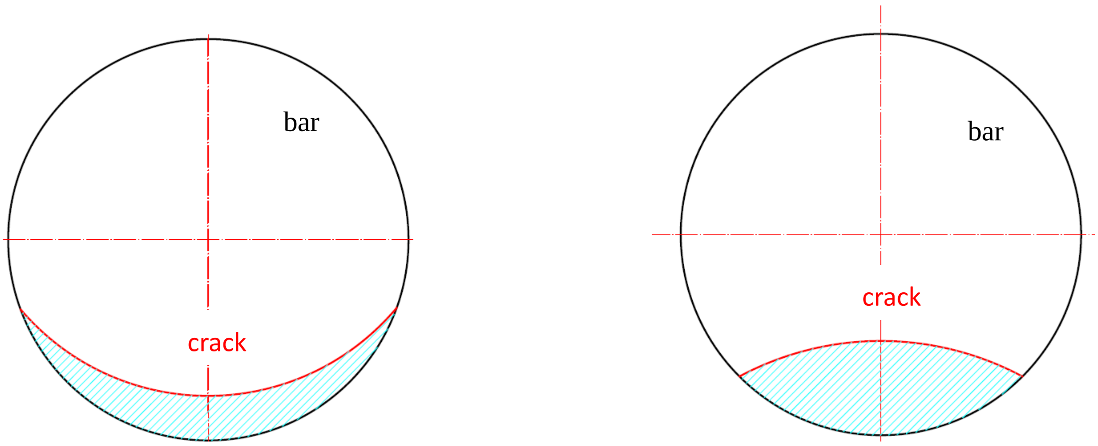

(a) ‘sickle’ crack

(b) ‘almond’ crack

Figure 1-3 Surface crack in a round bar

Some papers related to sickle-shaped cracks are available for bars with sharp or deep notches. Any model for calculating crack propagation and a lifetime to failure characteristics of a structure relies upon a knowledge of the stress intensity factor . Mattheck, C. et al [34] calculated the stress intensity factor at the deepest point of sickle-shaped cracks for a constant, a linear and a quadratic locally varying stress distribution by use of a weight function derived from finite element results. Caspers,

M. et al [35] studied the stress intensity factors for surface cracks in cylindrical bars applying the weight function obtained from the crack opening displacement of a reference loading using the finite element method. Hobbs, J. et al [36] used three-dimensional photoelasticity to analyze the effect of crack shape on the stress intensity factors at the tips of cracks in threaded connectors under axial and eccentric loads, especially for the crescent-shaped cracks. Carpinteri, A. et al [37, 38] studied the sickle-shaped crack in a round bar under complex mode I loading and cyclic tension and bending loading.

Most attempts to predict fatigue growth of a surface crack in an un-notched or very mild notched bar have focused on the ‘almond’ crack as its university in engineering. Some investigators have employed a circular arc which is deemed to be in good agreement with real fatigue crack surface to describe the crack front [31-32, 35, 39-44]. The crack front curvature was chosen to model shapes occurring in practice and to be the semi-circular crack. Edge crack of maximum depth and radius are taken into consideration in this configuration. Then the hypothesis that an actual part-through crack can be replaced by an equivalent elliptical arc edge flaw has been widely applied. Elliptical-arc surface flaw in around bar under fatigue loading is considered. And the relative depth $\xi = a/D$ of the deepest point A on the defect front and the flaw aspect ratio $\alpha = a/b$ define the crack configuration being examined, where a is the deepest depth of point A, and D is the diameter of the bar, as shown in Figure 1-4.

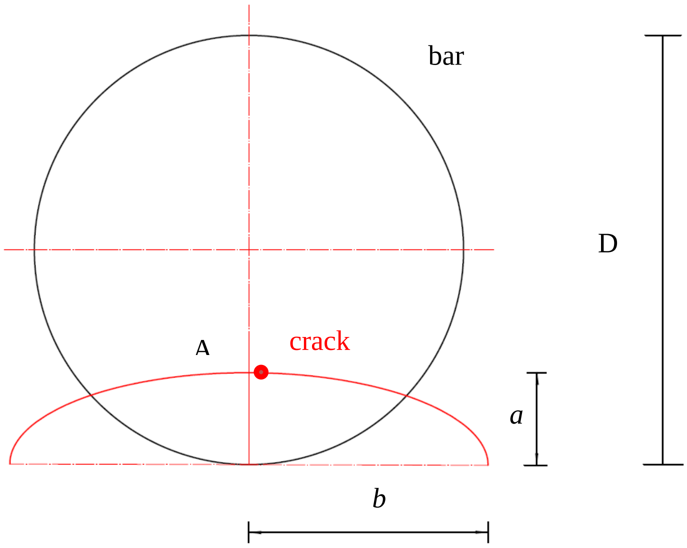

Figure 1-4 Configuration of elliptical-arc surface flaw

Lorentzen, T. et al [45] developed a theoretical method for calculating the stress intensity factor for semielliptical surface cracks in shafts subjected to a constant moment load, and the crack growth was calculated for the two points along the crack front with the Paris' law. Lin, X.B. and Smith, R.A. [46-47] employs an experimental Paris-type fatigue crack growth relation to calculate local crack advances at a few points along the crack front based on stress intensity factor along the crack front through finite element analysis. Toribio, J. et al [48] analyzed the dimensionless compliance evolution in a round bar subjected to fatigue with initial crack geometries and several Paris parameters. Branco, R. et al [49] monitored the crack initiation and crack growth using a high-resolution digital system.

Carpinteri, A. [50], as one of the most representative researchers on this topic, conducted extensive studies related to this configuration. Carpinteri, A. (1992) [51] discussed the influence of crack aspect ratio on the stress intensity factor of elliptical-arc edge flaws in solid round bars under tension or bending loading. Carpinteri, A. (1993) [52] studied the shape change of surface cracks in round bars under cyclic axial loading based on the calculating of stress intensity factor along the crack front. Carpinteri, A. (1994,1996) [53,54] analyzed a part-through cracked round bar subjected to constant amplitude cyclic bending loading and combined axial and bending loading respectively. Carpinteri, A. (2006, 2008) [55, 56] studied the surface cracks in notched and un-notched round bars under cyclic tension or bending with the stress concentration factor respectively.

However, regardless of whether they used a circular arc or elliptical arc, most researchers employed a certain shape with a fixed center, which transformed the fatigue calculations into one- or two-dimensional problems. Few efforts have been made by utilizing a three-parameter model. Although Carpinteri, A. (1996) [57] mentioned the three-parameter model previously, the fatigue crack propagation was only simply examined by applying the Paris-Erdogan law with the least square method as in almost all previous studies [58–60].

In addition to the experimental backtracking technique [61, 62] and normalized area-compliance method [63], some researches focused on the J-integral for elastic-plastic analysis for surface crack. Ismail, A.E. and Ariffin, A.K. [64] determined the J-integral around the crack front of the surface crack using an elastic-plastic finite element analysis. Ismail, A.E. et al [65] developed an analytical aspect for J-integral prediction of surface crack in round bars under combined mode I loading based on the local limit load approach considering a plastic deformation across the crack ligament. There is no further research regarding the method of surface crack prediction.

1.2 Objectives and methods

1.2.1 Evaluation of the energy release rate associated with crack kink

The objective of this topic was to evaluate the energy release rate associated with stress intensity factors at any angle under mixed-mode loading. In this thesis, a more concise and precise numerical method was established based on the concept that the energy release rate was equal to the change rate of the energy difference before and after the crack kink. A series of spatial inclined ellipses in Mode I-II and ellipsoids in Mode I-II-III with different propagation angles computed from a non-dimensional value ($K/\sqrt{EG}$) were fitted by MATLAB. Meanwhile, a theoretical expression of energy release rate with an angle for a crack tip under I-II-III mixed-mode crack was deduced based on the propagation mechanism of the crack tip under the influence of the stress field. It was confirmed that the theoretical expression deduced could provide accurate results as the proposed numerical method. The validity of the present method was shown by comparing with experimental data and previous literature.

1.2.2 Prediction of shape change for fatigue crack

The objective of the second topic was to predict the shape change of a fatigue crack in a round bar subjected to tension by employing fatigue crack growth circles, based on a three-parameter model using finite element analysis. A reduced shape restraints model with part-elliptical cracks whose center was allowed to move along the vertical axis was built, which could be more precise for expressing the actual crack shape front. The nominal aspect ratio of an ellipse, which was more meaningful, was proposed for the three-parameter model. Meanwhile, the fatigue crack growth circles, which were on a tangent to both current and new crack fronts, were developed to predict the crack path. The equivalent stress intensity factor ΔK_e based on both stress intensity factors along the current and new crack fronts was proposed to reduce the number of modeling computations with only a few iterations. The validity of the present method was shown by comparing its results with a simulation solution and experimental results.

1.3 Thesis organization

A discussion about the evaluation of the energy release rate and shape for a crack had been conducted based on the knowledge of fracture mechanics and fatigue damage.

The thesis was constituted with the following chapters.

Chapter 2 was focused on the evaluation of the energy release rate associated with crack kink firstly. The energy release rate associated with stress intensity factors under mixed-mode loading for aluminum alloy material was investigated using both numerical method and theoretical derivation. Based on the numerical method, a series of spatially inclined ellipses in Mode I-II and ellipsoids in Mode I-II-III with different propagation angles were computed by MATLAB, and the expression of energy release rate with the crack propagation angle was obtained. A theoretical expression of energy release rate at any propagation angle for a crack tip under I-II-III mixed-mode crack was deduced based on the propagation mechanism of the crack tip under the influence of a stress field. It was confirmed that the theoretical expression deduced could provide accurate results as the present numerical method.

Chapter 3 was the prediction of fatigue propagation of a surface crack in a round bar subjected to tension loads by using crack growth circles. The crack growth circles method was developed for the surface cracks of a round bar, and the circles were tangent to both current and new crack fronts. A three-parameter model with fewer shape restraints whose center is allowed to move along the vertical axis was built, and the shape change of a fatigue crack was predicted more precisely. The nominal aspect ratio of an ellipse, which was the ratio of the maximum crack depth to the chord length c, b_n/c, was taken into consideration, instead of the actual aspect ratio of an ellipse semi-axis. A relatively large crack growth increment was used by adopting the equivalent stress intensity factor ΔK_e based on the stress intensity factors along the current and new crack fronts. Finally, the present solutions were compared with other numerical solutions and experimental data.

Chapter 4 was the discussion and summary of the main contents and conclusion of this thesis.

Chapter 2 Evaluation of the energy release rate associated with crack kink

2.1 Stress Fields Ahead of Crack Tip

2.1.1 The stress intensity factor and energy release rate

For linear elastic materials, the energy release rate G describes global behavior, while K is a local parameter. As the most important parameters for fracture mechanics, K and G have been determined well on the assumption for crack propagation. Under Mode I loading, the relationship between K and G can be deduced with elastic modulus E and Poisson's ratio v by the Irwin's approach [66]:

$$G_I = \frac{1}{E} {K_I}^2 (plane\ stress),\ \ G_I = \frac{1-v^2}{E} {K_I}^2 (plane\ strain) \qquad (2\text{-}1)$$

Each mode of loading produces the $1/\sqrt{r}$ singularity at the crack tip. As an important parameter for stress fields ahead of a crack tip in an isotropic linear elastic material, the stress intensity factor is usually given a subscript to denote the mode of loading, such as K_I, K_{II}, K_{III}, shown in Figure 2-1.

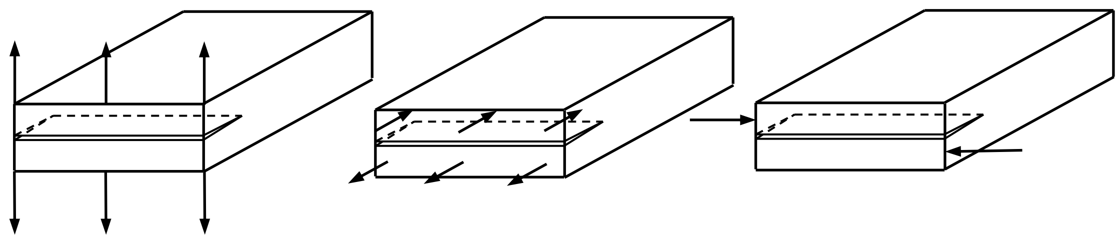

(a) Mode I (b) Mode II (c) Mode III

Figure 2-1 Cracked bodies under three different loading modes

When the crack is the Mode I, it grows along with the extension of the crack plane. However, the crack propagation is not collinear with the initial crack line under the combined loading condition, since the crack propagates in such a way as to maximize the energy release rate, there will be kinks for the extension and finally tends to propagate normal to the applied stress resulting in pure Mode I. In reality, as the asymmetry of load distribution and crack orientation, cracks are usually in a state of mixed deformation with Mode I, Mode II, and Mode III. When subjected to complex loads, the failure mode becomes more complex and the direction of crack propagation is unclear.

Energy is a common method to study linear elastic fracture for mixed crack. A crack expands when the energy released is equal to the energy required to form a new crack surface. The direction of crack propagation is determined by the maximum energy release rate.

2.1.2 Principle of superposition

Individual components of stress, strain, and displacement are additive for linear elastic materials in the same direction. Similarly, stress intensity factors are additive as long as the mode of loading is consistent:

$$K_I^{total} = K_I^{part\ 1} + K_I^{part\ 2} + K_I^{part\ 3} \tag{2-2}$$

the Equation (2-2) is a general relationship for Mode I, the above analysis can be repeated for other modes of loading. The superposition principle of stress intensity factor can be used to transform complex load problems into simple single load crack problems.

Similarly, contributions to energy release rate G from the three modes are additive because the energy release rate is a scalar quantity, shown in Equation (2-3):

$$G = \frac{K_I^2}{E} + \frac{K_{II}^2}{E} + \frac{K_{III}^2}{2\mu} \tag{2-3}$$

It is a self-similar crack growth, which is assumed to remain planar and maintain a constant shape as it grows.

2.2 Energy release rate for I-II mixed-mode crack

2.2.1 Numerical Analysis of 2D crack

2.2.1.1 Crack Simulation with ABAQUS

A rectangular plate with crack is under combined Mode I and Mode II loading in the top side, with fixed bottom side, $L = W = 50mm$, $A = 10mm$, shown in Figure 2-2(a). To reveal the relationship between stress intensity factors and energy release rate under I-II combined loading situation, finite element technology was applied, as shown in Figure 2-2 (b). Figure 2-2 (c) is the mesh around the crack tip, which is a collapsed element, using duplicate nodes and 1/4 displacement method to simulate the singularity of displacement of the crack tip region. The material is linear elastic homogeneous isotropic aluminum alloy, $E = 70000Mpa, v = 0.33$. The K and G are obtained by changing the value of $\sigma : \tau$.

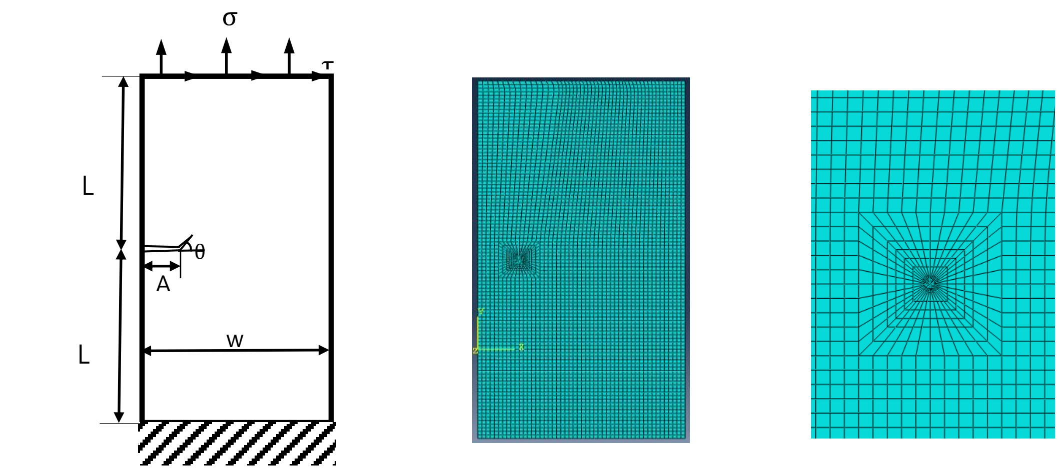

(**a**) A rectangular plate with a crack

(b) The finite element model

(c) Drawing of partial enlargement for crack

Figure 2-2 Finite element mesh for kinking problem

When $\Delta a = 0\,mm, \theta = 0^{\circ}, \tau = 0\,Mpa$, the value of σ changes from $20\,Mpa$ to $100\,Mpa$ with a step of 20. The result is shown in Figure 2-3. The simulation value output from ABAQUS is consistent with the reference value calculated by the literature [67]. The errors between the two values of each loading presented in Figure

2-3 (b) are about 0.53%. This simulation method verified will be applied in the following sections. Only one loading case is enough in this verification work as the linear elasticity of the material.

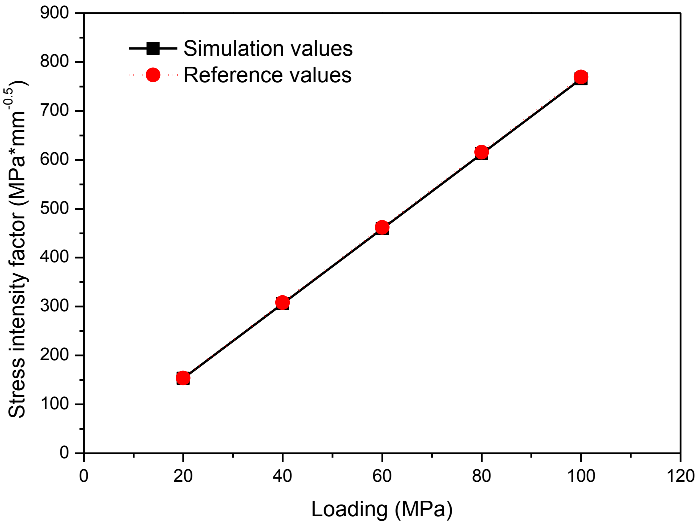

(**a**) Verification of simulation value output from ABAQUS

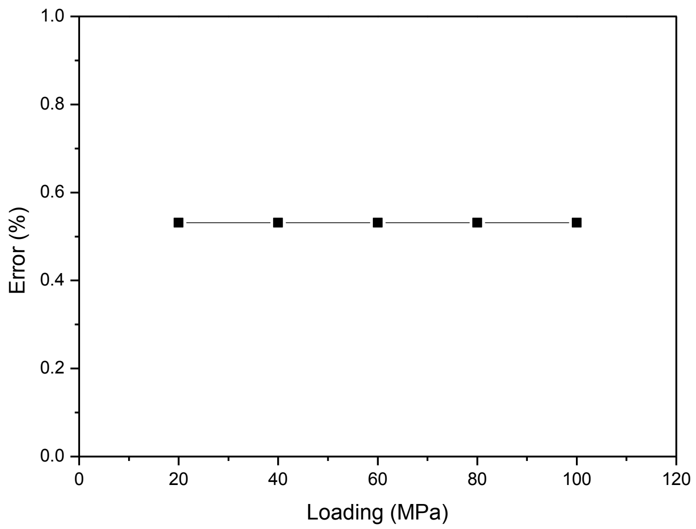

(b) Errors between the two values of each loading

Figure 2-3 Verification of simulation accuracy

2.2.1.2 The Theoretical Basis of Energy Release Rate Definition

A cracked plate in plane stress has an infinitesimal kink at angle θ from the plane of the crack, as illustrated in Figure 2-4(a)–(c). The energy release rate G, as a crack extension force, is a measure of the energy available for an increment of crack extension, which can be calculated approximately as:

$$G = -\frac{dU}{da} = -\lim_{a_2 \to a_1} \frac{(-U_2)-(-U_1)}{a_2 - a_1} \approx \frac{U_2 - U_1}{\Delta a} \tag{2-4}$$

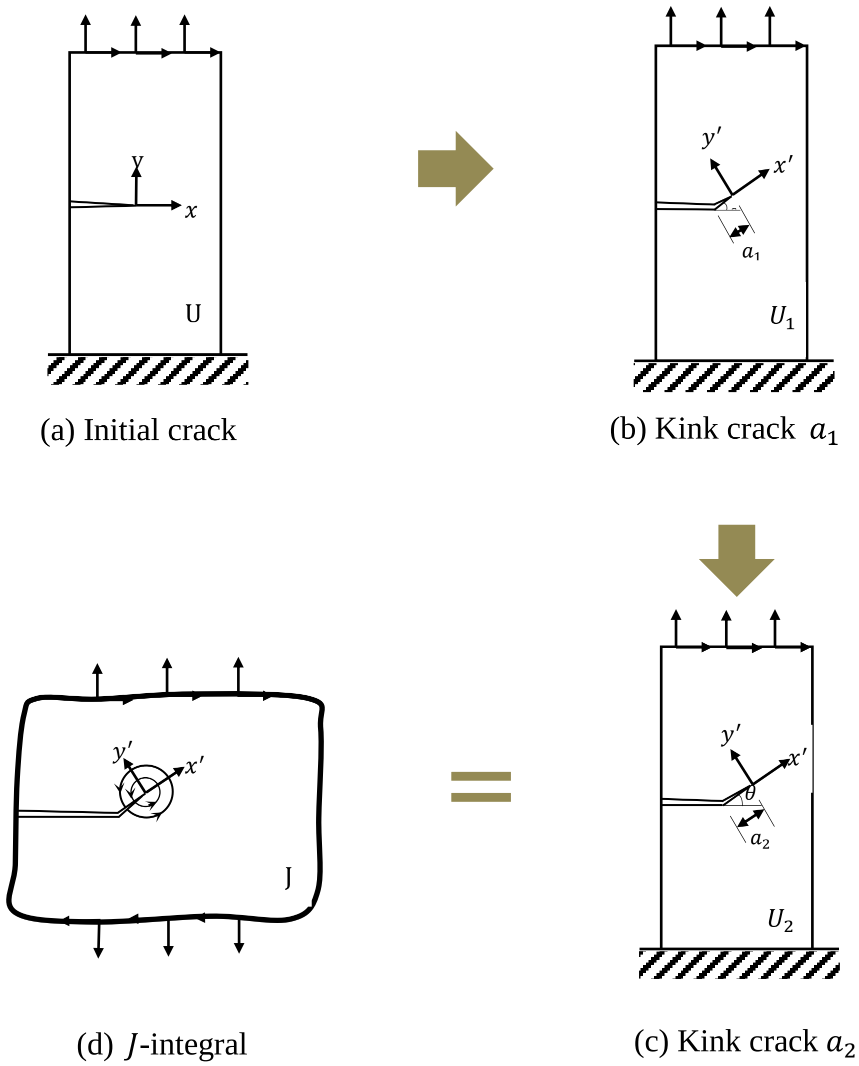

Figure 2-4 Extension of a kink crack

Irrespective of whether the crack extension is in its initial plane or kinked, the angle is θ, where U_1 and U_2 are the strain energy before and after the kink extension, respectively. And a is the length of the kink, which is measured from the original crack tip.

For an edge crack in the linear elastic body, the J-integral computed along a contour surrounding the crack tip is equal to the energy release rate (Figure 2-4(d)), which is revalidated by simulation work:

(1) Obtain the values of J and strain energy at these points $a_0 = 0\,mm,\ a_1 = 0.1\,mm,\ a_2 = 0.3\,mm,\ a_3 = 0.5\,mm,\ a_4 = 1\,mm.$

(2) Calculate the energy differences between a_0 and a_1, a_0 and a_2, a_0 and a_3, a_0 and a_4 , and divided by $a_1 - a_0 = 0.1\,mm,\ a_2 - a_0 = 0.3\,mm,\ a_3 - a_0 = 0.5\,mm,\ a_4 - a_0 = 1\,mm.$ It represents the energy release rate for the crack at *0.05 mm, 0.15 mm, 0.25 mm, 0.5 mm.*

(3) Determine that the minimum value of kink length for calculation is *0.1 mm*; since the kink crack becomes infinitesimally small, the values from the energy difference deviate from the J-integral.

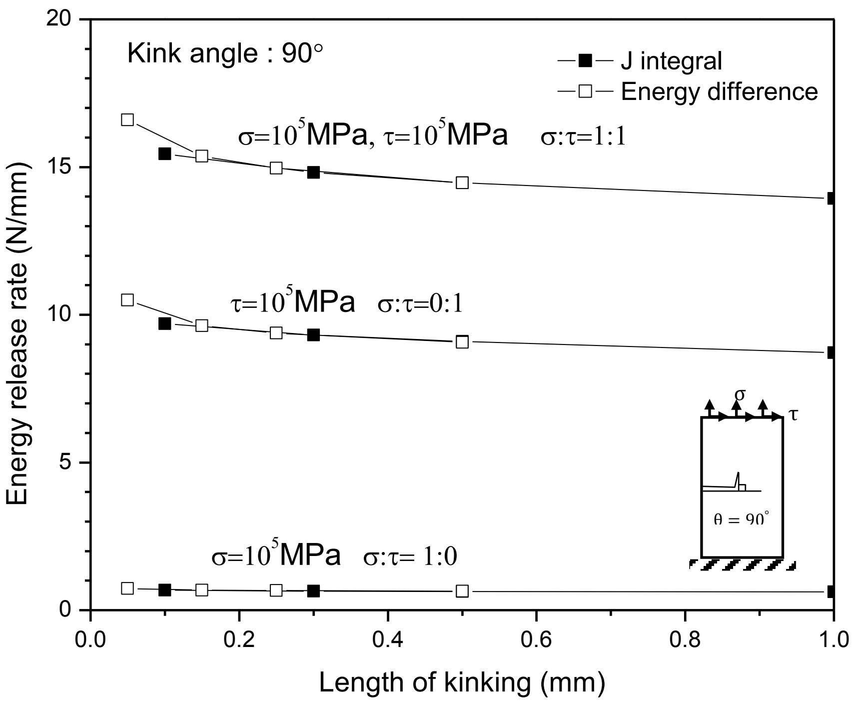

Figure 2-5 Determination of energy release rates as the length of kink crack approaches zero

The strain energy release rate and J-integral for a kink can be evaluated based on the output data of ABAQUS, as shown in Figure 2-5. It is shown that the energy release rate is in good agreement with the J-integral evaluated along the contour starting at one kink's crack surface and ending at the other kink's crack surface under arbitrary loading and kink angle conditions.

This validates the assumed connection between the strain energy release rate and J-integral. J-integral will be used in the following research as it is reliable and convenient.

2.2.1.3 Computational Analysis

From the output data of the simulation, the energy release rate and stress intensity factors can be obtained corresponding to the required condition. The method developed in the present study is described as follows:

(1) Determine J for kink cracks repeatedly, varying the kink length from $0.1\,mm$ to $1\,mm$ with four data points ($a = 0.1\,mm,\ 0.3\,mm,\ 0.5\,mm,\ 1\,mm$). Then, compute the energy release rate as the kink propagation vanishes on the curve of J versus kink length by the method of fitting. Figure 2-6 is the changing curve of J under an arbitrary loading, and the point of intersection with the vertical axis is the value of the energy release rate required.

(2) Determine K_I and K_{II} under arbitrary combined Mode I and Mode II loading conditions from the simulation work base on the Maximum energy release rate crack initiation criterion according to the same method with the value of J.

(3) Plot the non-dimensional value ($K_I/\sqrt{EG}, K_{II}/\sqrt{EG}$) for each kink angle ($\theta = 30^\circ, 60^\circ, 90^\circ, 120^\circ, 150^\circ$), as shown in Figure 2-7.

(4) Determine the parameters of inclined ellipses that fit the above data points using the curve fitting algorithm by MATLAB, and the corresponding ellipse equation is presented as follows:

$$\frac{(\frac{K_I}{\sqrt{EG}}\cos\alpha + \frac{K_{II}}{\sqrt{EG}}\sin\alpha)^2}{a^2} + \frac{(\frac{K_{II}}{\sqrt{EG}}\cos\alpha - \frac{K_I}{\sqrt{EG}}\sin\alpha)^2}{b^2} = 1 \tag{2-5}$$

where a, b, α are the semi-major axis, semi-minor axis, and inclination of the ellipse, respectively.

(5) Obtain the coefficients of quadratic of energy release rate in terms of stress intensity factors with a_{11}, a_{12} and a_{22}, defined as following

$$G = \frac{1}{E}(a_{11}K_I^2 + a_{12}K_I K_{II} + a_{22}K_{II}^2) \tag{2-6}$$

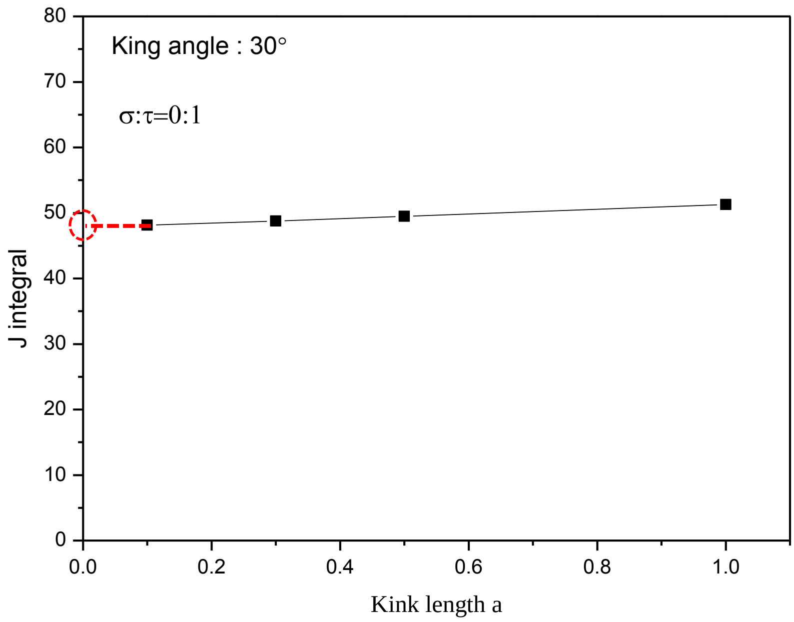

Figure 2-6 Variation of J with kink crack length for kink crack orientation 30 °and loading ratio 0:1

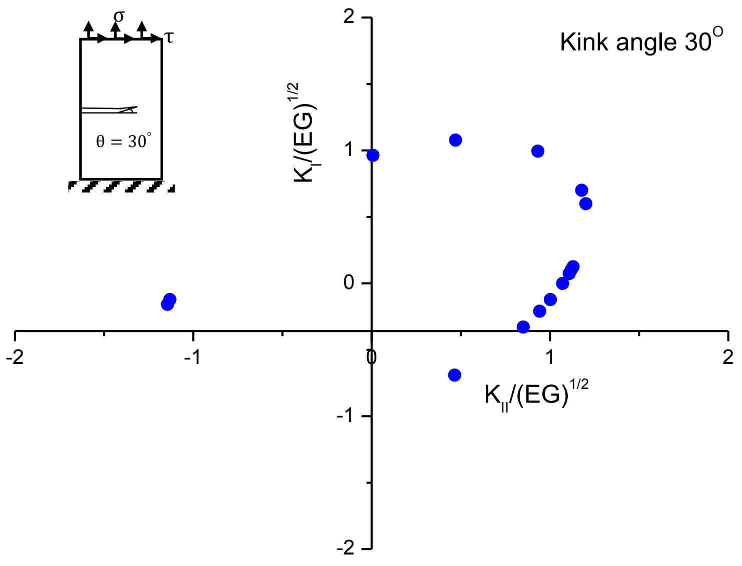

(a) Kink angle 30°

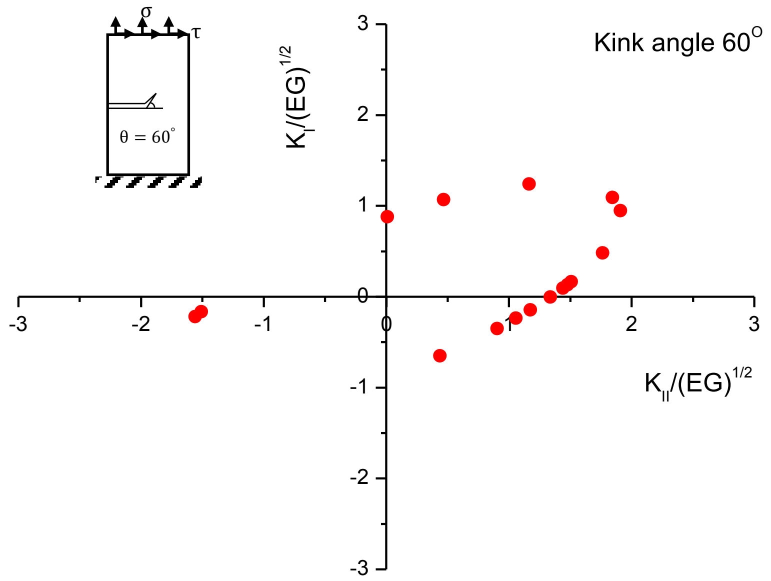

(b) Kink angle 60°

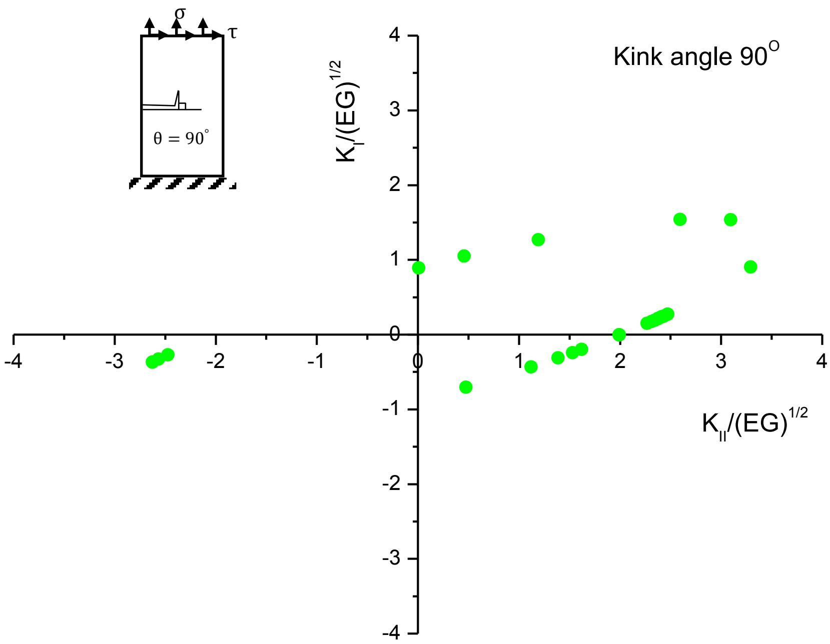

(c) Kink angle 90°

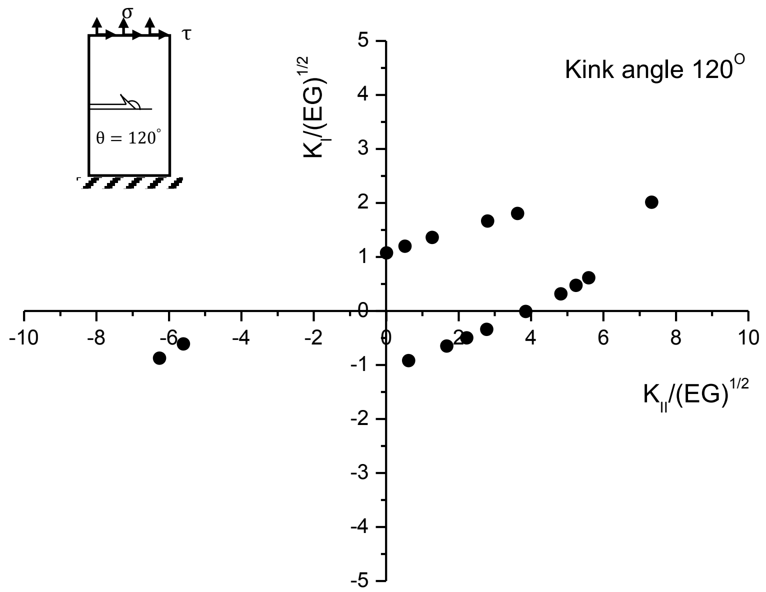

(d) Kink angle 120°

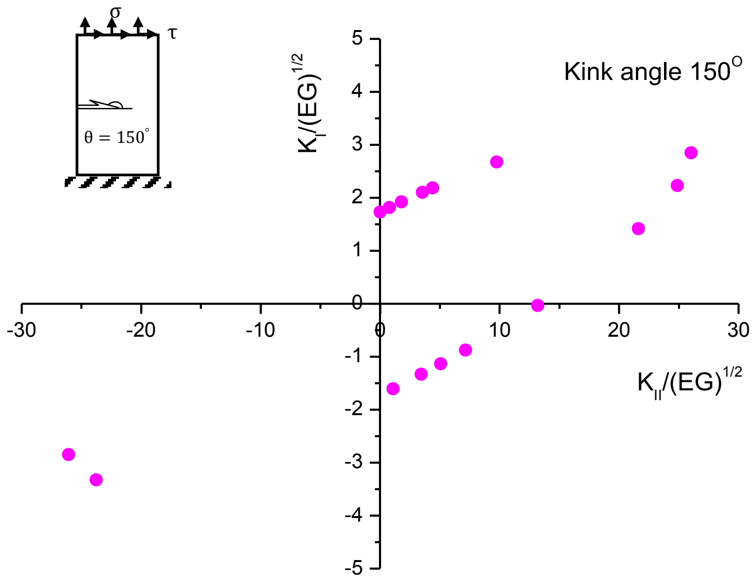

(e) Kink angle 150°

Figure 2-7 Non-dimensional value $(K_I/\sqrt{EG}\,, K_{II}/\sqrt{EG})$ for each kink angle

By fitting the database of non-dimensional value $(K_I/\sqrt{EG}\,, K_{II}/\sqrt{EG})$ calculated through the method proposed above for each kink angle, a series of inclined ellipses are presented with a certain angle and size, as shown in Figure 2-8. Figure 2-9 is the inclined angle α of Iso-energy release rate ellipses with kink angle θ. The variation of inclination for ellipses drops linearly with the increase of the kink angle. The trend of the semi-major axis and semi-minor axis of ellipses according to the variation of the kink angle has been shown in Figure 2-10. The coefficients of quadratics for energy release rate in terms of stress intensity factors are calculated for each kink angle based on the ellipse equations (Figure 2-11).

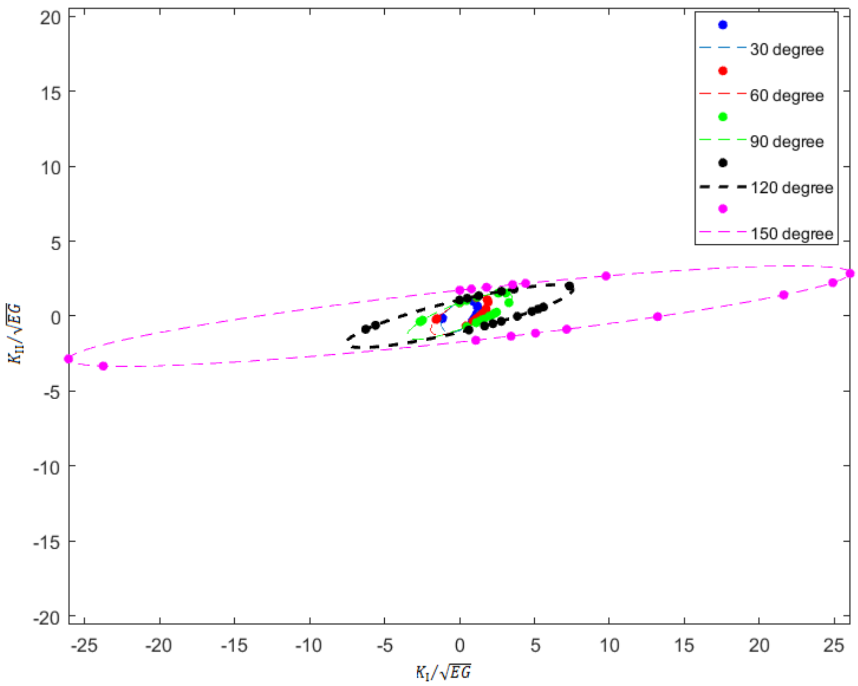

Figure 2-8 Iso-energy release rate ellipses on normalized mixed-mode stress intensity factors

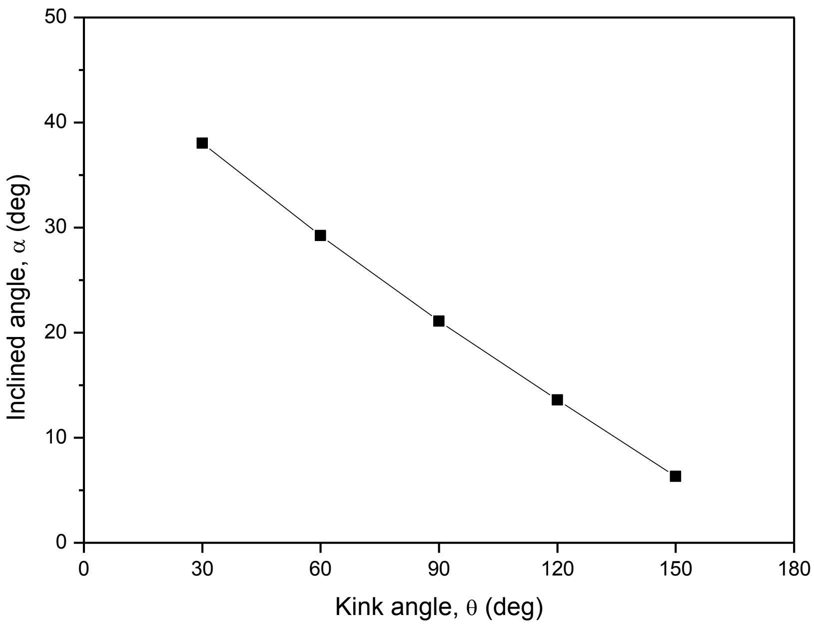

Figure 2-9 Inclined angle of the Iso-energy release rate

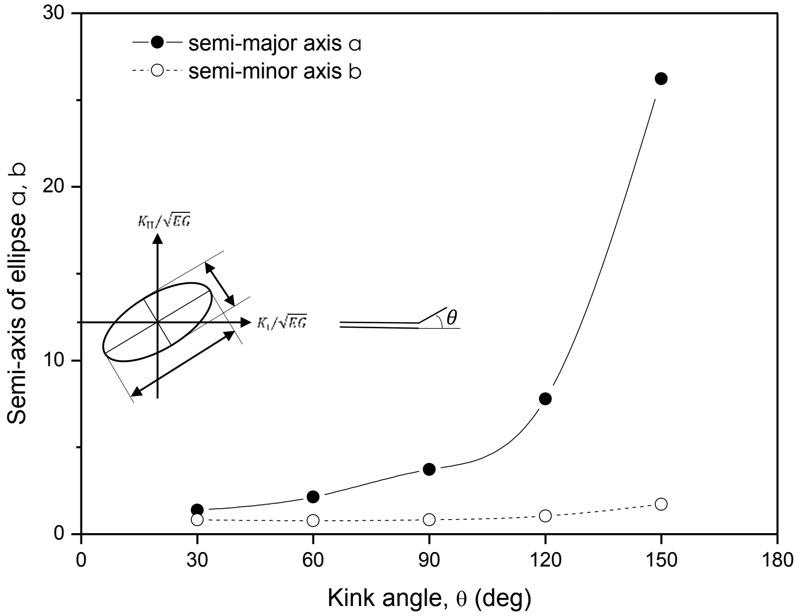

Figure 2-10 Semi-major and semi-minor axis of the Iso-energy release rate

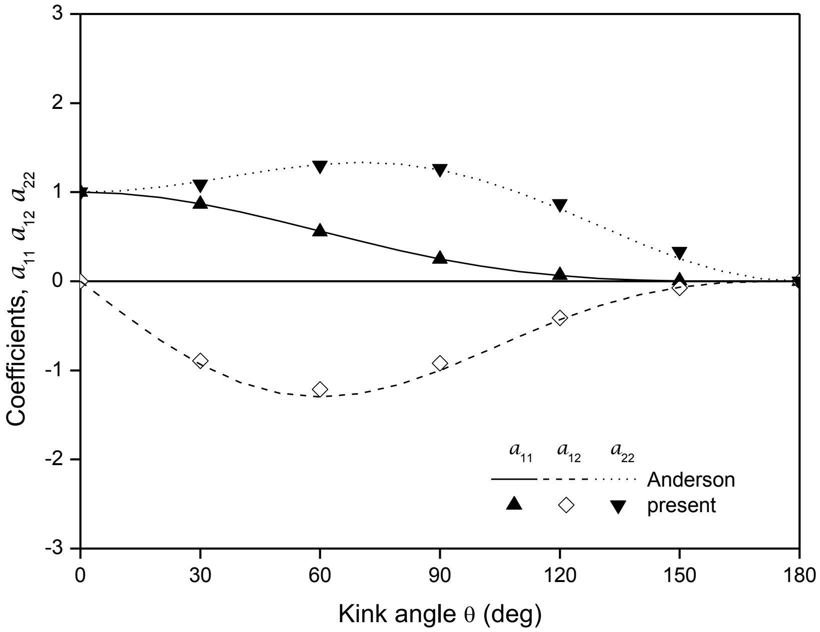

Figure 2-11 Coefficients of energy release rate

2.2.2 Comparison of Numerical Results with References

2.2.2.1 The validity of extended Irwin's formula

The Equation (1) for computing the energy release rate of $2D$ body can be extended to cracks under combined loading if the stress intensity factors involved are interpreted as the kink stress intensity factors, $k_I(\theta)$ and $k_{II}(\theta)$:

$$G(\theta) = \frac{{k_I}^2(\theta)+{k_{II}}^2(\theta)}{E} \quad (2\text{-}7)$$

The validity of extended Irwin's formula is reiterated by the numerical simulation under two arbitrary loading conditions, as shown in Table 2-1. Stress intensity factors $k_I(\theta)$ and $k_{II}(\theta)$ with the limiting process as the propagation kink goes to zero is obtained from the output of the ABAQUS, and $G(\theta)$ is obtained from equation (2-7). The value of G obtained from the present numerical method is consistent very well with the value from Irwin's formula. In other words, it is proved again that Irwin's formula indeed holds at the inception of kink for all kink angles, and is not limited to only the collinear crack extension [29].

Table 2-1 Comparison of G for two different methods

$\sigma = -10.4 \times 10^5 MPa, \tau = 2.5 \times 10^5 MPa$				
θ (deg)	$k_I(\theta)$ from ABAQUS ($MPa\sqrt{mm}$)	$k_{II}(\theta)$ from ABAQUS $MPa\sqrt{mm}$	$G(\theta)$ for Irwin's (mJ)	G for the present method (mJ)
30 °	1.31×10^5	9.90×10^5	4.84	4.84
60 °	-5.01×10^5	6.26×10^5	3.12	3.17
90 °	-7.72×10^5	1.30×10^5	2.98	2.98
120 °	-6.88×10^5	-2.42×10^5	2.58	2.58
150 °	-4.02×10^5	-3.22×10^5	1.29	1.29
180 °	0.00×10^0	0.00×10^0	0.00	0.00
$\sigma = 0\ MPa, \tau = 10^5\ MPa$				
θ (deg)	$k_I(\theta)$ from ABAQUS $MPa\sqrt{mm}$	$k_{II}(\theta)$ from ABAQUS $MPa\sqrt{mm}$	G for Calculation (mJ)	G for Simulation (mJ)

30 °	2.91×10^{6}	1.18×10^{6}	47.82	47.82
60 °	1.85×10^{6}	1.46×10^{6}	26.84	26.84
90 °	8.14×10^{5}	1.18×10^{6}	10.02	10.01
120 °	1.50×10^{5}	5.97×10^{5}	1.84	1.84
150 °	-8.86×10^{4}	1.02×10^{5}	0.09	0.09
180 °	0.00×10^{0}	0.00×10^{0}	0.00	0.00

2.2.2.2 Inaccuracy of Hussain's equation

In this section, Hussain's equation will be reviewed, some errors of Hussain's equation can be found through the comparison with the present technique. An L-shaped crack in the z-plane was mapped onto the unit circle in the ζ-plane, and $A'B'C'D'$ were respectively, the images of *ABCD*. Hussain formulated the problem in terms of a Cauchy integral equation along the path $B'C'D'$. The equation was then solved by iteration. In the process of iteration, the "simultaneous-expansion" procedure was introduced assumed that $B', D' \to C'$ as $r \to 0$ [68]. In the limit as $R \to 0,$ the path of integration in the ζ-plane corresponded to the integration around the crack tip in the z-plane (Figure 2-12). Then Hussain proposed the specific expression of the energy release rate for any angle in the limit as the propagation branch goes to zero using the elastic solution, as shown in Formula (2-8).

$$G(\theta) = \frac{1}{4E}\left(\frac{1-\theta/\pi}{1+\theta/\pi}\right)^{\theta/\pi}\left(\frac{4}{3+cos^2\theta}\right)^2\left\{(1+3cos^2\theta){K_I}^2 + 8\,sin\,\theta\,cos\,\theta K_I K_{II} + (9-5cos^2\theta)\,{K_{II}}^2\right\} \tag{2-8}$$

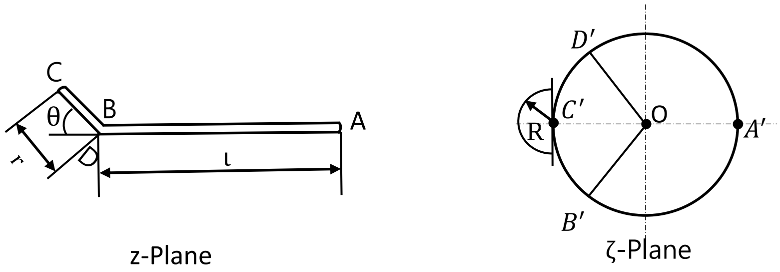

Figure 2-12 Mapping of the angled crack into the unit

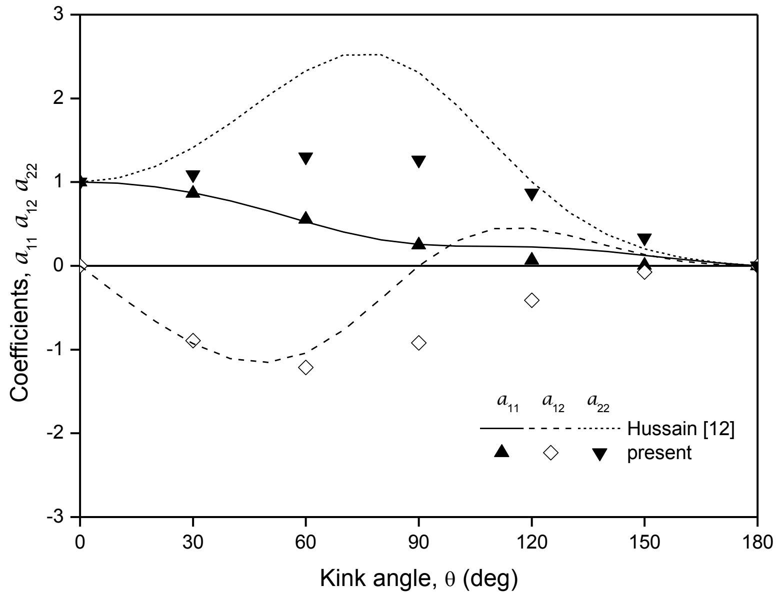

Figure 2-13 Energy release rate coefficients of present work compared with Hussain

Figure 2-13 was the comparison of the coefficients of energy release rate quadratics between Hussain's equation and the prior result investigated in this work. As Hussain's crack started from left, there was a difference of negative sign for a_{12}. The overall trend is consistent. However, the analytic expression from Hussain showed erroneous results for a_{22} and a_{1}, especially in the range of 60° to 120°.

Hussain obtained the same equation through two ways, one was to use J_1, J_2, and another was to use stress intensity factors $k_I(\theta), k_{II}(\theta)$. It was indicated that the J_1, J_2 of Hussain's expression were different from the conventional definition, such as Cherepanov, G.P. [69].

It was necessary to compute the energy release rate in an arbitrary direction θ for a crack tip located near the origin, as shown in Figure 2-14. The energy release rate referring to the new coordinate can be obtained using the transformation equations [70]:

$$J_1{}' = (\cos\theta)J_1 + (\sin\theta)J_2 \tag{2-9}$$

$$J_2{}' = (-\sin\theta)J_1 + (\cos\theta)J_2 \tag{2-10}$$

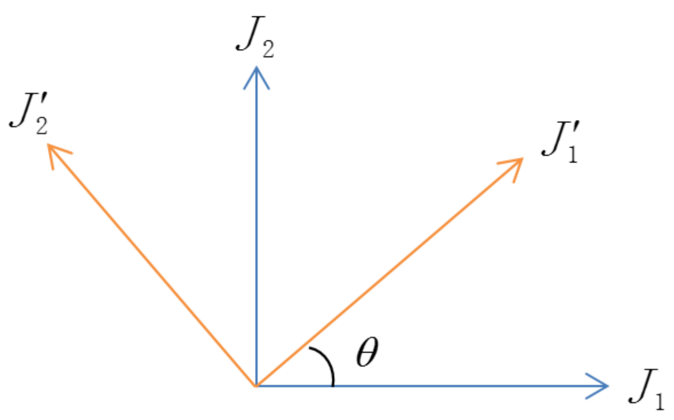

Figure 2-14 Rotation of the coordinate

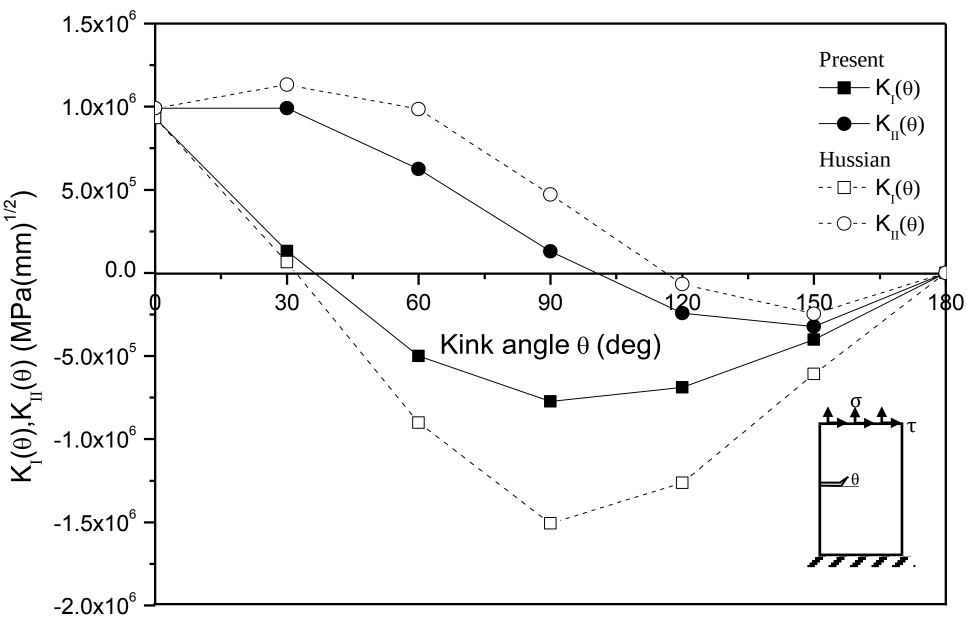

(a) Loading ratio: -10.4 : 2.5

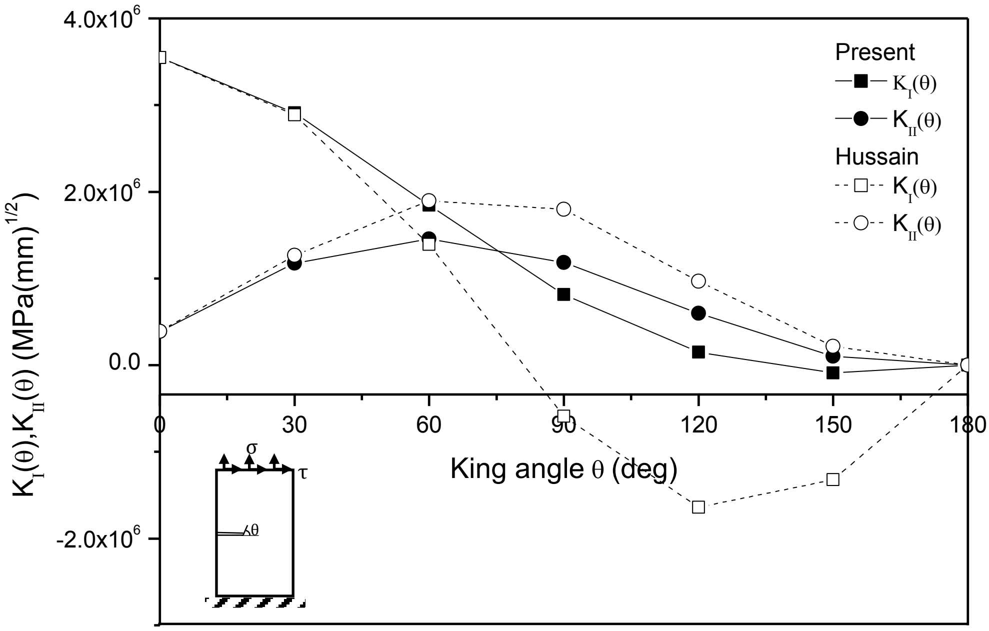

(b) Loading ratio: 0 : 1

Figure 2-15 The stress intensity factors of present work compared with Hussain

It was observed that Hussain just kept the energy release rate in the x' direction after translation, coherently with the inaccurate expression of stress intensity factors of Hussain. Figure 2-15 displayed the comparison of $k_I(\theta), k_{II}(\theta)$ between Hussain and present work for stress intensity factors under arbitrary loading conditions. When the kink angle was in the range of 30° to 150°, there was a significant difference between the two values of the stress intensity factor. The coefficients of $k_I(\theta), k_{II}(\theta)$ can be obtained from Hussain's equations.

$$k_{\mathrm{I}}(\theta) = (\frac{1-\theta/\pi}{1+\theta/\pi})^{\theta/2\pi}(\frac{4}{3+cos^2\theta})\left\{\cos\theta\, K_{\mathrm{I}} - \frac{3}{2}\sin\theta\, K_{\mathrm{II}}\right\} \tag{2-11}$$

$$k_{\mathrm{I}}(\theta) = (\frac{1-\theta/\pi}{1+\theta/\pi})^{\theta/2\pi}(\frac{4}{3+cos^2\theta})\left\{\cos\theta\, K_{\mathrm{II}} + \frac{1}{2}\sin\theta\, K_{\mathrm{I}}\right\} \tag{2-12}$$

Where the coefficients C_{ij} were obtained

$$C_{11} = (\frac{1-\theta/\pi}{1+\theta/\pi})^{\theta/2\pi}(\frac{4}{3+cos^2\theta})\cos\theta \tag{2-13}$$

$$C_{12} = -\frac{3}{2}(\frac{1-\theta/\pi}{1+\theta/\pi})^{\theta/2\pi}(\frac{4}{3+cos^2\theta})\sin\theta \tag{2-14}$$

$$C_{21} = \frac{1}{2}(\frac{1-\theta/\pi}{1+\theta/\pi})^{\theta/2\pi}(\frac{4}{3+cos^2\theta})\sin\theta \tag{2-15}$$

$$C_{22} = (\frac{1-\theta/\pi}{1+\theta/\pi})^{\theta/2\pi}(\frac{4}{3+cos^2\theta})\cos\theta \tag{2-16}$$

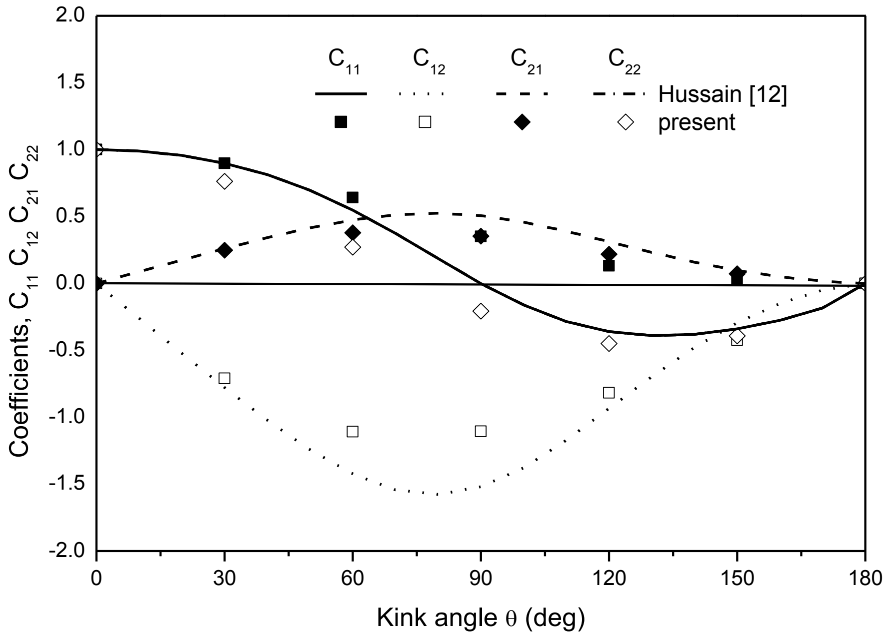

Figure 2-16 Coefficients $C_{11}, C_{12}, C_{21}, C_{22}$ of present work compared with Hussain

Figure 2-16 illustrated the huge gap between the present work and Hussain, especially for the C_{11} and C_{12}. Hence, in general, the error which led to the fundamental inaccuracy was the derivatives of two stress functions in the mapping function during the “simultaneous expansion” procedure are incorrect.

2.2.2.3 Comparison with Anderson’s equation

The results obtained by the proposed method were more evident through the comparison with Anderson. Anderson’s analytic work introduced the local SIFs, which were functions of nominal SIFs—the local SIFs represent the true stress strength in front of a kink crack, shown as the following:

$$k_{\mathrm{I}}(\theta) = \sigma_{yy}\sqrt{2\pi r} = C_{11}K_{\mathrm{I}} + C_{12}K_{\mathrm{II}} \tag{2-17}$$

$$k_{\mathrm{II}}(\theta) = \tau_{xy}\sqrt{2\pi r} = C_{21}K_{\mathrm{I}} + C_{22}K_{\mathrm{II}} \tag{2-18}$$

Where the coefficients C_{ij} were given by

$$C_{11} = \frac{3}{4}cos\left(\frac{\alpha}{2}\right) + \frac{1}{4}cos\left(\frac{3\alpha}{2}\right) \tag{2-19}$$

$$C_{12} = -\frac{3}{4}\left[sin\left(\frac{\alpha}{2}\right) + sin\left(\frac{3\alpha}{2}\right)\right] \tag{2-20}$$

$$C_{21} = \frac{1}{4}\left[sin\left(\frac{\alpha}{2}\right) + sin\left(\frac{3\alpha}{2}\right)\right] \tag{2-21}$$

$$C_{22} = \frac{1}{4}cos\left(\frac{\alpha}{2}\right) + \frac{3}{4}cos\left(\frac{3\alpha}{2}\right) \tag{2-22}$$

And the energy release rate expression with angle α can be found as the following formula:

$$G = \frac{1}{8}(3 + 4\,cos\,\alpha + cos\,2\alpha){K_I}^2 - \left(sin\,\alpha + \frac{1}{2}sin\,2\alpha\right)K_I K_{II} + \frac{1}{8}(7 + 4\,cos\,\alpha - 3\,cos\,2\alpha){K_{II}}^2 \tag{2-23}$$

Where the coefficients a_{ij} were shown as following:

$$a_{11} = \frac{1}{8}(3 + 4\cos\alpha + \cos 2\alpha) \tag{2-24}$$

$$a_{12} = -\left(\sin\alpha + \frac{1}{2}\sin 2\alpha\right) \tag{2-25}$$

$$a_{22} = \frac{1}{8}(7 + 4\cos\alpha - 3\cos 2\alpha) \tag{2-26}$$

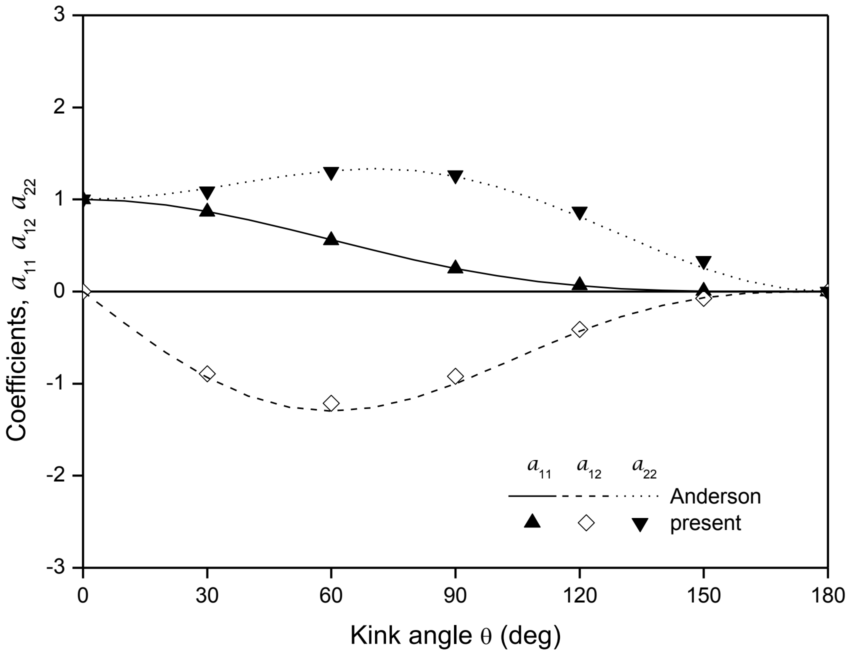

(a) Energy release rate coefficients

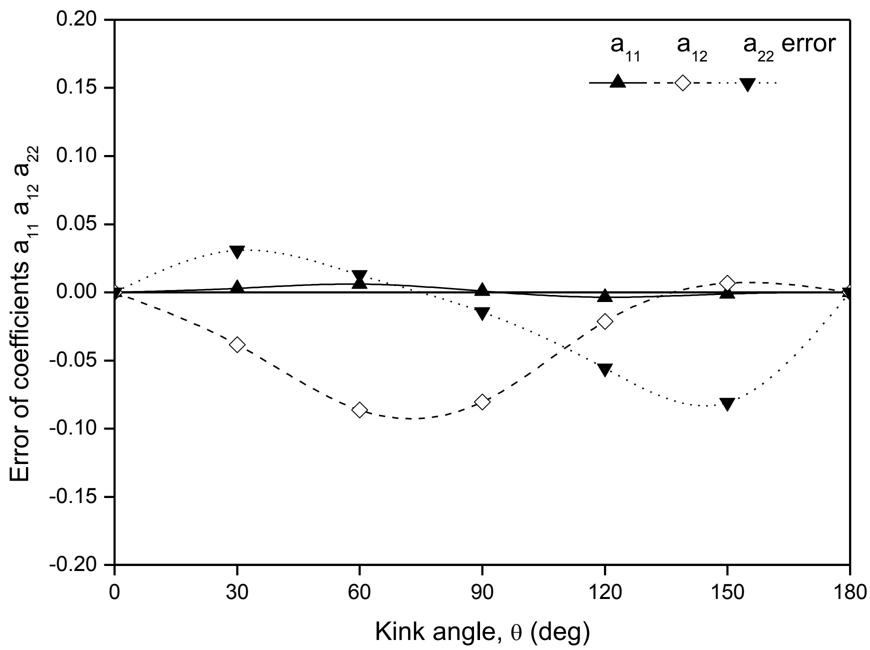

(b) Error

Figure 2-17 Energy release rate coefficients of the present work compared with Anderson

Figure 2-17(a) was the coefficients calculated by Anderson's theory and the proposed method. The values of coefficients a_{11}, a_{12} and a_{22}calculated by Anderson and the proposed method was surprisingly consistent. Figure 2-17(b) was the errors between the two results for each kink angle. It was observed that the coefficients a_{12} and a_{22} had relatively larger differences between the two methods. The maximum error was less than 0.09 for a_{12} and a_{22} at the point of 60° and 150°, respectively. The accuracy was better for a_{11}, the discrepancy varied from -0.004 to 0.006. The average error between each kink angle was less than 1%, which illustrated that the results obtained by the present work agreed well with Anderson's.

However, the slight deviation found was imputable to the fact that the kink extension was not sufficiently small with respect to the initial crack: the effect remote load was thus underestimated. To obtain more accurate estimations, higher-order terms in the expansions of stress fields, or non-linear models must be taken into consideration [71].

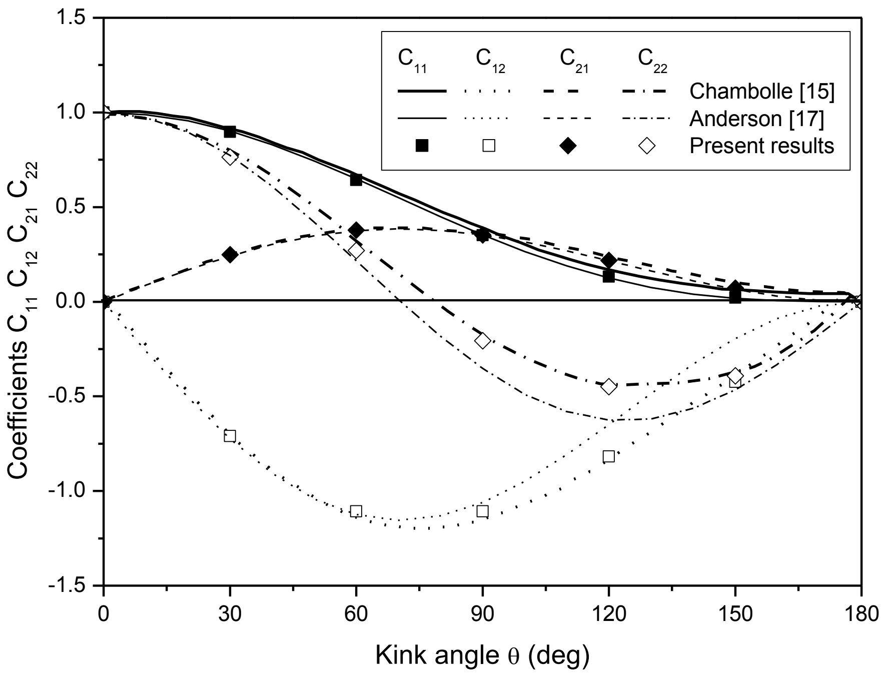

Figure 2-18 Coefficients $C_{11}, C_{12}, C_{21}, C_{22}$ of present work compared with Chambolle and Anderson

The above interpretation for deviation also can be proved by Chambolle, A. [28]

with the semi-analytical and semi-numerical method. Using the expansion of Amestoy, M and Leblond, J.B. [8] in the interval $[0^{\circ}, 80^{\circ}]$, the curve-fitting for larger angles yields the numerical curves for the coefficients of stress intensity factors. Figure 2-18 compared the coefficients $C_{11}, C_{12}, C_{21}, C_{22}$ between Chambolle and Anderson. The error of coefficients C_{12}, C_{22} for Chambolle is distinctly smaller than Anderson with reference to present results (Figure 2-19), as the higher-order expression was concerned.

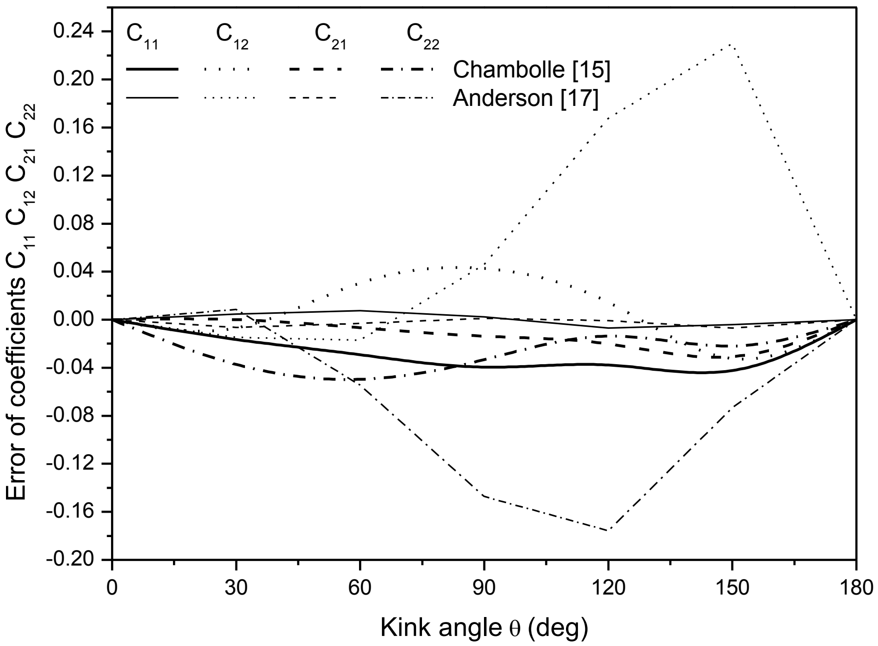

Figure 2-19 Errors of coefficients $C_{11}, C_{12}, C_{21}, C_{22}$ for Chambolle and Anderson with reference to the present

2.3. Fracture Parameters for 3D Crack

2.3.1. The Theoretical Derivation for I-II-III Mixed Mode Crack

2.3.1.1 Stress analysis of crack

Each mode of loading produces the $1/\sqrt{r}$ singularity at the crack tip, but the proportionality constants the stress intensity factor K and f_{ij} depend on the mode.

Thus, the stress fields ahead of a crack tip in an isotropic linear elastic material can be written as:

$$\left.\begin{aligned}\lim_{r\to 0}\sigma_{ij}^{(I)} &= \frac{K_I}{\sqrt{2\pi r}}f_{ij}^{(I)}(\theta)\\ \lim_{r\to 0}\sigma_{ij}^{(II)} &= \frac{K_{II}}{\sqrt{2\pi r}}f_{ij}^{(II)}(\theta)\\ \lim_{r\to 0}\sigma_{ij}^{(III)} &= \frac{K_{III}}{\sqrt{2\pi r}}f_{ij}^{(III)}(\theta)\end{aligned}\right\} \tag{2-27}$$

Table 2-2 Stress fields for mixed-mode crack

Stress Fields		Mode I	Mode II	Mode III
σ_{xx}		$\frac{K_I}{\sqrt{2\pi r}}\cos\left(\frac{\theta}{2}\right)\left[1-\sin\left(\frac{\theta}{2}\right)\sin\left(\frac{3\theta}{2}\right)\right]$	$-\frac{K_{II}}{\sqrt{2\pi r}}\sin\left(\frac{\theta}{2}\right)\left[2+\cos\left(\frac{\theta}{2}\right)\cos(\frac{3\theta}{2}\right)$	0
σ_{yy}		$\frac{K_I}{\sqrt{2\pi r}}\cos\left(\frac{\theta}{2}\right)\left[1+\sin\left(\frac{\theta}{2}\right)\sin\left(\frac{3\theta}{2}\right)\right]$	$\frac{K_{II}}{\sqrt{2\pi r}}\sin\left(\frac{\theta}{2}\right)\cos\left(\frac{\theta}{2}\right)\cos\frac{3\theta}{2}$	0
τ_{xy}		$\frac{K_I}{\sqrt{2\pi r}}\cos\left(\frac{\theta}{2}\right)\sin\left(\frac{\theta}{2}\right)\cos(\frac{3\theta}{2})$	$\frac{K_{II}}{\sqrt{2\pi r}}\cos\left(\frac{\theta}{2}\right)\left[1-\sin\left(\frac{\theta}{2}\right)\sin\left(\frac{3\theta}{2}\right)\right]$	0
σ_{zz}	Plane stress	0	0	0
	Plane strain	$v(\sigma_{xx}+\sigma_{yy})$	$v(\sigma_{xx}+\sigma_{yy})$	
τ_{xz}		0	0	$-\frac{K_{III}}{\sqrt{2\pi r}}\sin(\frac{\theta}{2})$
τ_{yz}		0	0	$\frac{K_{III}}{\sqrt{2\pi r}}\cos(\frac{\theta}{2})$

Detailed expressions for the singular stress fields for Mode I, Mode II, and Mode III are given in Table 2-2[21].

Based on the principle of linear superposition, in a mixed-mode problem, the individual contributions to a given stress component are additive for Modes I, II, and III, respectively.

$$\sigma_{ij}^{(total)} = \sigma_{ij}^{(I)} + \sigma_{ij}^{(II)} + \sigma_{ij}^{(III)} \tag{2-28}$$

Accordingly, the stress fields ahead of the crack front for Mode I, Mode II, and Mode III are obtained as following:

$$\left.\begin{aligned}
\sigma_{xx} &= \frac{K_I}{\sqrt{2\pi r}}\cos\left(\frac{\theta}{2}\right)\left[1-\sin\left(\frac{\theta}{2}\right)\sin\left(\frac{3\theta}{2}\right)\right]-\frac{K_{II}}{\sqrt{2\pi r}}\sin\left(\frac{\theta}{2}\right)\left[2+\cos\left(\frac{\theta}{2}\right)\cos\left(\frac{3\theta}{2}\right)\right]\\
\sigma_{yy} &= \frac{K_I}{\sqrt{2\pi r}}\cos\left(\frac{\theta}{2}\right)\left[1+\sin\left(\frac{\theta}{2}\right)\sin\left(\frac{3\theta}{2}\right)\right]+\frac{K_{II}}{\sqrt{2\pi r}}\sin\left(\frac{\theta}{2}\right)\cos\left(\frac{\theta}{2}\right)\cos\frac{3\theta}{2}\\
\tau_{xy} &= \frac{K_I}{\sqrt{2\pi r}}\cos\left(\frac{\theta}{2}\right)\sin\left(\frac{\theta}{2}\right)\cos\left(\frac{3\theta}{2}\right)+\frac{K_{II}}{\sqrt{2\pi r}}\cos\left(\frac{\theta}{2}\right)\left[1-\sin\left(\frac{\theta}{2}\right)\sin\left(\frac{3\theta}{2}\right)\right]\\
\sigma_{zz} &= \begin{cases}\frac{\sqrt{2}K_I}{\sqrt{\pi r}}\cos\left(\frac{\theta}{2}\right)-\frac{\sqrt{2}K_{II}}{\sqrt{\pi r}}\sin\left(\frac{\theta}{2}\right) & \text{(Plane strain)}\\ 0 & \text{(Plane strain)}\end{cases}\\
\tau_{xz} &= -\frac{K_{III}}{\sqrt{2\pi r}}\sin\left(\frac{\theta}{2}\right)\\
\tau_{yz} &= \frac{K_{III}}{\sqrt{2\pi r}}\cos\left(\frac{\theta}{2}\right)
\end{aligned}\right\} \quad (2\text{-}29)$$

2.3.1.2 The Modified Expression of Energy Release Rate for Mixed Mode crack

The stress intensity factor defines the amplitude of the crack-tip singularity. The stresses near the crack tip increase in proportion to K. Moreover, the stress intensity factor completely defines the crack tip conditions; if K is known, it is possible to solve for all components of stress, strain, and displacement as a function of r and θ. This single-parameter description of crack tip conditions turns out to be one of the most important concepts in fracture mechanics.

Considering the meaning of SIFs, K_I, K_{II}, K_{III} denote the intensity of tensile stress, in-plane stress, and out-of-plane stress in a 3D crack, as shown in Figure 2-20. When a crack kink occurs, the local SIFs at the crack tip should be recalculated under the influence of the stress field. A local $x' - y' - z'$ the coordinate system at the tip of the kink is defined and assumes that the remote stress fields in polar coordinates defined the local stress field. The transformation of the $x' - y'$ plane is shown in Figure 2-21.

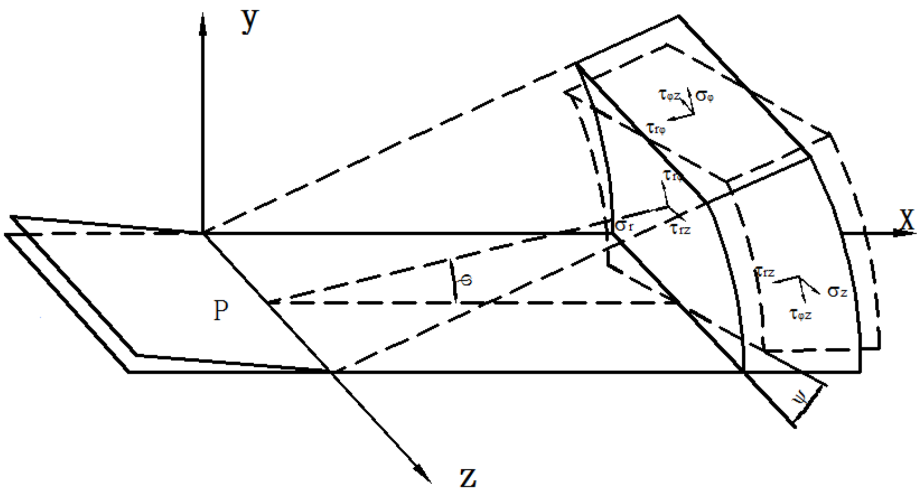

Figure 2-20 Stress field at the crack tip

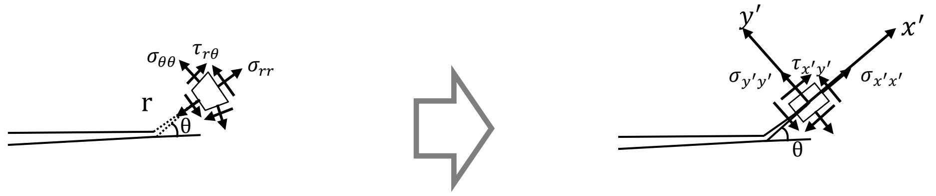

(a) The crack-tip stress fields in polar coordinate system

(b) The local stress fields in $x' - y'$ coordinates system

Figure 2-21 Infinitesimal kink at the tip in different coordinates

For the stress fields to be useful at the crack tip in local coordinates, it is needed to determine K from remote loads in polar coordinates. The closed-form solutions for stress fields ahead of the crack front for Mode I, Mode II, and Mode III at an angle θ in polar coordinates are shown in Equation (2-30) [73].

$$\left.\begin{aligned}
\sigma_{rr} &= \frac{K_I}{\sqrt{2\pi r}}\left[\frac{5}{4}cos\left(\frac{\theta}{2}\right)-\frac{1}{4}cos\left(\frac{3\theta}{2}\right)\right]+\frac{K_{II}}{\sqrt{2\pi r}}\left[-\frac{5}{4}sin\left(\frac{\theta}{2}\right)+\frac{3}{4}sin\left(\frac{3\theta}{2}\right)\right]\\
\sigma_{\theta\theta} &= \frac{K_I}{\sqrt{2\pi r}}\left[\frac{3}{4}cos\left(\frac{\theta}{2}\right)+\frac{1}{4}cos\left(\frac{3\theta}{2}\right)\right]+\frac{K_{II}}{\sqrt{2\pi r}}\left[-\frac{3}{4}sin\left(\frac{\theta}{2}\right)-\frac{3}{4}sin\left(\frac{3\theta}{2}\right)\right]\\
\tau_{r\theta} &= \frac{K_I}{\sqrt{2\pi r}}\left[\frac{1}{4}sin\left(\frac{\theta}{2}\right)+\frac{1}{4}sin\left(\frac{3\theta}{2}\right)\right]+\frac{K_{II}}{\sqrt{2\pi r}}\left[\frac{1}{4}cos\left(\frac{\theta}{2}\right)+\frac{3}{4}cos\left(\frac{3\theta}{2}\right)\right]\\
\sigma_z &= \begin{cases}\frac{\sqrt{2}K_I}{\sqrt{\pi r}}\cos\left(\frac{\theta}{2}\right)-\frac{\sqrt{2}K_{II}}{\sqrt{\pi r}}\sin\left(\frac{\theta}{2}\right) & \text{(Plane strain)}\\ 0 & \text{(Plane strain)}\end{cases}\\
\tau_{rz} &= \frac{K_{III}}{\sqrt{2\pi r}}sin\left(\frac{\theta}{2}\right)\\
\tau_{\theta z} &= \frac{K_{III}}{\sqrt{2\pi r}}cos\left(\frac{\theta}{2}\right)
\end{aligned}\right\} \tag{2-30}$$

The directions of the local stress field for the kink tip in a local $x' - y' - z'$ coordinate system are consistent with those of the polar coordinate, as shown in Figure 2-21. Thus, the stress at the kink tip between the polar coordinate and local $x' - y' - z'$ coordinate has the following relationship:

$$\left.\begin{aligned}
\sigma_{x'x'} &= \sigma_{rr}\\
\sigma_{y'y'} &= \sigma_{\theta\theta}\\
\tau_{x'y'} &= \tau_{r\theta}\\
\sigma_z &= \sigma_z\\
\tau_{x'z'} &= \tau_{rz}\\
\tau_{y'z'} &= \tau_{\theta z}
\end{aligned}\right\} \tag{2-31}$$

Consider a through crack in a stress plane plate experiences combined Mode I, Mode II, and Mode III loading in $x' - y' - z'$coordinate system with $\theta = 0$, which are created by the resolved normal and shear components form applied stress. The stress normal to the crack plane, $\sigma_{y'y'}$, produces pure Mode I loading, $\tau_{x'y'}$ applies Mode II loading to the crack, and $\tau_{y'z'}$ applies Mode III loading, the stress intensity factors for the plate with crack can be inferred as following:

$$\left.\begin{aligned}
K_I &= \sigma_{y'y'}(\theta = 0)\sqrt{2\pi r}\\
K_{II} &= \tau_{x'y'}(\theta = 0)\sqrt{2\pi r}\\
K_{III} &= \tau_{y'z'}(\theta = 0)\sqrt{2\pi r}
\end{aligned}\right\} \tag{2-32}$$

Accordingly, in the Figure 2-21, the local stress intensity factors $k(\theta)'$for the infinitesimal kink at the arbitrary extend angle θ were deduced by combining Equations (2-30), (2-31), (2-32), respectively:

$$\left.\begin{array}{c} k_I'(\theta) = \sigma_{y'y'}\sqrt{2\pi r} = C_{11}K_I + C_{12}K_{II} \\ k_{II}'(\theta) = \tau_{x'y'}\sqrt{2\pi r} = C_{21}K_I + C_{22}K_{II} \\ k_{III}'(\theta) = \tau_{y'z'}\sqrt{2\pi r} = C_{33}K_{III} \end{array}\right\} \tag{2-33}$$

where the coefficients can be calculated as following:

$$\left.\begin{array}{c} C_{11} = \frac{3}{4}\cos\left(\frac{\theta}{2}\right) + \frac{1}{4}\cos\left(\frac{3\theta}{2}\right) \\ C_{12} = -\frac{3}{4}sin\left(\frac{\theta}{2}\right) - \frac{3}{4}sin\left(\frac{3\theta}{2}\right) \\ C_{21} = \frac{1}{4}sin\left(\frac{\theta}{2}\right) + \frac{1}{4}sin\left(\frac{3\theta}{2}\right) \\ C_{22} = \frac{1}{4}\cos\left(\frac{\theta}{2}\right) + \frac{3}{4}\cos\left(\frac{3\theta}{2}\right) \\ C_{33} = \cos\left(\frac{\theta}{2}\right) \end{array}\right\} \tag{2-34}$$

Reviewing the expression of the classical energy release rate, the new expression for the I-II-III mixed-mode crack can be modified as Equations (2-35):

$$G(\theta) = \frac{k_I'^2(\theta)}{E} + \frac{{k_{II}'}^2(\theta)}{E} + \frac{{k_{III}'}^2(\theta)}{2\mu} \tag{2-35}$$

2.3.2. Numerical Analysis of 3D Crack

2.3.2.1. 3D Model of Crack Simulation

As there are few relevant studies of fracture of crack under mode I, II, III. A finite element model of mixed crack was established based on the research of 2D crack above. The pattern of stress and deformation for the component is different from the plane stress before. The stress intensity factor and J-integral values are generated at each node of the crack tip along the thickness direction.

A 3D model with a mixed-mode crack is considered here (Figure 2-22): $L = 50\,mm, W = 50\,mm,\ D = 20\,mm,\ A = 10\,mm$. The bottom is fixed, and normal stress and shear stress are applied at the top. The front of the surface cracks in the 3D model exhibits a straight line.

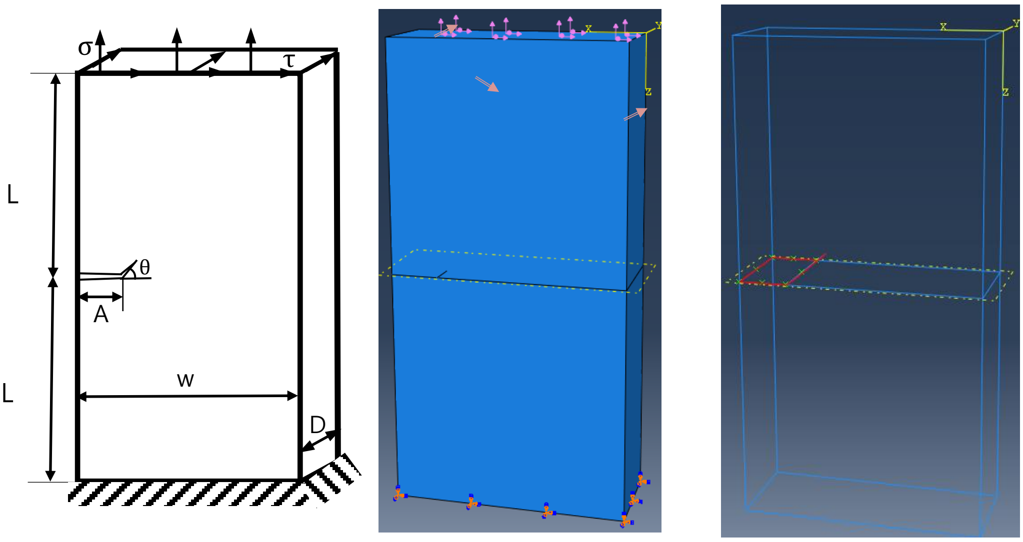

(a) A 3D model with a mixed-mode crack

(b) Loaded solid model

(c) Definition of crack for three-dimensional specimen

Figure 2-22 Crack model with mixed-mode I-II-III in ABAQUS

Quadratic hexahedral elements are used with the 20-nodes collapsed element in the crack tip region by the1/4-node displacement method [74, 75] to simulate the singularity of the displacement at the crack tip. Figure 2-23 shows the finite element model with a partially enlarged drawing of mesh generation at the crack front. Several circles of the cylindrical hexahedral element are arranged around the crack tip as the transition section. The mesh size increases gradually to ensure the refinement of the crack tip and reduces the number of overall elements. This meshing method can not only ensure the accuracy of calculation but also improves the efficiency.

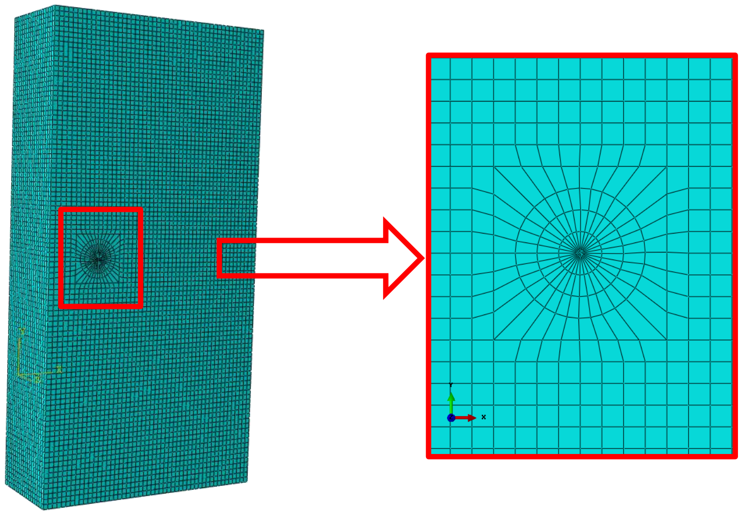

(a) Overview of model (b) Crack tip meshes

Figure 2-23 Finite element model

2.3.2.2. Computational Analysis

The data processing for K and G under the I-II-III mixed-mode crack simulation is more complex than the I-II mixed-mode crack—not only for the value K_{III} added, but also for much more data on the crack tip line. To obtain the fracture parameter K, the present study is described as follows:

(1) Determine K and J for kink cracks repeatedly, varying the kink length from $0.1\,mm$ to $1\,mm$ with four data points ($a = 0.1\,mm$, $0.3\,mm$, $0.5\,mm$, $1\,mm$). Then, compute the energy release rate and stress intensity factors as the kink propagation vanishes on the curve of K and J versus kink length through fitting each node along the crack tip line.

(2) Plot the non-dimensional value $(K_I/\sqrt{EG}, K_{II}/\sqrt{EG}, K_{III}/\sqrt{EG})$ for each kink angle $(\theta = 30^{\circ}, 60^{\circ}, 90^{\circ}, 120^{\circ}, 150^{\circ})$

(3) Determine the parameters of inclined ellipsoids that fit the above data points using a fitting method for quadric surfaces in space by MATLAB, and the corresponding ellipsoid equation is presented as follows:

$$\frac{(\frac{K_I}{\sqrt{EG}}\cos\alpha+\frac{K_{II}}{\sqrt{EG}}\sin\alpha)^2}{a^2}+\frac{(\frac{K_{II}}{\sqrt{EG}}\cos\alpha-\frac{K_I}{\sqrt{EG}}\sin\alpha)^2}{b^2}+\frac{(\frac{K_{III}}{\sqrt{2\mu G}})^2}{c^2}=1 \tag{2-36}$$

where a, b, c, α are the semi-major axis, semi-middle axis, semi-minor axis, and inclination of an ellipse, respectively.

(4) Obtain the coefficients of quadratic of energy release rate in terms of stress intensity factors, and defined as

$$G = \frac{1}{E}[a_{11}K_I^2 + a_{12}K_I K_{II} + a_{22}K_{II}^2 + a_{33}(1+v)K_{III}^2] \quad (2\text{-}37)$$

The results of fitting the non-dimensional value are shown in Figure 2-24. A series of conclusions can be summarized as follows:

(1) A series of ellipsoids are fitted based on the non-dimensional value ($K_I/\sqrt{EG}$, $K_{II}/\sqrt{EG}$, $K_{III}/\sqrt{EG}$) transformed from the data output from ABAQUS, which stands for (x, y, z) respectively in a three-dimensional coordinate system.

(2) At each presupposed extended angle (30°~150°), the scattered points of dimensionless data output by ABAQUS under different loadings are all on the surface of the same inclined ellipsoid. Here to show this phenomenon clearly, the perspective of $y = x$ observation is adopted.

(3) The coefficients of quadratics for energy release rate in terms of stress intensity factors are calculated for each kink angle based on the ellipsoid equations.

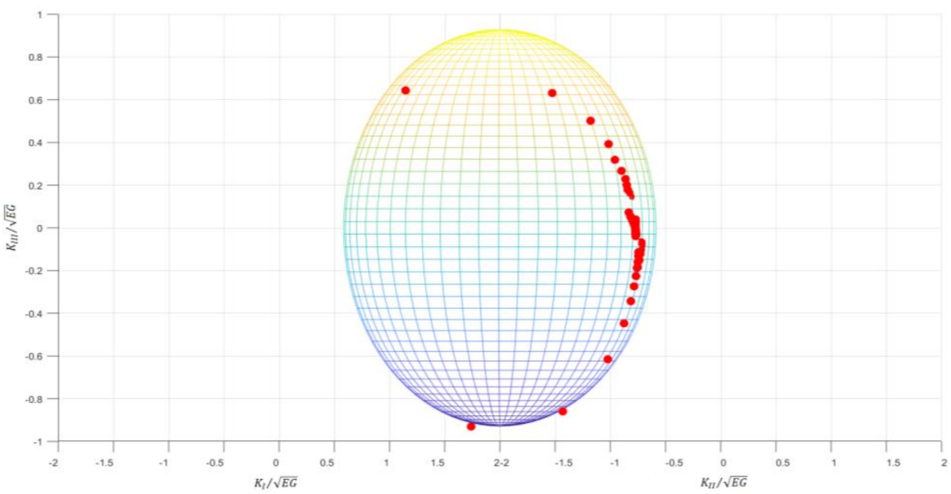

a) 30°

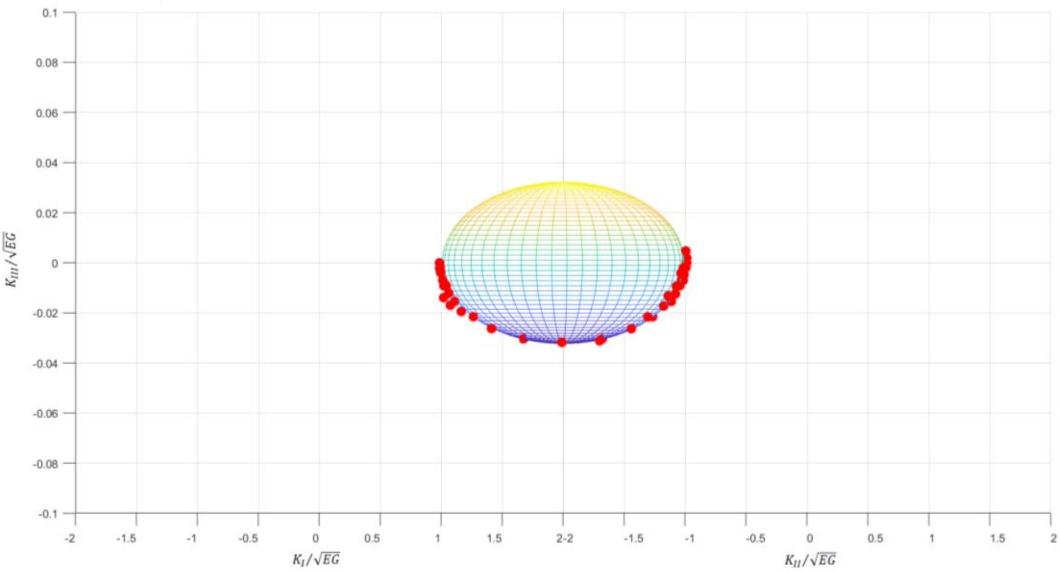

0.1
0.08
0.06
0.04
0.02
0
-0.02
-0.04
-0.06
-0.08
-0.1
$K_{III}/\sqrt{EG}$
-2
-1.5
-1
-0.5
0
0.5
1
1.5
2-2
-1.5
-1
-0.5
0
0.5
1
1.5
2
$K_I/\sqrt{EG}$
$K_{II}/\sqrt{EG}$

(b) 60°

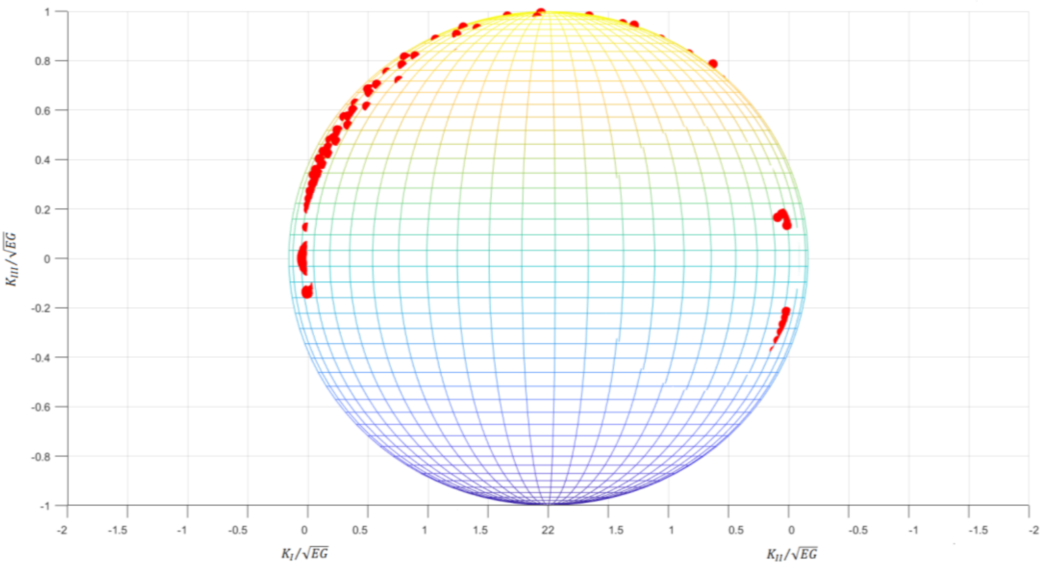

1
0.8
0.6
0.4
0.2
0
-0.2
-0.4
-0.6
-0.8
-1
$K_{III}/\sqrt{EG}$
-2
-1.5
-1
-0.5
0
0.5
1
1.5
22
1.5
1
0.5
0
-0.5
-1
-1.5
-2
$K_I/\sqrt{EG}$
$K_{II}/\sqrt{EG}$

(c) 90°

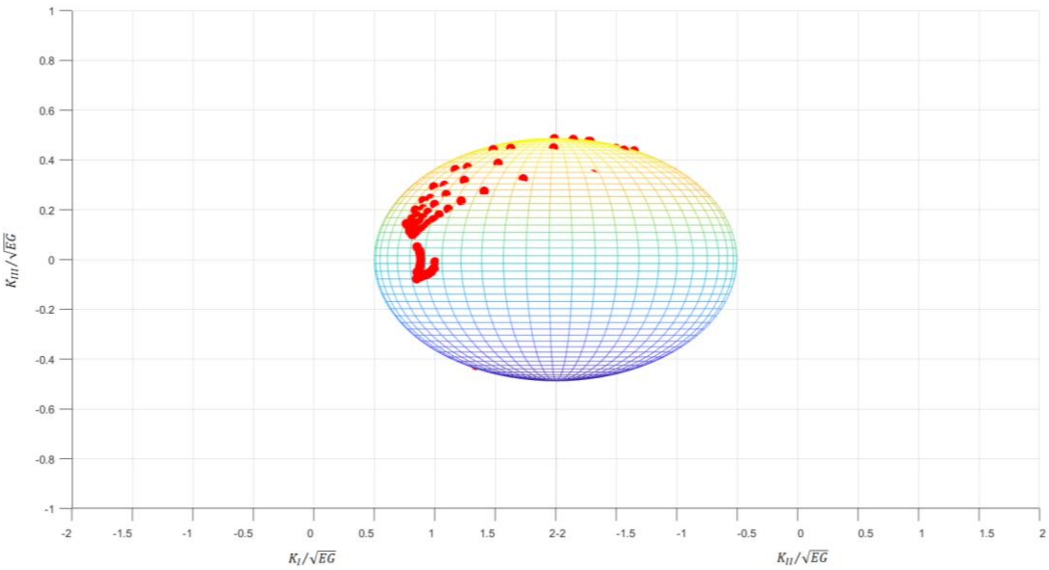

(d) 120°

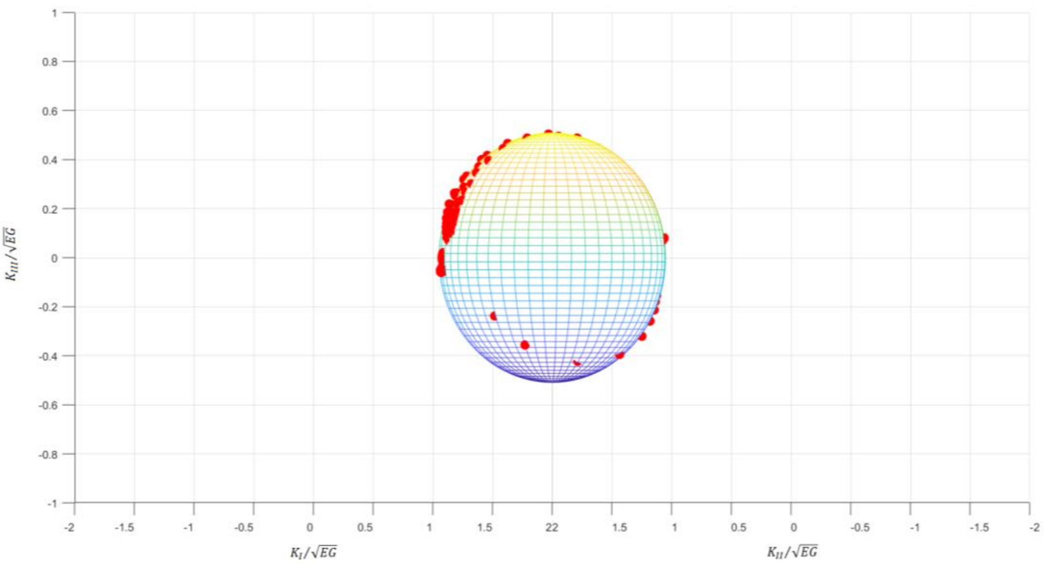

（e）150°

Figure 2-24 Iso-energy release rate ellipsoids on normalized mixed-mode stress intensity factors

2.3.3. Discussion of Theoretical and Numerical Results

Based on the research of I-II mixed-mode crack, the method extent to I-II-III mixed-mode crack, not only added out-of-plane loading but also considered the thickness factor. Therefore, the nodes along the thickness direction in a finite element model can output multi-group values of K and G.

An arbitrary loading had been imposed on a crack model, the energy release rate

G can be obtained based on the numerical method, and $G(\theta)$ was calculated with the obtained global stress intensity factor K through the theoretical expression (2-35). Figure 2-25 was the $G/G(\theta)$ along the thickness direction, the values at node 4~17 were at about a constant value of 1.1, while the values at node 1, 2, 3 and 18, 19, 20 which were adjacent to the free surface are offset highly from 1.1. It was confirmed that the theoretical expression deduced could provide accurate results as the proposed numerical method. The reason for deviation for the two solutions was not only the influence of the free surface at both ends of the crack front but also the stress coupling effect.

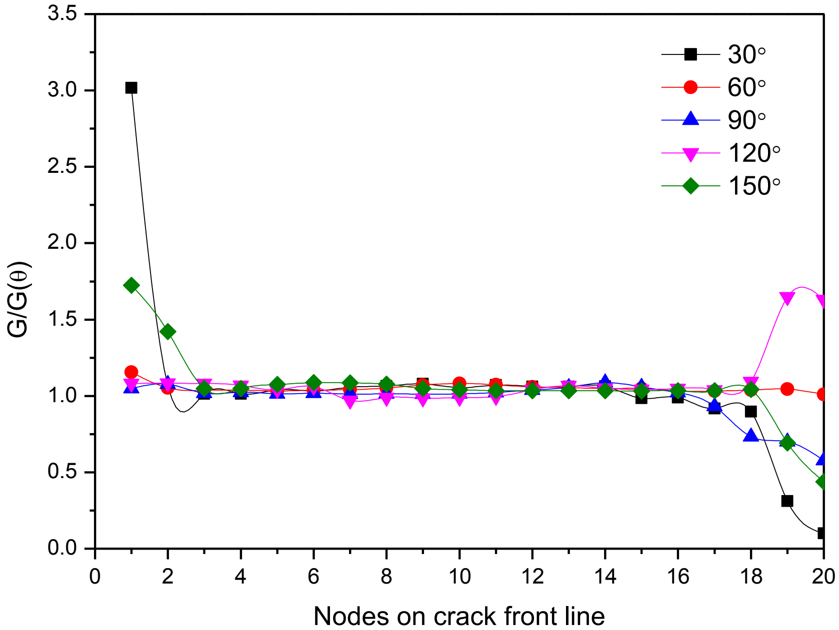

Figure 2-25 $G/G(\theta)$ for each expansion angle

The case to be considered was the specimen subject to in-plane shear loading, as shown in Figure 2-26. In this case, the generated K_{II} values were rather constant in the inner part of the specimen. But the values for nodes near the free surface increase remarkably, which means that the singularity changed in the vicinity of the free surface. The stress intensity factor K_{III} was generated, even if the external loading of the specimen did not include an out-of-plane shear component. This phenomenon was defined as the stress coupling effect [76, 77]. The in-plane shear loading not only create K_{II} , but also K_{III} as the imbalance of stress about the neutral layer. However, there was no normal stress created by the shear loading influence, so the K_I was inexistent throughout. The absolute values of K_{III} were enlarged gradually from the middle node of the crack tip to both sides, which illustrated the coupling effect enhanced by the free surface. Due to the absolute values of K_{III} were less than K_{II}, especially in the inner part of the specimen, the coupling effect was called weak coupling.

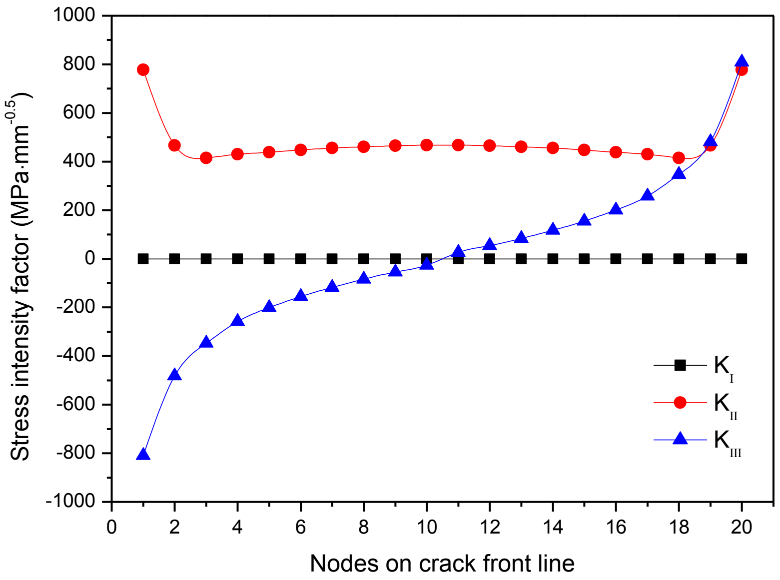

Figure 2-26 Distribution of stress intensity factor on the crack tip line under mode II loading

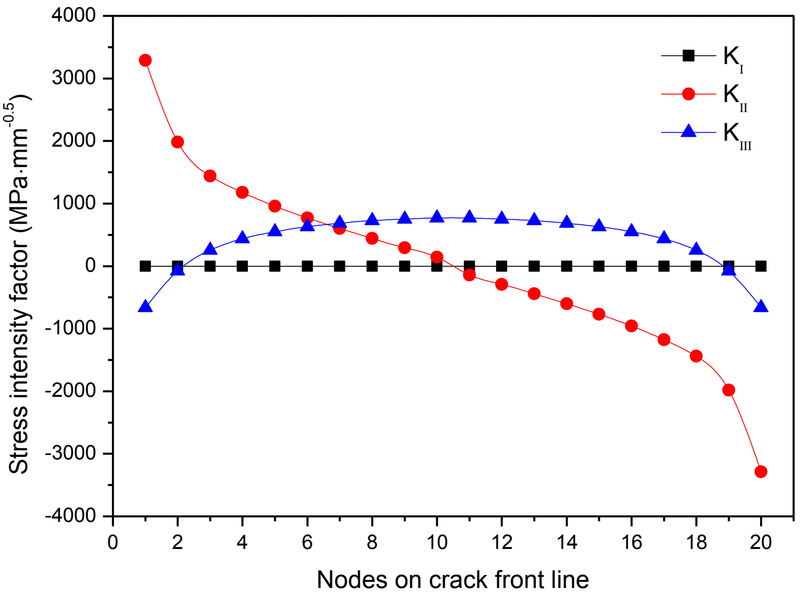

Figure 2-27 Distribution of stress Intensity factor on the crack tip line under mode III loading

Figure 2-27 showed the out-of-plane shear loading case. In this case, the pure mode III loading generated K_{III} and K_{II}, and the absolute value K_{II} of nodes adjacent to the free surfaces exceeds the value of K_{III}, which was called the strong coupling effect. Regarding the I-II-III mixed-mode crack simulation, the induced K_{II} and K_{III} had a significant influence on their theoretical value due to the coupling effect, which can result in the deviation between G and $G(\theta)$.

2.4 Experiment of Mixed Mode Crack for Verification

2.4.1 Fundamentals of Experimental Design

The fracture mechanics test is the foundation of studying fracture mechanics theory, and the preparation of the fracture sample is related to the accuracy of the test. Various forms of fracture specimens have been used to determine the fracture parameters of cracks, and only the test method of mode I crack was identified for criterion, such as Compact Tension (CT), Three-Points Bending(3PB), C tensile specimen. As there is no standard sample to determine the fracture parameters for mixed-mode crack, standard samples for mode I is improved here.

To research the law of crack propagation under combined loading, the uniaxial oblique crack experiment was carried out. An oblique crack in a plate where the normal to the crack plane was oriented at an angle β with the stress axis is shown as in Figure 2-28(a). The crack experienced combined Mode I and Mode II loading when $\beta \neq 0$; And $K_{III} = 0$ as long as the stress axis and the crack normal both lied in the plane of the plate. For the convenience of analysis, the coordinate axis was redefined to coincide with the crack orientation (Figure 2-28(b)), so the applied stress will be resolved into normal and shear components. The stress normal to the crack plane was $\sigma_{y'y'}$, which produced pure Mode I loading, and shear stress $\tau_{x'y'}$ applies Mode II loading to the crack. The stress intensity factors can be calculated by Formula (38), which was relating $\sigma_{y'y'}$ and $\tau_{x'y'}$ to σ and β through Mohr's circle [25]:

$$\left.\begin{aligned} K_I &= \sigma_{y'y'}\sqrt{\pi a} = \sigma\sqrt{\pi a}\sin^2\beta \\ K_{II} &= \tau_{x'y'}\sqrt{\pi a} = \sigma\sqrt{\pi a}\sin\beta\cos\beta \end{aligned}\right\} \tag{2-38}$$

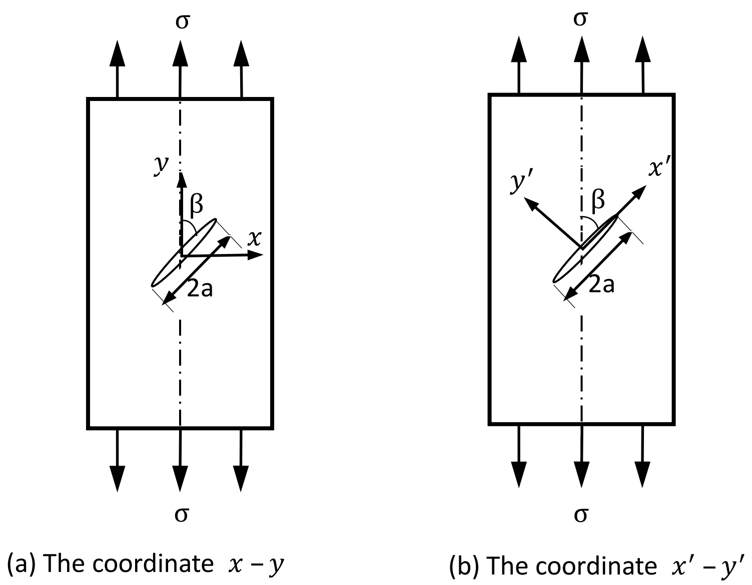

Figure 2-28 Uniaxial oblique crack

Note that Equation (38) transformed to the pure Mode I solution when $\beta = 0$;

The maximum K_{II} occurs at $\beta = 45^{\circ}$, where the shear stress was also at a maximum. And reference [72] verified the validity of specimen for mixed-mode fracture experiment.

2.4.2 Tensile Test of Uniaxial oblique crack

The composition of the 6061-T6 aluminum alloy which was used to manufacture test specimens is shown in Table 2-3. A rectangular plate was fabricated with length $50mm$, width $25\,mm$, and thickness $2\,mm$ containing a $5mm$ edge crack as showing in Figure 2-29. Samples were processed by middle-speed WEDM, and the accuracy was $0.2\,mm$. The surface roughness of the specimens was controlled by a polishing treatment to reduce the effect of roughness on the direction of crack propagation.

Table 2-3 Composition of 6061-T6 aluminum alloy

Chemical composition	Al	Si	Fe	Mn	Mg	Zn	Cr	Ti	Cu	other
Ratio	95.8	0.6	0.7	0.15	0.8~1.2	0.25	0.3	0.15	0.2~0.4	0.15

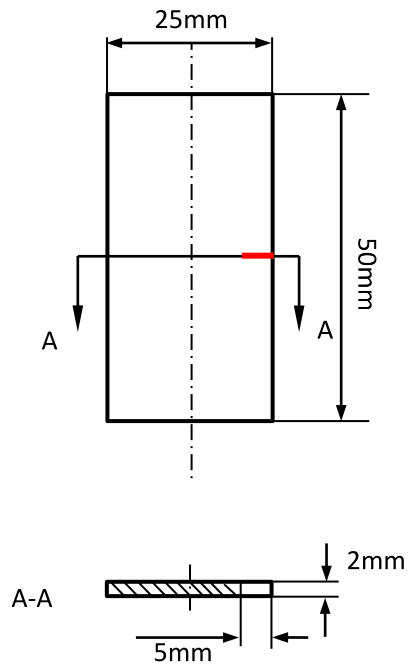

Figure 2-29 Dimensions of an edge crack specimen

A propagating crack seeks the path of least resistance (or the path of the maximum driving force) and need not be confined to its initial plane. If the material is isotropic and homogeneous, the crack will propagate in such a way as to maximize the energy release rate. What follows is an evaluation of the energy release rate as a function of propagation direction in mixed-mode problems. To study the propagation of the mixed-mode crack, the angle between the crack and loading was changed to obtain the different rate of K_I/K_{II}. Therefore, the specimens were divided into three groups by inclination angle $\beta = 30^{\circ}, 60^{\circ}, 90^{\circ}$. To avoid accidental errors, each group had three replications, as shown in Figure 2-30.

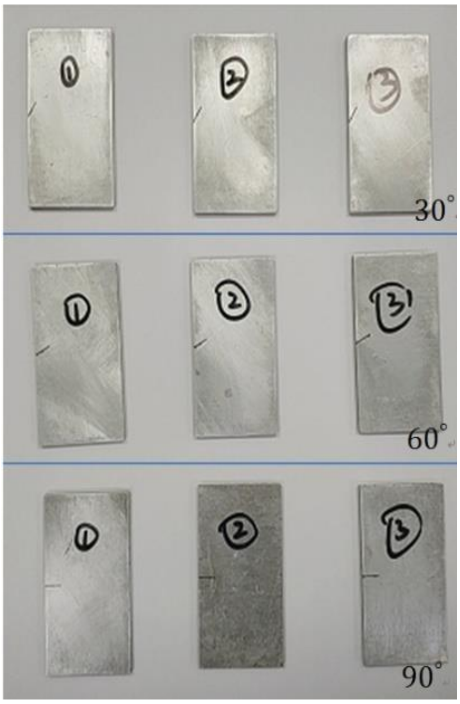

Figure 2-30 Single side inclined crack specimen

The test pieces were prepared in accordance with the American Society for Testing Materials, ASTM E8/E8M-15a Standard Test Methods for Tension Testing of Metallic Materials. Figure 2-31 was the Universal Hydraulic Testing Machine (type LD26.105) with the capability of 100 kN in axial load, which was used to accomplish the test at room temperature. The samples with oblique crack were of the exerted displacement boundary condition on the top end at a speed of $0.2\,mm/s$ and fixed on the bottom end until the crack started propagation.

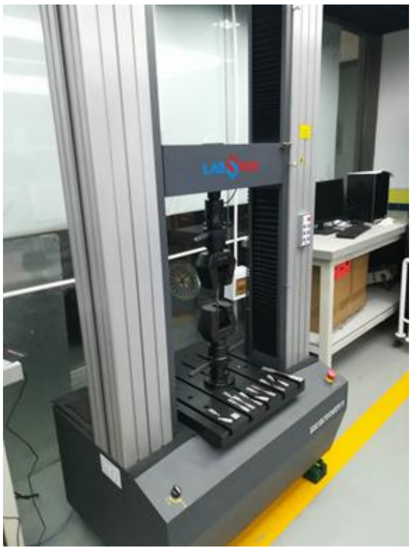

Figure 2-31 Universal Testing Machine

As the specimen contains a crack, stress concentration will occur at the crack tip with the increase of tension at both ends of the clamping specimen. The crack propagation will start from the crack tip until fracture. Figure 2-32 showed the propagation of single side oblique crack for 90° under the uniaxial tensile force. Equivalent loading was adopted slowly for each group of specimens with the same loading mode.

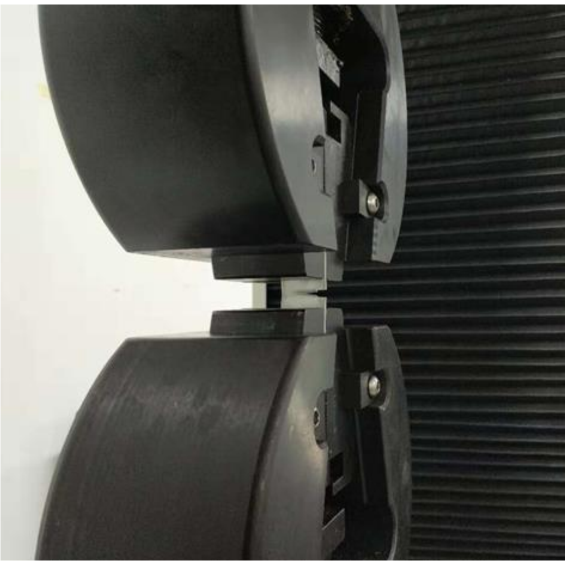

Figure 2-32 Uniaxial tensile test of single side oblique crack for 90°

2.4.3 Experimental result

As shown in Figure 2-33(a), it was revealed that when the inclination angle was 90° (Mode I crack), the crack extended in a self-similar manner that propagated along the direction of the initial crack, while the phenomenon was unsuitable for 30° and 60° (mixed I-II crack) extension situations. Crack propagation under these two angles deviated from the initial direction, which illustrated that the assumption for the mixed-mode crack extension path along its initial plane was wrong.

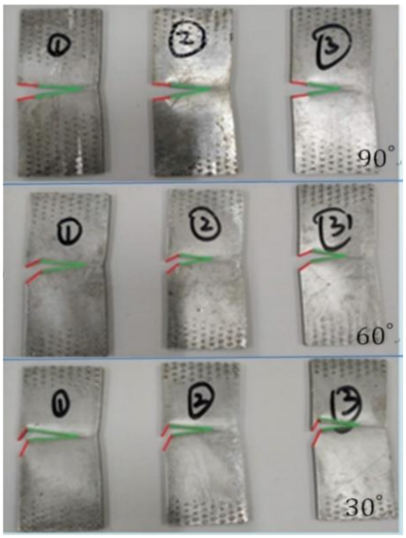

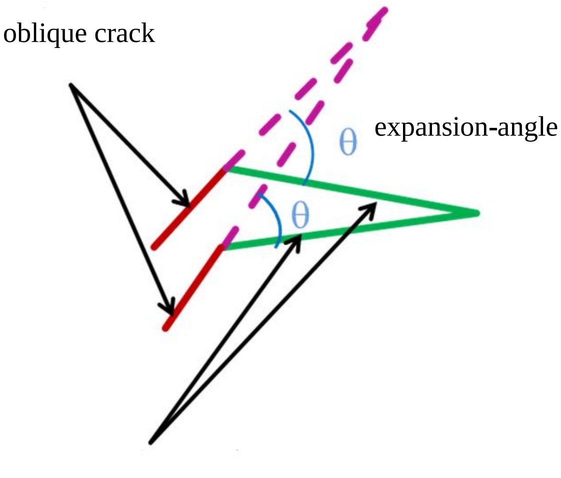

(**a**) Samples with extension crack (**b**) Schematic diagram of crack extension

Figure 2-33 Crack propagation path of experimental results

From the experimental results, the actual extension angles were measured through kink crack as shown in Figure 2-33(b). The stress intensity factors for cracked specimens were obtained through the analytical expression (2-38) of the stress field at the oblique crack tip based on the output force curve of the test machine. Then the energy release rate $G(\theta)$ can be calculated by the formula (2-35) from the present result. And the extension angles were deduced by the MG-criterion, and the results were shown in Table 2-4:

Table 2-4 Calculated extension angle and experimental extension angle

Crack Angle (deg)	Sample Number	Calculated Extension Angle (deg)	Experimental Extension Angle (deg)	Experimental Extension Angle (Average) (deg)	Error (%)
	1	−60	−59		
30	2	−60	−59.5	−58.7	2.17
	3	−60	−57.6		
	1	−43	−41.5		
60	2	−43	−40.8	−41.2	4.26
	3	−43	−41.2		
	1	0	0		
90	2	0	0	0	0
	3	0	0		

Relatively similar results between the calculated extension angle and an experimental extension angle were observed. As the specimens were not manufactured by ideal elastic material, the error value (lower than 5%) was reasonable.

2.5 Chapter summary

The energy release rate associated with stress intensity factors under mixed-mode loading for aluminum alloy material had been investigated using both numerical method and theoretical derivation. The present results demonstrate the simpler, accurate calculation process and accurate evaluation of the energy release rate with infinitesimal crack kink, which can be used to study the propagation of branch kink, and then conduct fracture prediction and analysis in practical engineering applications. The following conclusions can be drawn：

(1) A relatively simple and precise numerical method was established to evaluate the energy release rate associated with the stress intensity factors under mixed-mode loading, based on the concept that the energy release rate is equal to the change rate of the energy difference before and after crack kink.

(2) Based on the numerical method, a series of spatial inclined ellipses in Mode I-II and ellipsoids in Mode I-II-III with different propagation angles computed from

the non-dimensional value ($K/\sqrt{EG}$) were fitted by MATLAB, and the expression of the energy release rate with the crack propagation angle was obtained.

(3) A theoretical expression of energy release rate at any propagation angle for a crack tip under I-II-III mixed-mode crack was deduced based on the propagation mechanism of the crack tip under the influence of a stress field. It was confirmed that the theoretical expression deduced could provide results as accurately as the present numerical method.

(4) The present results were consistent with the experimental data. The error, which is lower than 5%, can be accepted considering that the specimens were not manufactured by an ideal elastic material. Consequently, the proposed method can achieve an accurate evaluation of energy release rate, with concise calculation.

Chapter 3 Prediction of the shape change of a fatigue surface crack in a round bar

3.1 Assessment of components with surface cracks

The crack will cause fracture under low stress, which occurs and develop under fatigue loads in engineering structures. In addition to the cracks formed by the defects of the material, most of the cracks formed originated from the surface with a high-stress level under fatigue loading.

For the failure assessment of cracked components of metallic materials, the geometry of surface crack, both real defects found during nondestructive evaluation and hypothetical cracks are modeled as planar, having semi-elliptic contours and being loaded normal to the plane.

For a better estimation, the shape of the semielliptical crack may be determined according to Figure 3-1. The length $2C$ is the mean value of the maximum crack extension in the length direction and crack extension at the surface of the body. The crack depth a is the maximum depth of the smoothened contour of the real crack. The shape of real cracks usually deviates little from a semi-ellipse as long as plastic deformations in the crack vicinity are small.

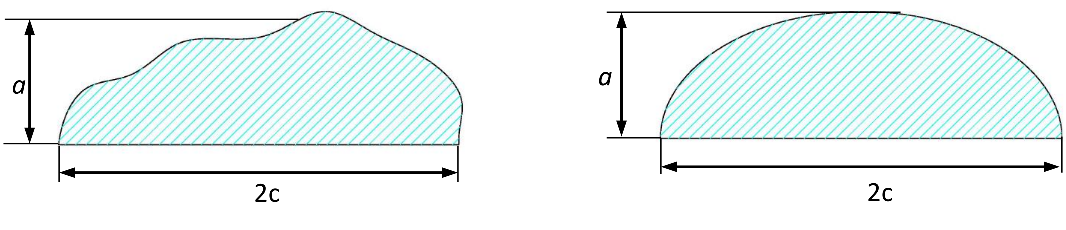

Figure 3-1 Idealization for surface crack shape

Except general cases, there are hole wall surface crack, corner crack and hole wall corner crack, as shown in Figure 3-2.

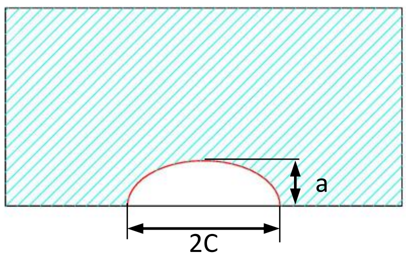

(a) Semi-elliptical surface crack

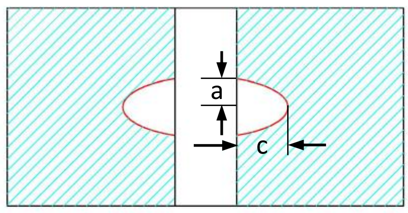

(b) Semi-elliptical crack from a hole

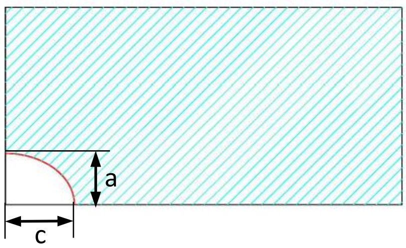

(c) Corner crack

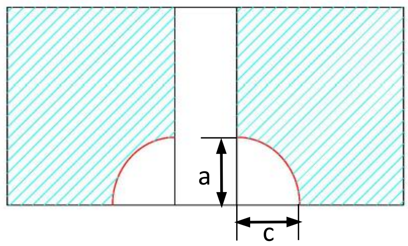

(d) Corner crack emanating from a hole

Figure 3-2 Three dimensional crack

For analytical evaluation of surface crack, although the stress intensity factor varies along the crack front, those at the deepest point and the intersection with the free surface are used as representative values for estimating crack growth in the depth and length directions. Meanwhile, the power-law relations are used widely between the defective stress intensity factor range and the crack growth per cycle.

3.2 Numerical propagation process

3.2.1 Model of simulation

3.2.1.1 Three-Parameter Model

A surface crack in a smooth round bar with a diameter D_0 and height $L(L \gg D_0)$ subjected to fatigue tension are taken into consideration. The geometry of the round bar is shown in Figure 3-3. A part-elliptical surface flaw which is in the median cross-section of the bar is defined by three parameters: (1) major axis of an ellipse a, (2) minor axis of an ellipse b, and (3) center of the ellipse O_y. (Figure 3-4). When the aspect ratio of the ellipse $b/a = 1$, the crack is a so-called part-circular crack. When $b/a \to 0$, the crack is regarded as a straight crack. And any other intermediate crack geometry between the two above limiting cases can be defined by the aspect ratio of the ellipse b/a.

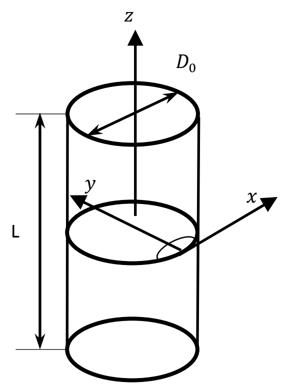

Figure 3-3 A round bar

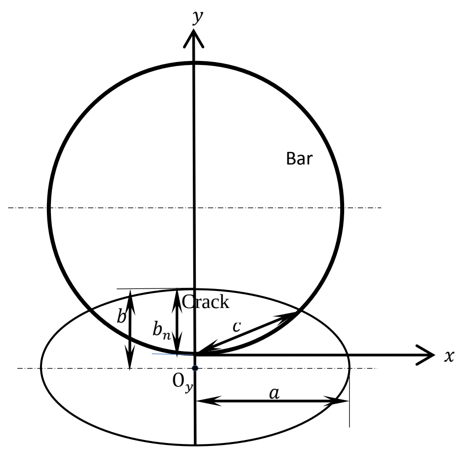

Figure 3-4 A surface crack

3.2.1.2 Numerical simulation

The typical model of a round bar with a diameter D_0 and length L that contains a surface crack in its median cross-section has been used in many experimental tests and numerical simulations. Yang, F.P. [62] presented the experimental results of fatigue crack growth for a straight-fronted edge crack in an elastic bar under axial loading with a diameter of $12\,mm$, a length of $90\,mm$, and carbon steel S45 as the material. Table 3-1 is material parameters for steel S45. Carpinteri, A. [52, 55] calculated the surface cracks in round bars with $50\,mm$ diameters through finite-element analysis. Since the propagation of crack shape is defined by the crack configuration for a given loading type [58], in the present paper, the models are established for different values of these initial parameters to compare the fatigue crack propagation with the experimental and simulation results from Yang, F.P. [62] and Carpinteri, A. [52,55].

Table 3-1 Material parameters for steel S45

Monotonic Tensile Yield Strength $\sigma_0(MPa)$	Nominal Ultimate Tensile Strength $\sigma_{\mathrm{m}}(MPa)$	True Ultimate Tensile Strength $\sigma_f(MPa)$	Young's Modulus $E(MPa)$	Poisson's Ratio v	Crack Growth Parameter m
635.07	775.65	2101.65	$2.06e^5$	0.33	3

Since the bar geometry and applied loads present two planes of symmetry, 3D finite element analysis is performed by modeling a quarter of the round bar. The load is applied at the rear ends in the form of uniform tensile stress, and the cross-section of the surface crack is restrained with symmetry, as shown in Figures 3-5.

The finite element analysis software ABAQUS TM (France) is used to simulate the scenario. About 350,000–380,000 quadratic hexahedral elements have been employed in each model. The 1/4-node displacement method and fine meshing with a $0.02\,mm$ mesh size has been used around the crack front to model the stress field singularity and improve the accuracy of the contour integral calculation, as shown in Figure 3-6.

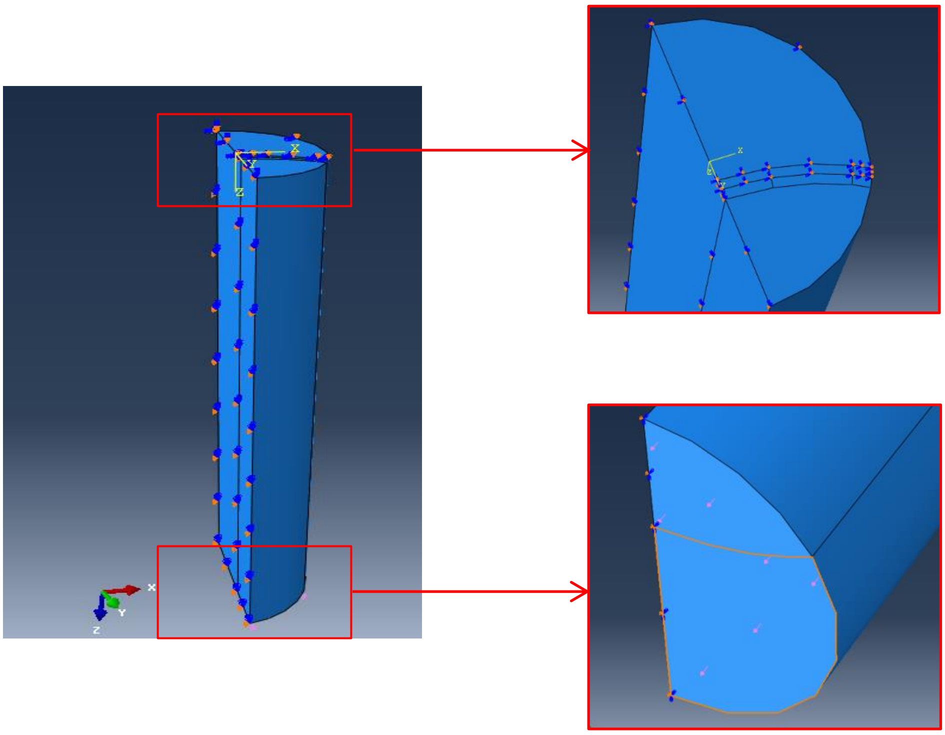

Figure 3-5 3D model with load constraint

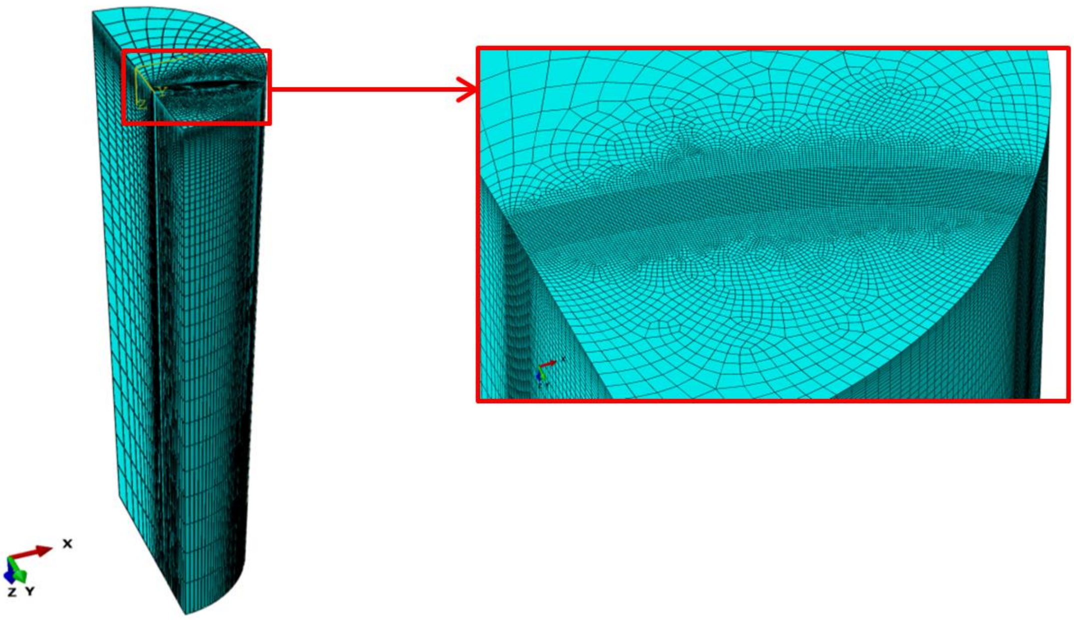

Figure 3-6 The finite element models of a surface-cracked round bar

3.2.2 Fatigue Crack Propagation

3.2.2.1 Stress intensity factors for surface crack

The manner of fatigue crack growth is affected by multiple factors, such as load ratio, frequency and amplitude, plastic zone, microstructure, mean stress, stress concentration factors, and so on. Based on the previous study, it is indicated that the range of stress intensity factor ΔK is the major factor for fatigue crack growth, based on previous fatigue crack growth experiments.

The finite element method is employed to estimate the stress intensity factors along the crack front. As the output stability of J-integral for simulation, the stress intensity factor K_I in mode I is estimated at each node lying on the crack front based on the following equation in elastic analysis condition.

$$J = G_I = \frac{1 - v^2}{E} {K_I}^2 \tag{3-1}$$

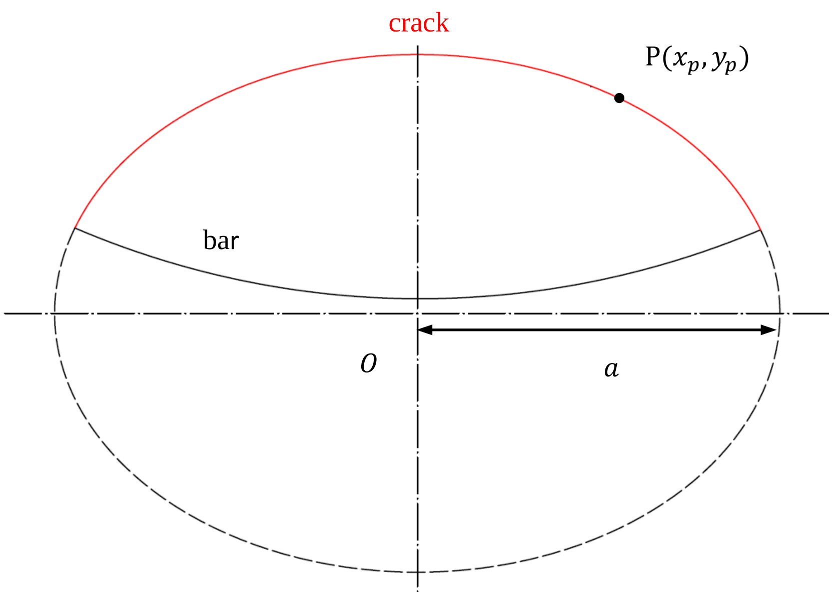

Figure 3-7 Crack fronts for database

Figure 3-7 shows the surface crack front along which the point P is between the two intersections with the bar. The stress intensity factor K is varying along the crack front for an arbitrary loading condition and initial shape of the crack (Figure 3-8), it is symmetrical with the axis of the deepest point on the crack front. The values of the stress intensity factor K for two intersections are bigger than the middle ones.

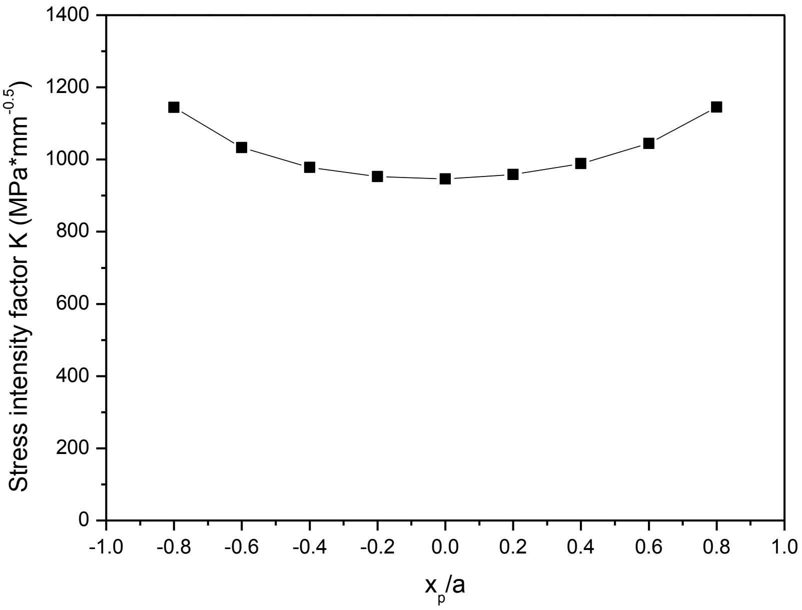

Figure 3-8 Stress intensity factor varying along the crack front of a given initial crack

3.2.2.2 Fatigue crack growth law

For fatigue growth rate, three regions can usually be observed in the experiment. Crack growth is dependent on material microstructure in the first region, the threshold ΔK_{th} is the main parameter for crack growth. The second region is called power-law growth, which is usually referred to as Paris law (Equation 3-2) of fatigue crack growth. Both the coefficient C and exponent m account for the material and environmental effects affect the crack growth rate da/dN, which is proposed in ASTM E647-88[78]. The third region represents rapid crack growth, and fracture occurs when $K_{max} \geq K_{Ic}$, K_{Ic} is the fracture toughness.

$$\frac{da}{dN} = C(\Delta K)^m \tag{3-2}$$

To apply the stress intensity factor calculation to the fatigue crack propagation, σ and K_I are replaced by $\Delta\sigma$ and ΔK_I, and the defect is assumed to grow according to Paris- Erdogan law of the second region.

3.2.3 Prediction of shape for fatigue Crack

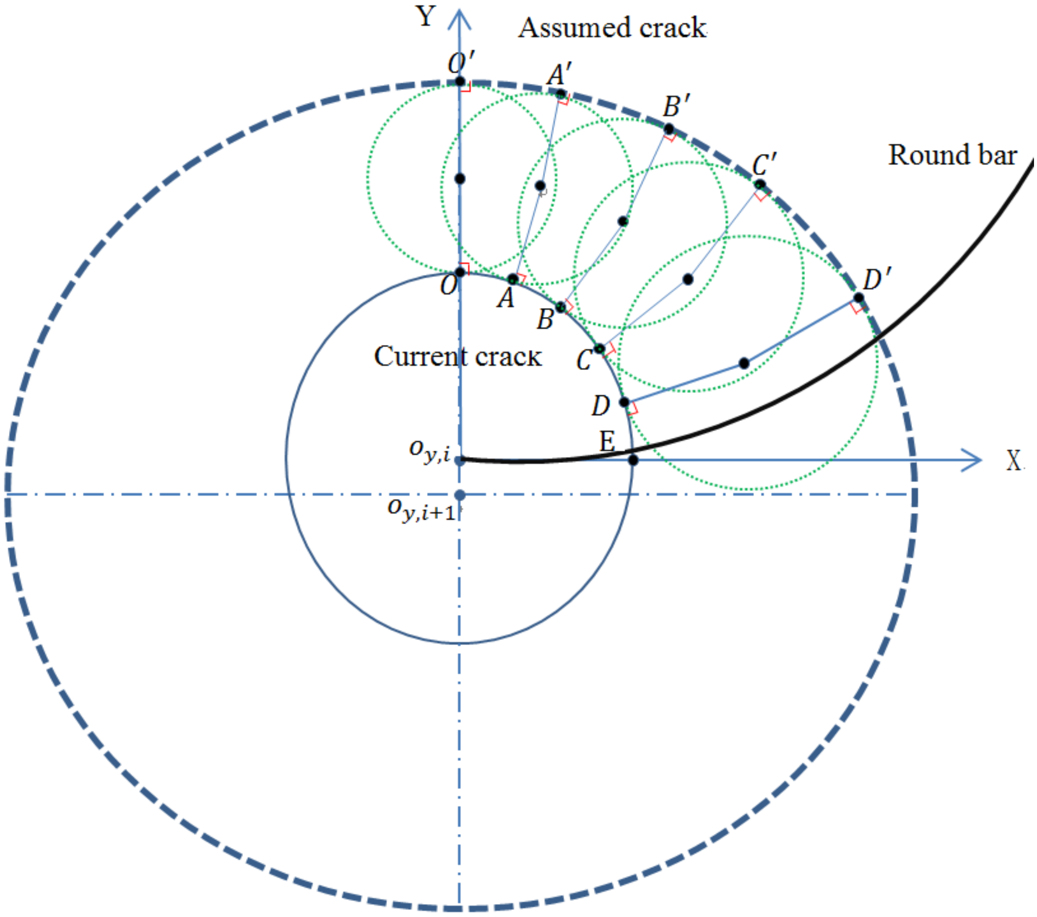

Figure 3-9 Determination of a new crack front by fatigue crack growth circles

The propagation of a surface crack in a round bar under cyclic tension is predicted by employing fatigue crack growth circles [79] (Figure 3-9). If the crack front presents an ellipse shape up to the ith loading step, the initial ellipse whose center is located on the surface of the specimen can be defined with given a_i and b_i, as represented by the following equation.

$$\frac{x^2}{{a_i}^2} + \frac{y^2}{{b_i}^2} = 1 \tag{3-3}$$

Points O, A, B, C, and D in Figure 3-9 with coordinates (x_{ji}, y_{ji}) are deployed equidistantly along the current crack front, where the subscript J refers to the points O, A, B, C, and D.

The growth of a new crack front lying on an ellipse with semi-axes a_{i+1}, b_{i+1}, and center O_{i+1} after one cyclic loading step to a new configuration can be described by the following equation

$$\frac{x^2}{(a_{i+1})^2} + \frac{(y - O_{y,i+1})^2}{(b_{i+1})^2} = 1 \tag{3-4}$$

The assumed crack growth circles, which pass points O, A, B, C, and D, respectively, are tangent to both current and new crack fronts. The new crack front points $O^{'}, A^{'}, B^{'}, C^{'}$ and $D^{'}$ with coordinates $(x_{j,(i+1)}, y_{j,(i+1)})$ are the points of tangency between crack growth circles and the new crack front. Meanwhile, the centers of crack growth circles can be determined as $(x_{j,c},\ y_{j,c})$.

The crack growth increment for these points can be determined by applying the Paris-Erdogan law (Equation 3-2).

After each computed crack configuration, an increment of crack growth at the interior point $O^{'}$ is given. The crack growth length of other points A', B', C', and D' can be determined as following:

$$\Delta l_j = \left(y_{O,i+1} - y_{O,i}\right)\frac{\left(\Delta K_{ej}\right)^m}{(\Delta K_{eO})^m} \tag{3-5}$$

Here, ΔK_e stands for the equivalent stress intensity factor related to the stress intensity factors of both current and new crack fronts.

The stress intensity factor ΔK is assumed to be a linear function of crack growth increment. An arbitrary number of crack growth steps can be assumed. Using

$$da = C(\Delta K)^m dN, \tag{3-6}$$

the crack growth length is increased to $a + da$ repeatedly in each step to the last step by adjusting material constant C. The equivalent stress intensity factor ΔK_e with stepping coefficient μ can be obtained appropriately through the crack growth plot of da/dN vs. N.

$$\Delta K_{ej} = \mu\left(K_{ij}\right)^m + (\frac{1}{2}(K_{i,j} + K_{(i+1),j}))^m + (1-\mu)\left(K_{(i+1),j}\right)^m \quad 0 < \mu < 1 \tag{3-7}$$

At the beginning of iteration, sometimes a relatively large value of μ can be used to avoid diverging.

The distance from the center of crack growth circles to points $O^{'}, A^{'}, B^{'}, C^{'}$ and

D' along the new crack front are calculated using the geometrical relationship

$$\Delta d_j = \sqrt{(x_{j,(i+1)} - x_{j,c})^2 + (y_{j,(i+1)} - x_{j,c})^2} \tag{3-8}$$

An error equation can be derived as

$$Error = \sum \left|\Delta d_j - \Delta l_j/2\right| \tag{3-9}$$

The values of a_{i+1} and O_{i+1} minimize the error equation through iterative methods and repeat all of the above steps based on the obtained crack front. The parameters of the ellipse for each new crack front can be determined until the results converge.

3.3 Results and Discussion

3.3.1. Evolution of the Crack Shape

3.3.1.1 Crack growth circles

Figure 3-10 illustrates the fatigue shape evolution by the crack growth circles in a round bar subjected to tension for the initial condition $b_0/a_0 = 1, b_0/D_0 = 0.1\,, m = 2$ and $m = 4$.

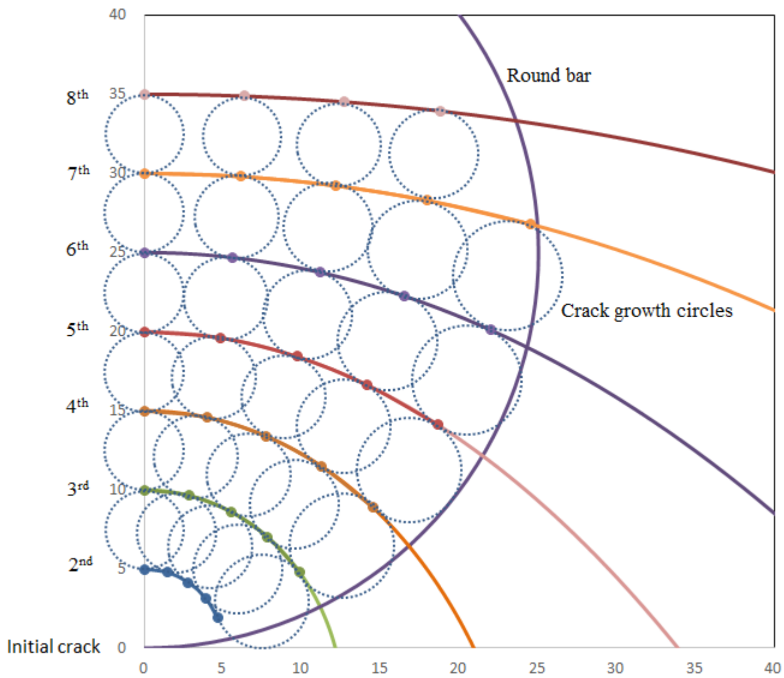

(a) $b_0/a_0 = 1, b_0/D_0 = 0.1\,, m = 2$

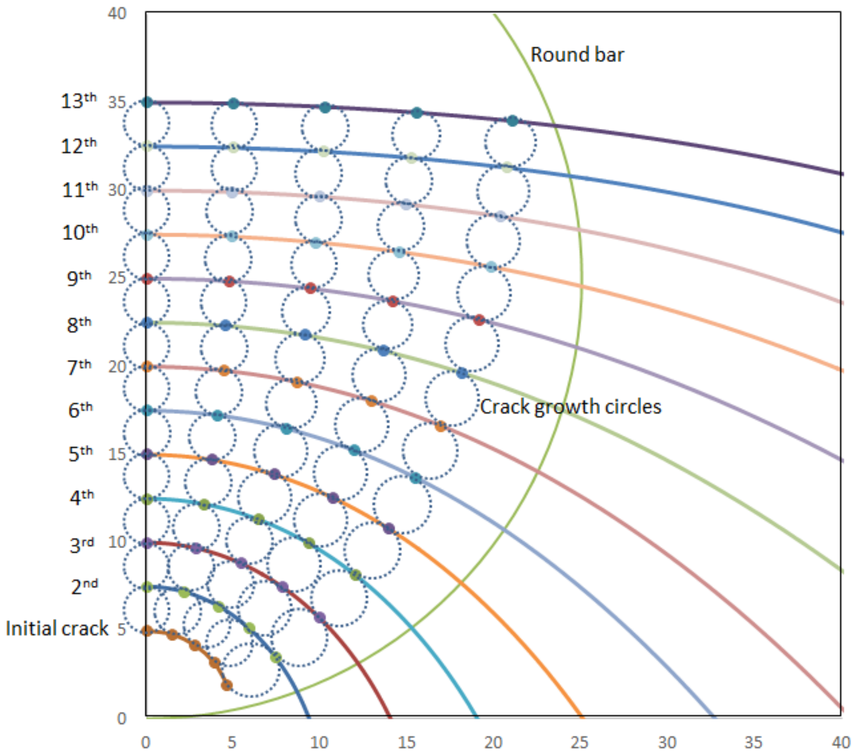

(a) $b_0/a_0 = 1, b_0/D_0 = 0.1\,, m = 4$

Figure 3-10 Successive determination of crack fronts by the crack growth circles with initial crack $b_0/a_0 = 1, b_0/D_0 = 0.1$

For $b_0/a_0 = 1, b_0/D_0 = 0.1\,, m = 2,$ seven crack front profiles displayed are deduced from roughly 29 crack growth circles in less than 20 iterations. The outermost crack growth circle rolls along the internal profile of the round bar approximately. When the point of tangency between crack growth circle with crack front approaches very closely to the surface of the bar, such as crack front 6 in Figure 3-10 (a), the outermost crack growth circle will disappear in the next propagation. For $b_0/a_0 = 1, b_0/D_0 = 0.1\,, m = 4,$ eleven crack front profiles displayed with a smaller step size of increment. Although more crack growth circles and iterations are needed, the outermost crack growth circles are far from the internal profile of the round bar, the number of crack growth circles is consistent always, as shown in Figure 3-10(b).

Figure 3-11 illustrates the fatigue shape evolution by the crack growth circles in a round bar subjected to tension for the initial condition $b_0/a_0 = 0,\ b_0/D_0 = 0.08\,,$

$m = 2\ and\ m = 3.$

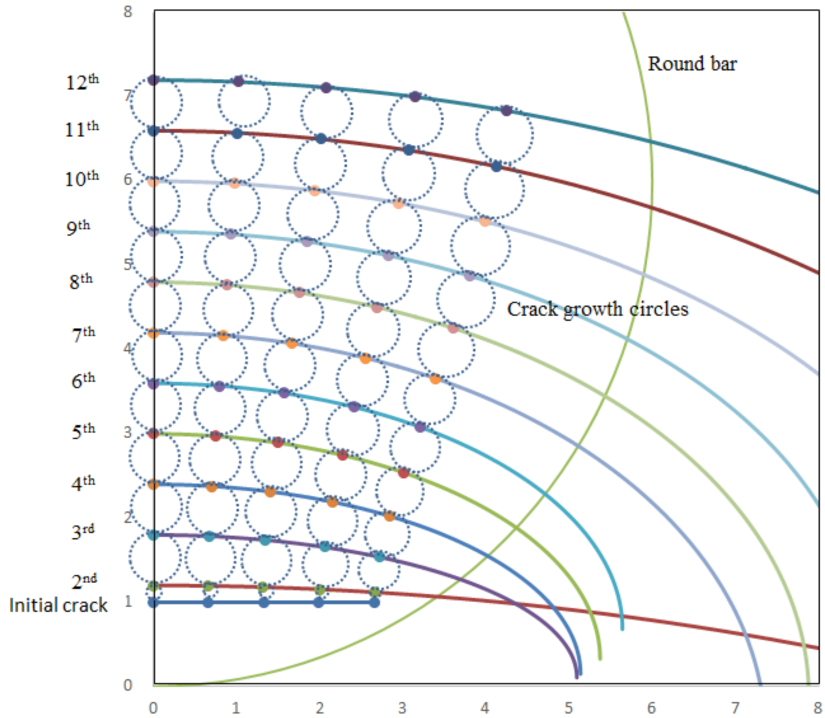

(a) $b_0/a_0 = 0, b_0/D_0 = 0.08, m = 2$

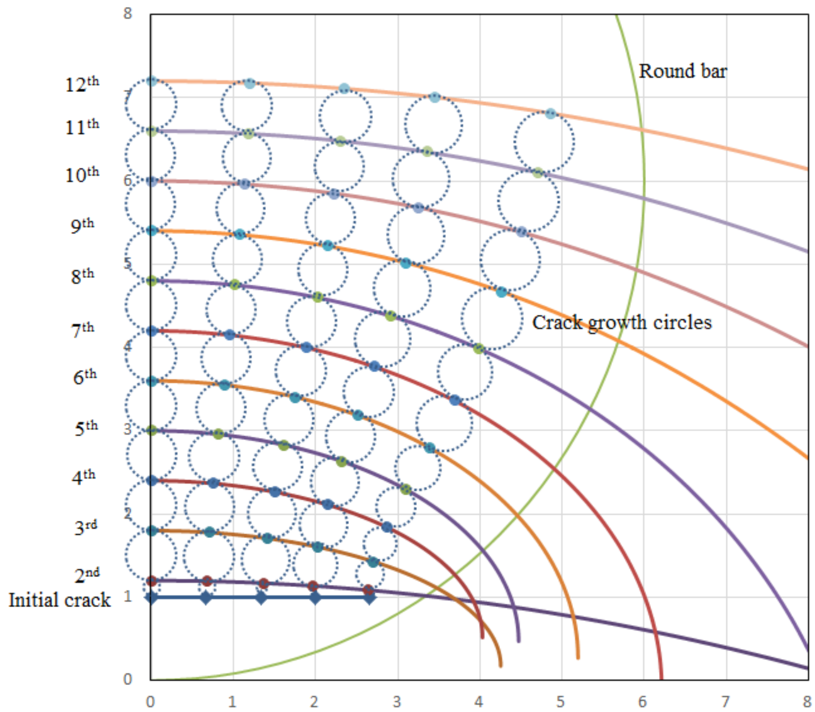

(b) $b_0/a_0 = 0, b_0/D_0 = 0.08, m = 3$

Figure 3-11 Successive determination of crack fronts by the crack growth circles with initial crack $b_0/a_0 = 0, b_0/D_0 = 0.08$

For $b_0/a_0 = 0, b_0/D_0 = 0.08, m = 2, m = 3$, there are twelve crack front profiles displayed by roughly 55 crack growth circles in less than 36 iterations. The outermost crack growth circles are far from the internal profile of the round bar as the small step of increment of crack propagation in the vertical direction, and the curvature of ellipses present smaller for the first several steps. As the initial crack is straight, the increment should be smaller based on multiple tests, or else it is difficult to converge for iteration.

Figure 3-12 illustrates the fatigue shape evolution by the crack growth circles in a round bar subjected to tension for the initial condition $b_0/a_0 = 1$, $b_0/D_0 = 0.05$, $m = 2$. Twelve crack front profiles displayed are deduced from roughly 52 crack growth circles in less than 36 iterations. The outermost crack growth circle rolls also tend to approach the internal profile of the round bar, and the outermost crack growth circle disappeared from the crack front 9.

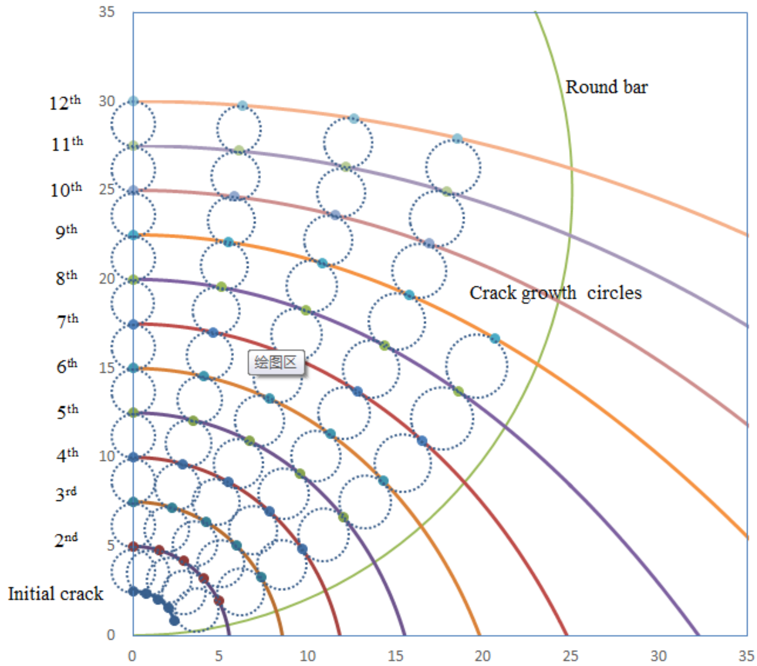

Figure 3-12 Successive determination of crack fronts by the crack growth circles with initial crack $b_0/a_0 = 1, b_0/D_0 = 0.05, m = 2$

3.3.1.2 Ellipses of crack fronts

The rate of crack propagation can be observed intuitionally by the size of crack growth circles. As shown in Figure 3-13, the optimum simulation result for the center of an ellipse is not fixed on the surface of the bar but is reciprocating along the *y*-axis. Therefore, the actual crack shape can be expressed accurately by the three-parameter model. The center locations of ellipses are around the outermost surface of the round bar mostly with the initial crack $b_0/a_0 = 0, b_0/D_0 = 0.08$. The crack fronts tend to be flat as the straight curve of the initial crack.

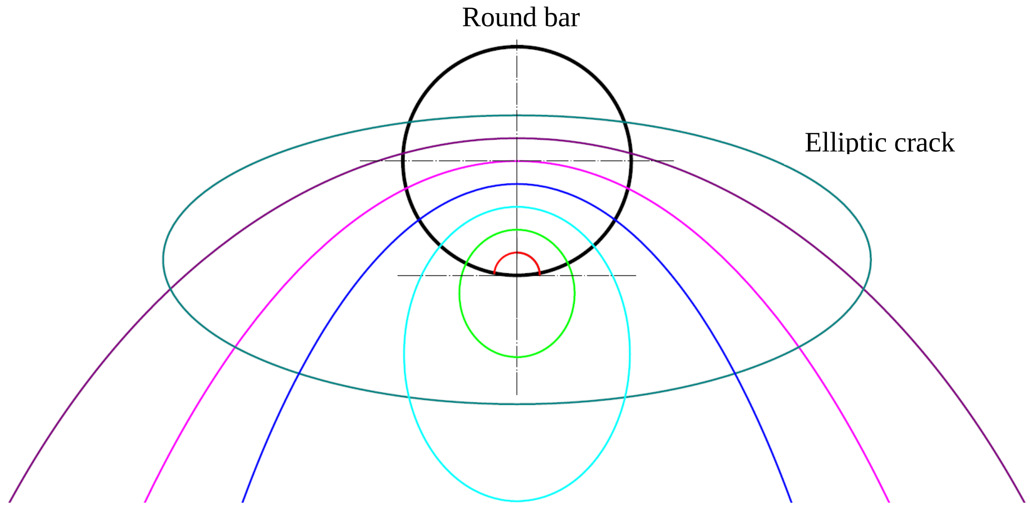

(a) $b_0/a_0 = 1, b_0/D_0 = 0.1\,, m = 2$

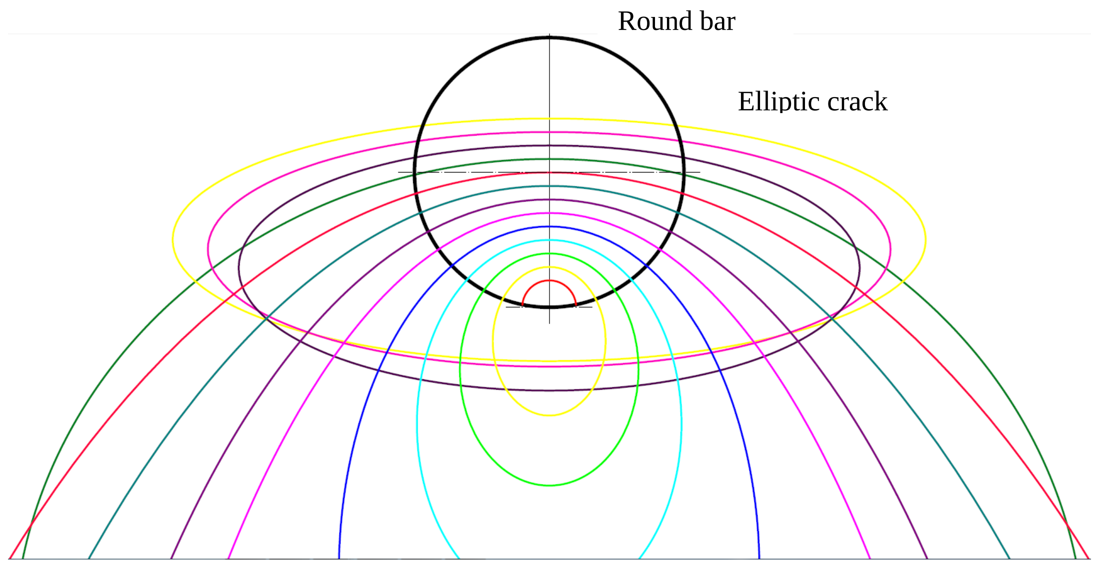

(b) $b_0/a_0 = 1, b_0/D_0 = 0.1\,, m = 4$

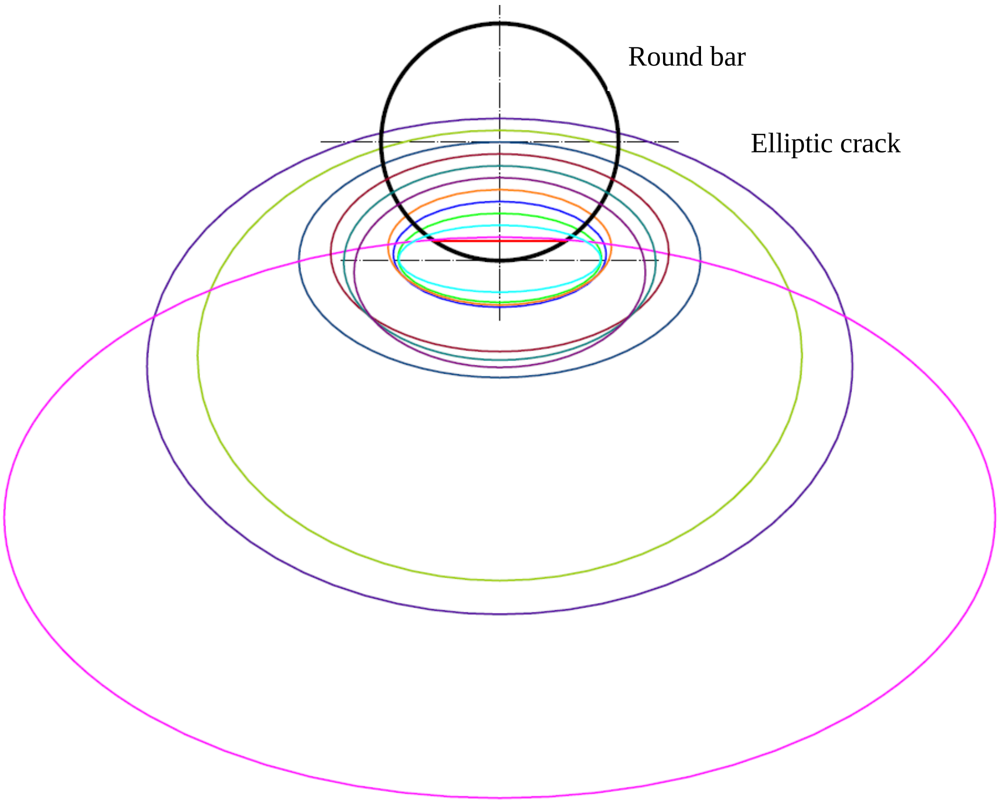

(c) $b_0/a_0 = 0, b_0/D_0 = 0.08 , m = 2$

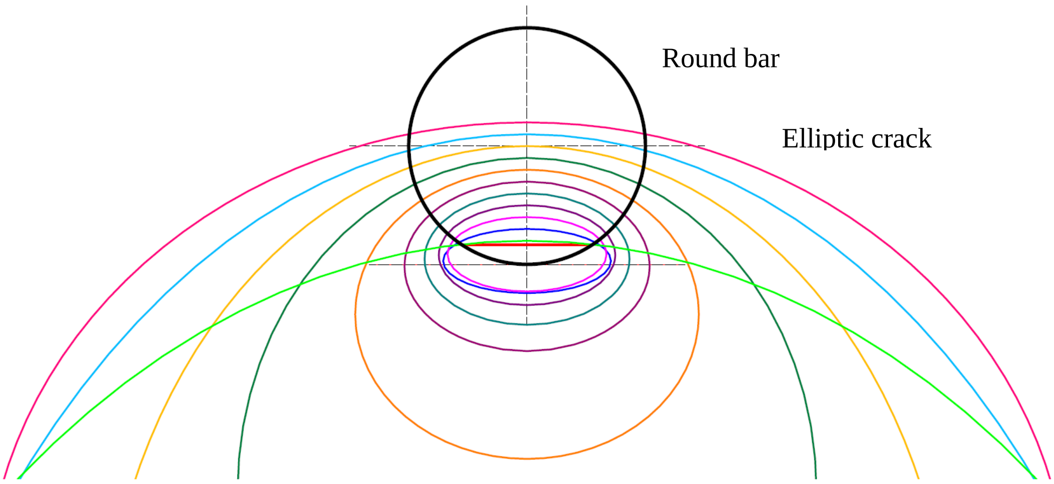

(d) $b_0/a_0 = 0, b_0/D_0 = 0.08 , m = 3$

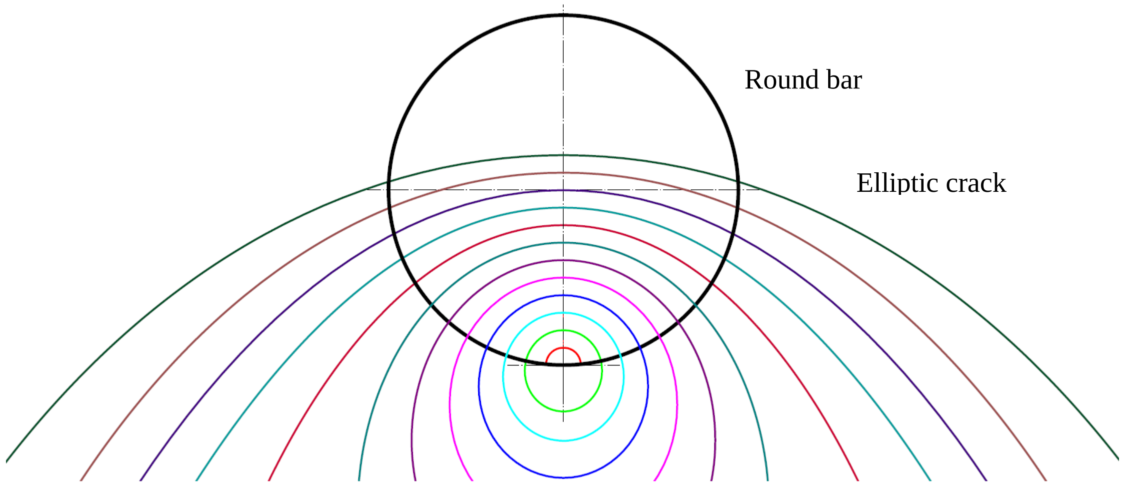

(e) $b_0/a_0 = 1, b_0/D_0 = 0.05\,, m = 2$

Figure 3-13 Ellipses used to determine crack fronts

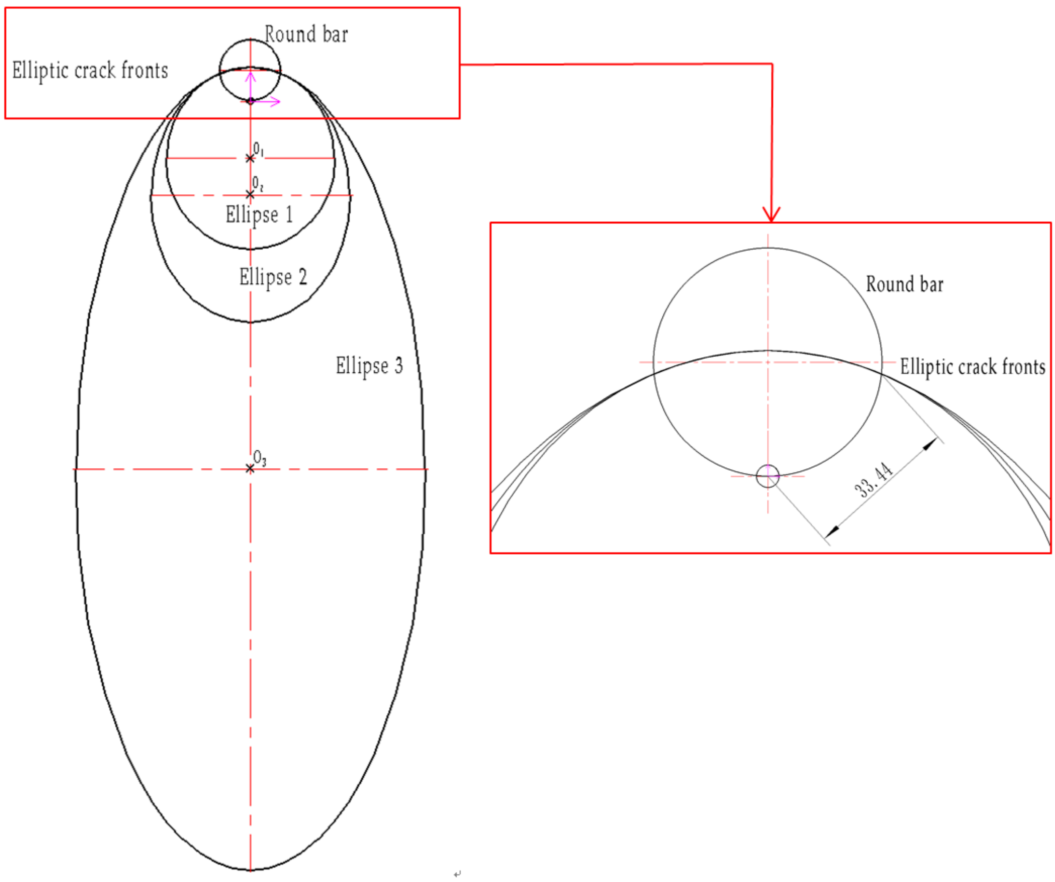

Figure 3-14 Crack front as a part of an ellipse

In the simulation process, once the center is not fixed, several different ellipses with the same chord length can be replaced to describe one actual crack front, since only part of an ellipse is used (Figure 3-14). A large variation of ellipse actual aspect ratio is obtained with undifferentiated iteration error, as shown in Figure 3-15. Hence, the actual aspect ratio of the ellipse semi-axis is meaningless for the three-parameter model to describe the crack front.

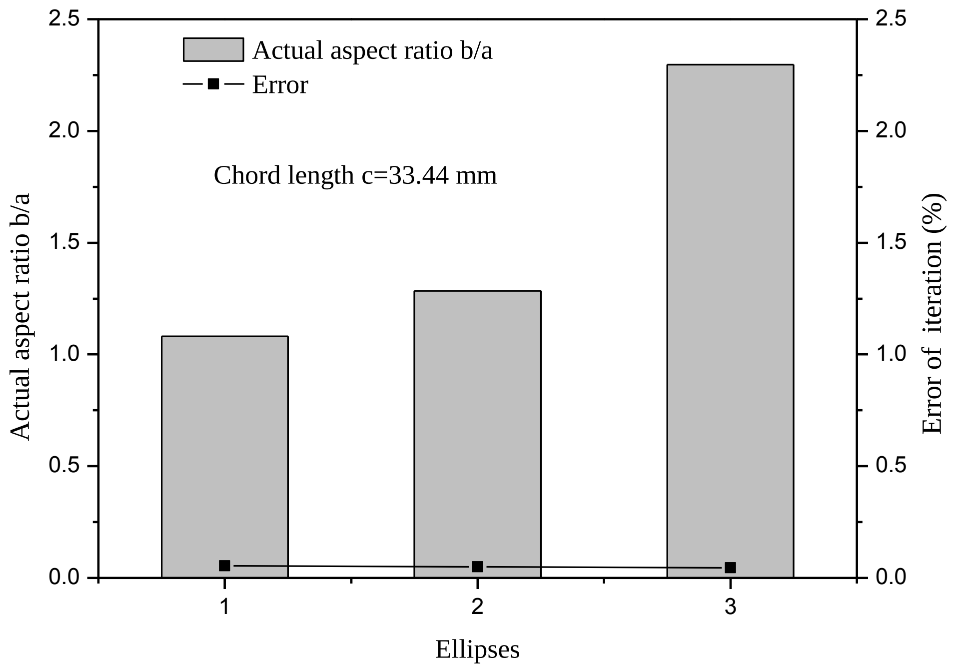

Figure 3-15 Change of actual aspect ratio with the same chord length c

Figure 3-16 illustrates the fatigue shape evolution for five cases. The aspect ratio of the initial ellipse $b_0/a_0 = 0, 1,$ and the relative crack depth $b_n/D_0 = 0.05, 0.08,$ and 0.1, while the material constants in the Paris-Erdogan law are assumed to be m = 2, 3, and 4. The trends of crack propagation are adequately demonstrated.

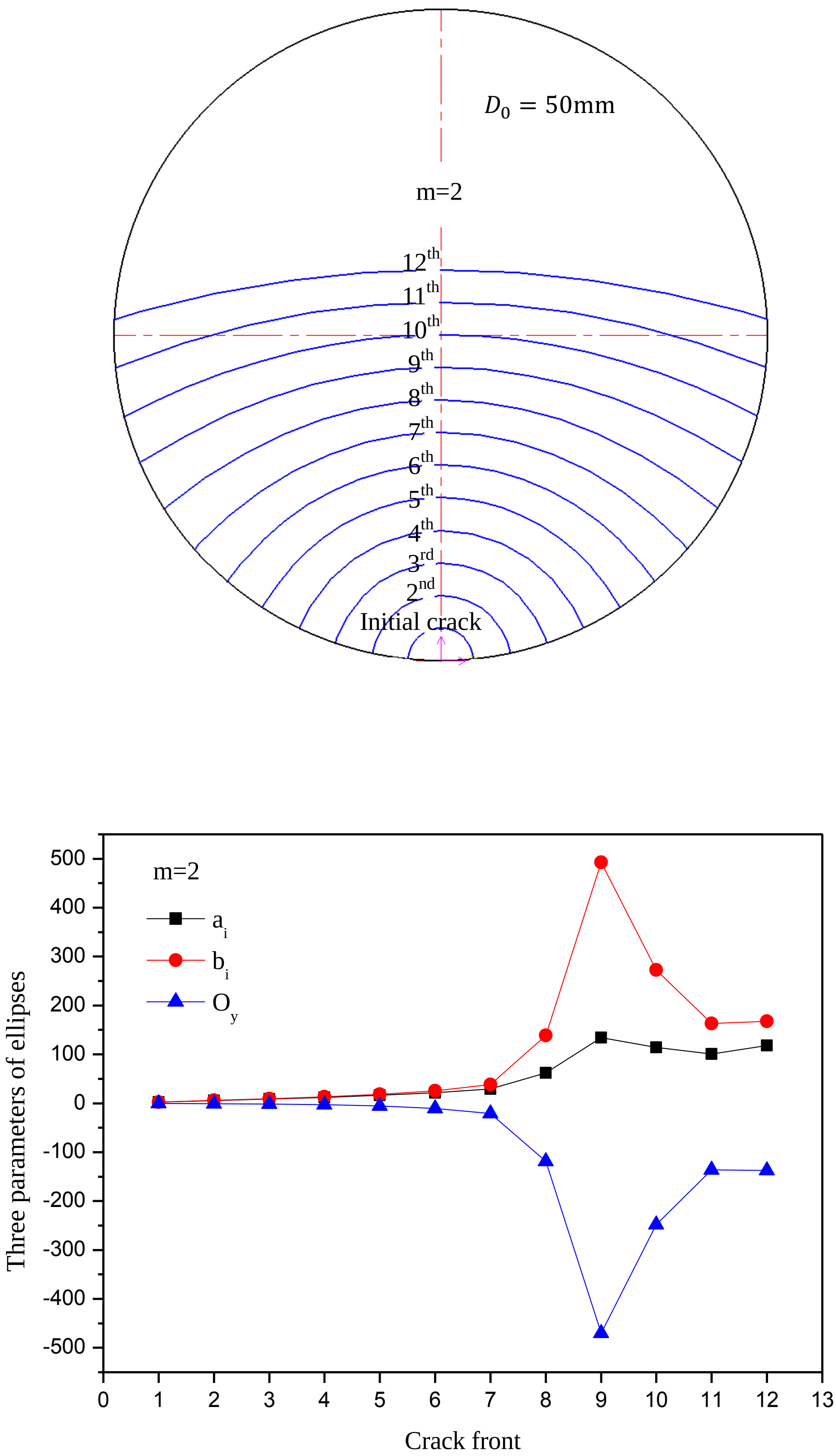

(a) $b_0/a_0 = 1, b_0/D_0 = 0.05$

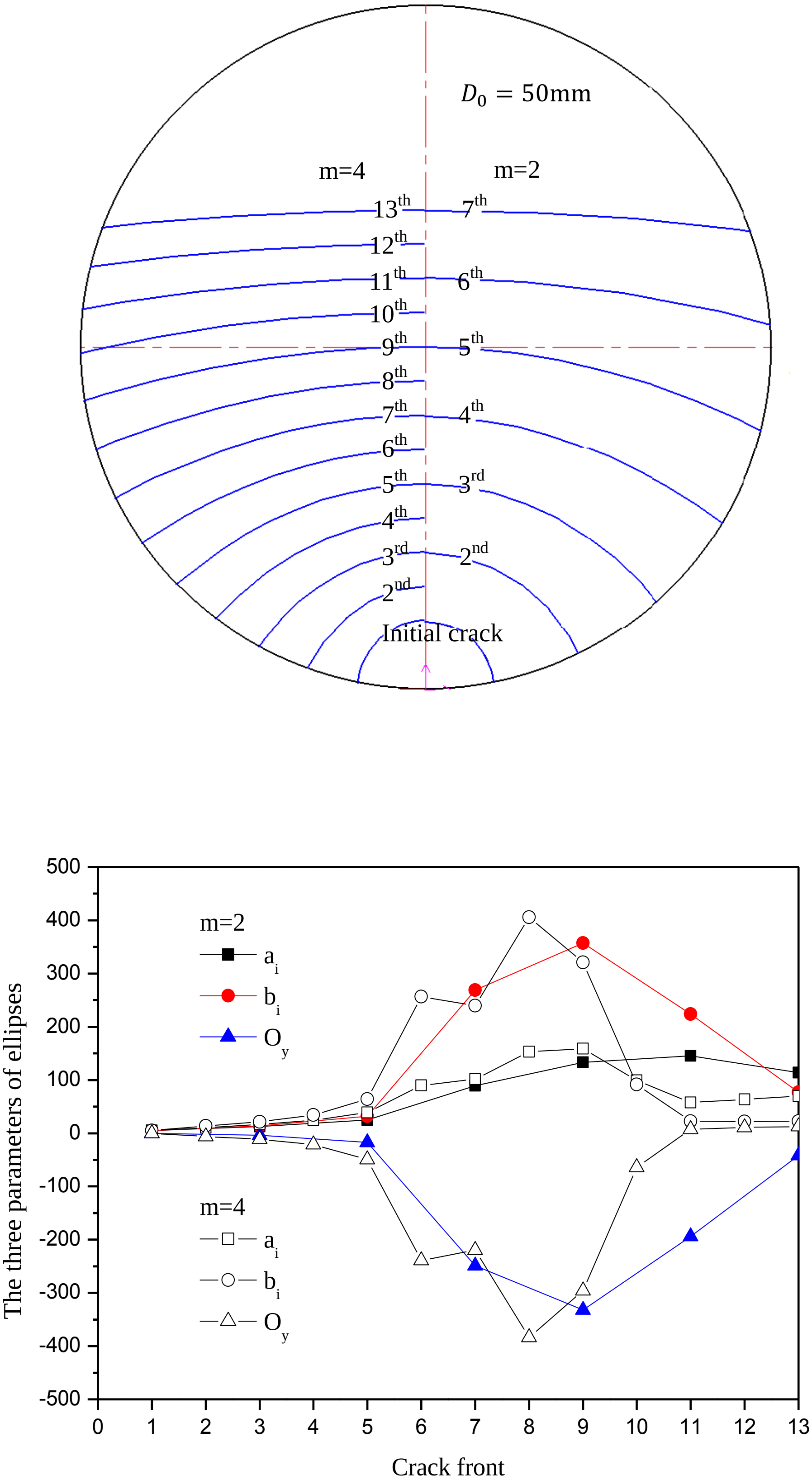

(b) $b_0/a_0 = 1,\ b_0/D_0 = 0.1$

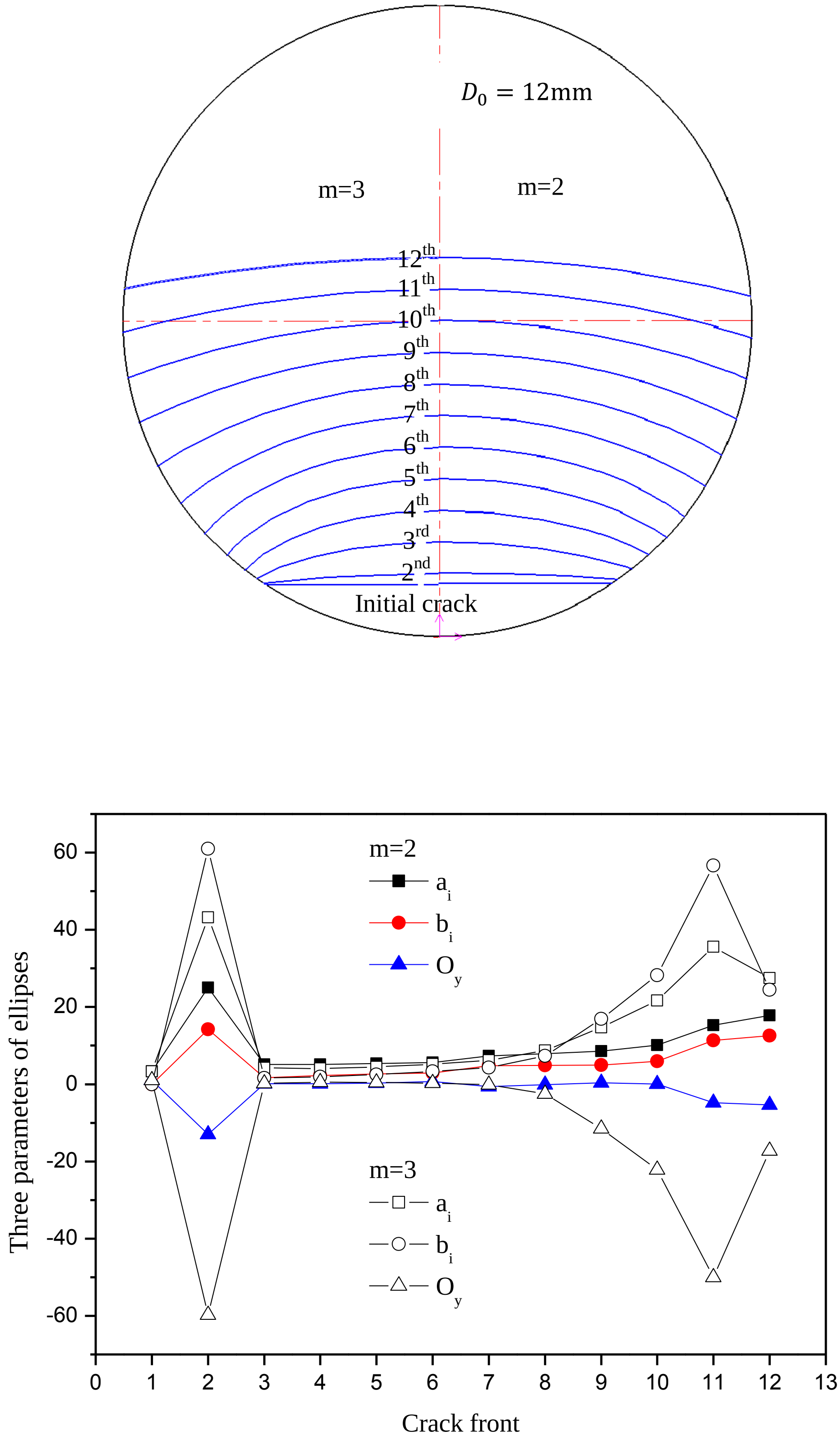

(c) $b_0/a_0 = 0, b_0/D_0 = 0.08$

Figure 3-16 Shape change of different initial crack for different fatigue crack growths exponent m values.

3.3.1.3 Analysis of propagation

As mentioned previously, the nominal aspect ratio of an ellipse, which is the ratio of the maximum crack depth to the chord length c, b_n/c can be considered here. It is noteworthy that, as shown in Figure 3-17, both initial crack dimensions and Paris law exponent m affect the evolution of different parameters. The trends of crack propagation are consistent with the same initial crack aspect ratio, although the beginning propagation is affected by the crack depth provisionally. Meanwhile, a difference of transition can be noticed between the crack propagation with different Paris law exponent m values. In Figure 3-17, it can be found that the nominal aspect ratio change is very sensitive to the initial crack geometry during early growth, and the nominal aspect ratios for all cases are converged and become constant around $b_n/D_0 \approx 0.4$. It is shown that the flaws tend to follow preferential propagation paths that flatten gradually when the crack depth becomes larger.

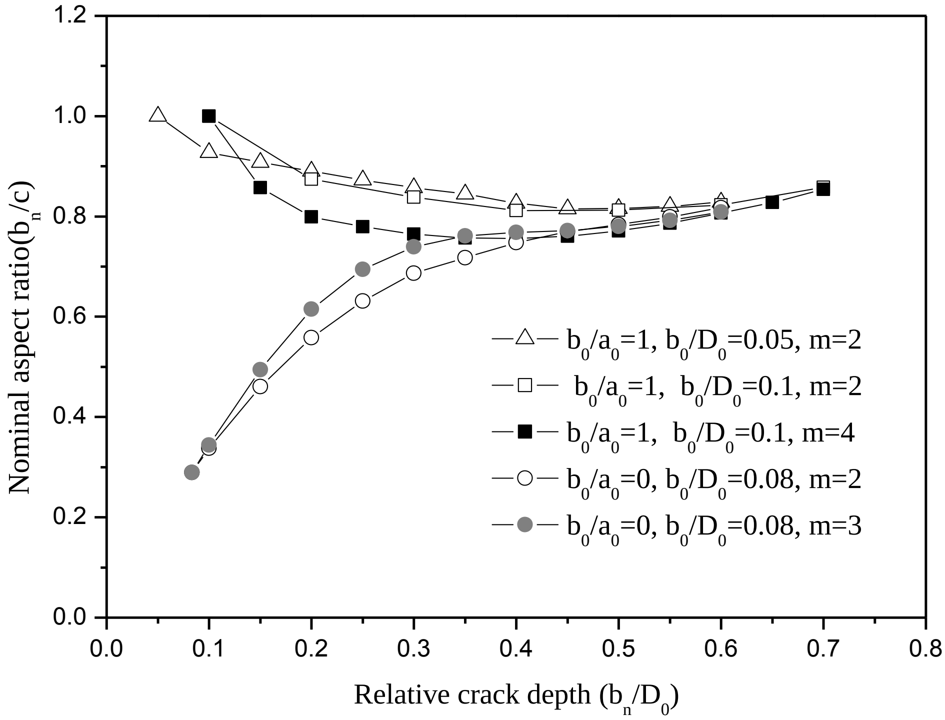

Figure 3-17 Nominal aspect ratio vs. relative crack depth

The propagation of fatigue crack along with b_n/D_0 and c/D_0 under cyclic loading with different initial parameters is shown in Figure 3-18. It can be seen that the crack propagation paths differ with different initial flaws, It's shown obviously that the same shape of initial flaws ($b_0/a_0 = 1\ or\ b_0/a_0 = 0$) generate the generally consistent propagation, no matter the size of the initial flaw. However, they will converge asymptotically ultimately.

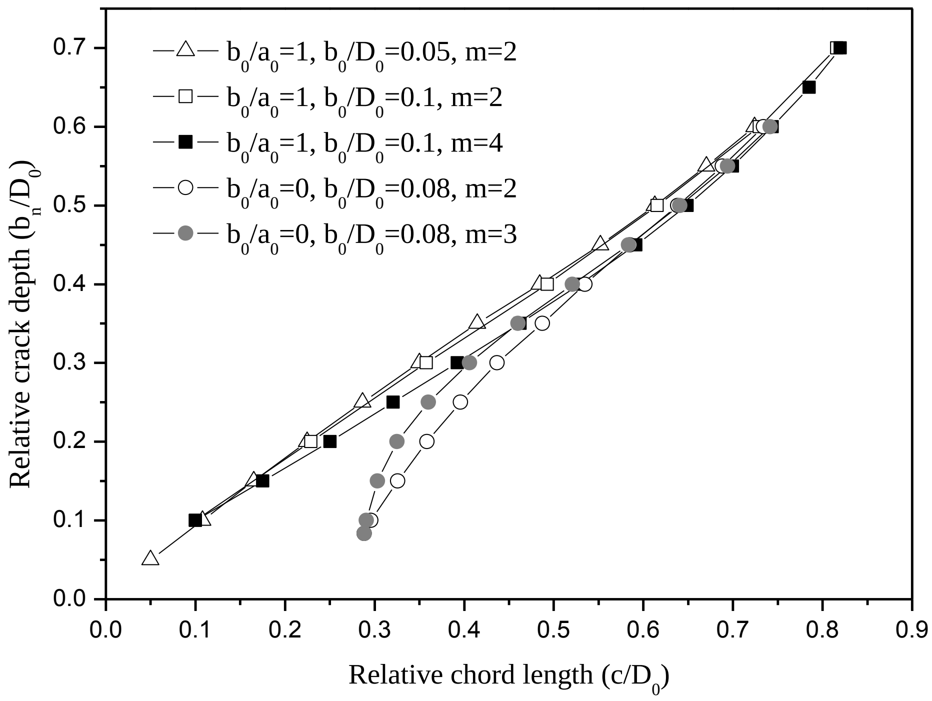

Figure 3-18 Relative crack depth vs. relative chord length with different initial parameters

Furthermore, in the process of expansion, the crack growth rate for the center and outermost points are variable, which is deduced from the gradient of two type lines with initial flaws $b_0/a_0 = 0, 1$. This can be seen more precisely in Figure 3-19. For the case of an initial crack $b_0/a_0 = 1$ shown in Figure 3-19(a), the ratio of crack growth (db/dc) is always less than 1 for most propagation processes, which means the crack growth rate for the central point is always slower than the outermost point until the relative crack depth $b_n/D_0 \approx 0.6$. However, the change in growth ratio will slow down from the beginning to the stage of $b_n/D_0 \approx 0.6$ for all the cases with initial flaws $b_0/a_0 = 1$, and then increase distinctly. For the case of an initial crack with $b_0/a_0 = 0$, as shown in Figure 3-19(b), the crack growth along the vertical central line is always greater than the growth adjacent to the horizontal surface until the relative crack depth satisfies $b_n/D_0 \approx 0.4$, since the gradient line exceeds 1. Furthermore, the rate decreases sharply at the beginning propagation, especially for m = 3. Larger values of Paris law exponent m convey more drastic changes. It can be deduced that in the early propagation stage, the exponent m in the Paris law has a distinct effect on the evolution of the crack. The change of crack growth rate for the central point is bigger for a large value of m. It is considered to be related to plasticity which suppresses the crack propagation on the outermost surface.

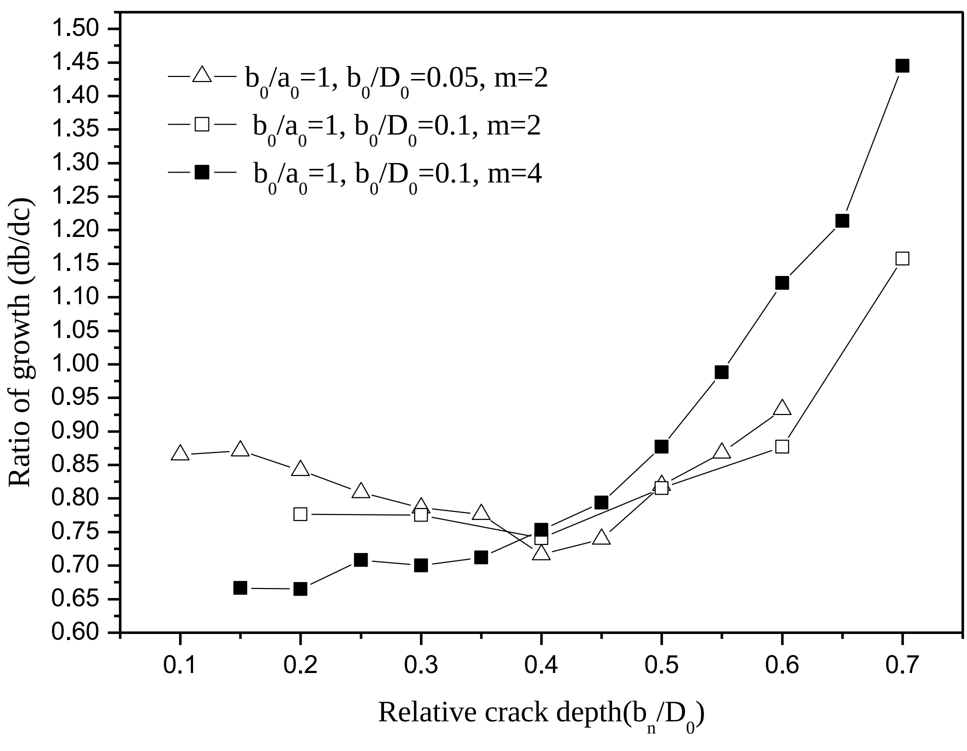

(a) $\mathrm{b}_0/\mathrm{a}_0 = 1$

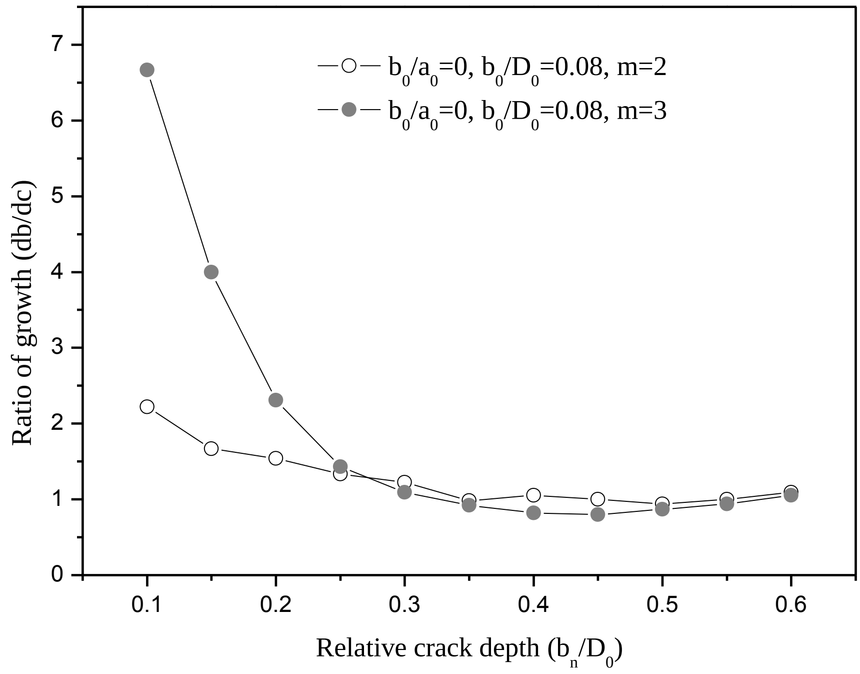

(b) $b_0/a_0 = 0$

Figure 3-19 Ratio of crack growth along the vertical centerline and toward the horizontal surface

3.3.2 Comparison with Other Numerical Solutions and Experimental Results

In Figure 3-20, the fatigue propagation of the initial crack $b_0/a_0 = 1$, $b_0/D_0 = 0.05$ and 0.1 is compared with numerical solutions from Carpinteri, A. [52, 55]. The curves in the present results are similar in all cases. However, a certain discrepancy between the present result and Carpinteri can be seen, especially for the initial crack $b_0/a_0 = 1, b_0/D_0 = 0.05$. The deviation is mainly due to the difference in the crack growth method adopted and the idealized crack front geometry in the above comparison. A two-parameter elliptical-arc shape with a fixed center is assumed only by employing the Paris-Erdogan law ordinarily by Carpinteri [52,55]. The two-parameter shape assumption method mentioned above can simplify the fatigue calculations, but it is also clear that better predictions should be obtained if the shape restraint can be reduced, such as those generated by the proposed method.

Moreover, the crack growth circles, which are tangent to the new crack front as well as to the current crack front, can accurately represent the real path of the fatigue crack and thus obtain more accurate results. Also, the better mesh refinement demonstrated in this paper leads to improved prediction accuracy.

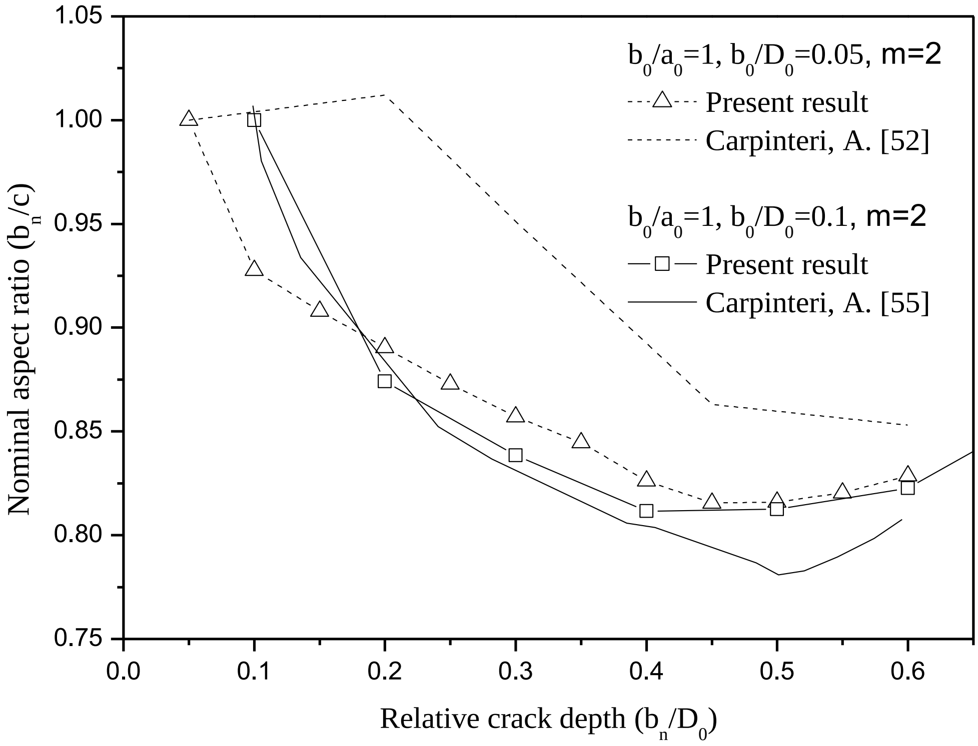

Figure 3-20 Crack propagation patterns compared with numerical solutions

Figures 3-21 and 3-22 are the comparisons of the crack propagation result with the experimental data deduced from Yang, F.P. [62]. It is shown that the present results agree well with the experimental data. For the relationship of crack propagation with depth and chord length, the overall trend remains consistent, although most data of experiment are beyond the simulation results slightly, as shown in Figure 3-21.

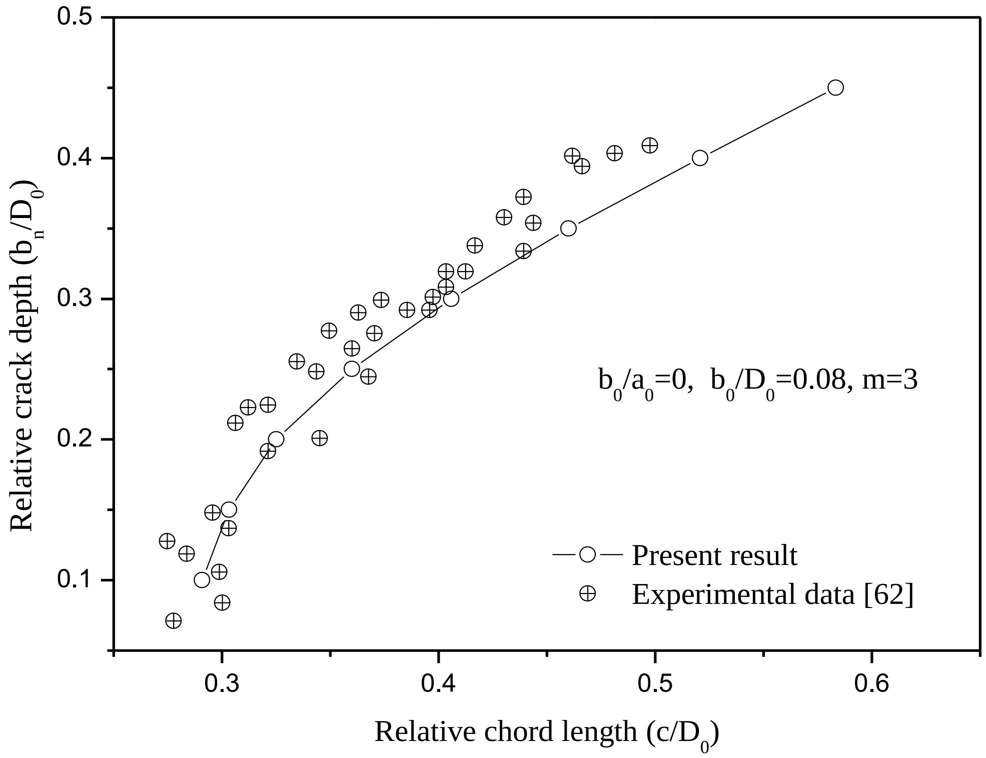

Figure 3-21 Relationship of crack propagation with depth and chord length compared with experimental data

In Figure 3-22, the consistency of the comparison with the two results is good, especially for the propagation of the previous stage. Nevertheless, the experimental result deviates abnormally around the relative crack depth of $b_n/D_0 = 0.4$. The maximum discrepancy is approximately 12%. The deviation of the two solutions are acceptable, as the fracture begins to happen in the experimental method approach the relative crack depth $b_n/D_0 = 0.4$, the discreteness of the experiment is inevitable. It is confirmed that the proposed method could provide relatively good accuracy.

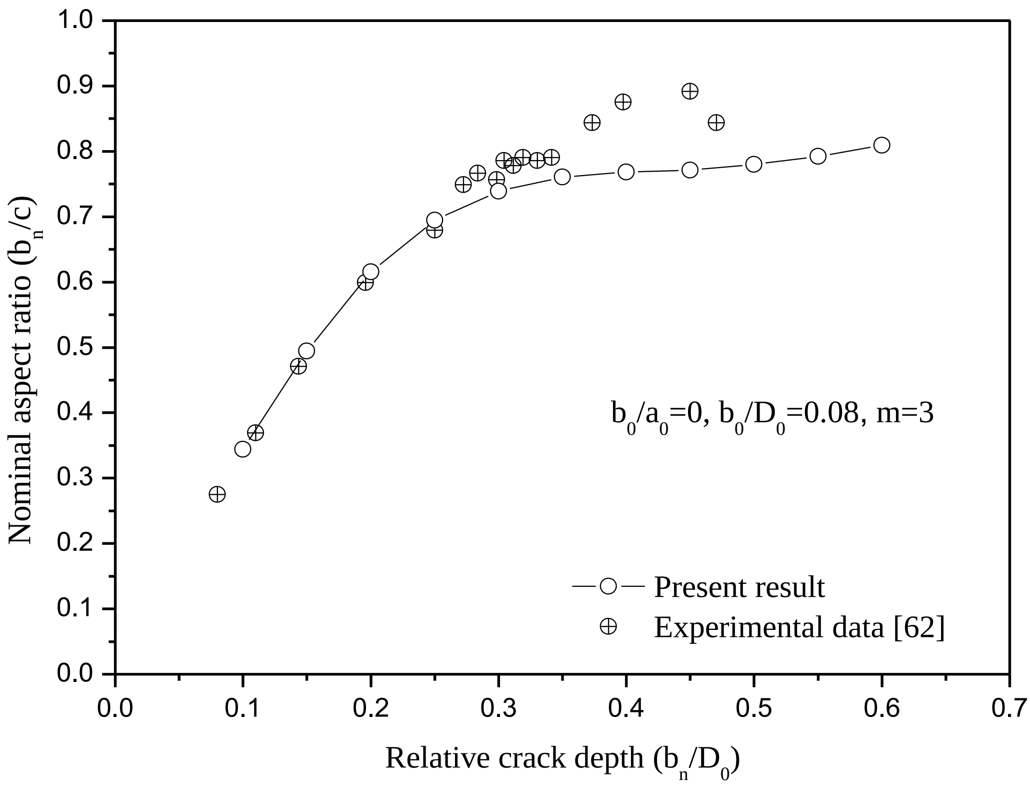

Figure 3-22 Crack propagation patterns compared with experimental data

3.4 Chapter summary

The fatigue propagation of a surface crack in a round bar subjected to tension loads has been investigated by using crack growth circles. It is illustrated that the proposed method can achieve good convergence speed and accurate prediction of crack shape patterns. The following conclusions can be drawn:

(1) The crack growth circles method is developed for the surface cracks of a round bar, and the circles are tangent to both current and new crack fronts. In this way, good simulation accuracy can be achieved with less iteration.

(2) A three-parameter model with fewer shape restraints whose center is allowed to move along the vertical axis is established, and the shape change of a fatigue crack is predicted more precisely. The nominal aspect ratio of an ellipse, which is the ratio of the maximum crack depth to the chord length c, b_n/c, is considered, instead of the actual aspect ratio of an ellipse semi-axis.

(3) A relatively large crack growth increment can be used by adopting the equivalent stress intensity factor ΔK_e based on the stress intensity factors along the current and new crack fronts.

(4) The crack propagation process is described accurately based on the ratio of vertical growth toward the horizontal surface. It can be seen that the crack propagation paths differ with different initial flaws, but will converge asymptotically. The ratio of crack growth is always less than 1 for the case of initial crack $b_0/a_0 = 1$, and the crack growth along the vertical centerline is always greater than the growth toward the horizontal surface. For the case of an initial crack $b_0/a_0 = 0$, a greater Paris law exponent m value generates more drastic change.

(5) The present solutions are compared with other numerical solutions and experimental data. It is shown that the proposed solutions agree well with the experimental data and are better than other numerical solutions.

In this paper, the dimensions of the initial crack and the material parameters are considered. The main reason is these factors are directly related to the method employed here.

Conclusions

The crack problem as an important impact on the safety of engineering components is a significant research area. Crack propagation evaluation method based on fracture mechanics and fatigue damage is conducted in this thesis, involving the evaluation of energy release rate related to crack kink and simulation of surface crack shape change of round bar. The following conclusions can be drawn:

(1) The energy release rate related to crack kink under mixed-mode loading for aluminum alloy material has been investigated using both a numerical method and theoretical derivation.

A relatively simple and precise numerical method was established to obtain the expression of energy release rate associated with the stress intensity factors under mixed-mode loading by a series of spatially inclined ellipses in Mode I-II and ellipsoids in Mode I-II-III with different propagation angles, based on the concept that the energy release rate is equal to the change rate of the energy difference before and after crack kink.

A theoretical expression of energy release rate at any propagation angle for a crack tip subjected to I-II-III mixed-mode crack was deduced based on the propagation mechanism of the crack tip under the influence of a stress field.

An experiment is carried out to verify the present methods. The results of the proposed method are consistent with the experimental data. It is illustrated that the proposed method can achieve an accurate evaluation of the energy release rate, with concise calculation.

(2) The fatigue propagation of a surface crack in a round bar subjected to tension loads has been investigated.

A series of crack growth circles, which are tangent to both current and new crack fronts, is developed to predict the shape of the surface cracks for a round bar under tension loads base on a three-parameter model with fewer shape restraints whose center is allowed to move along the vertical axis. It shows that good simulation accuracy can be achieved with less iteration.

An equivalent stress intensity factor ΔK_e based on the stress intensity factors along the current and new crack fronts is proposed to increase the crack growth increment of simulation.

The crack propagation process is described accurately based on the ratio of vertical growth toward the horizontal surface. It can be seen that the crack propagation paths differ with different initial flaws, but will converge asymptotically.

Comparisons have been done to verify the present solutions with other numerical solutions and experimental data. It is indicated that the present solutions agree well with the experimental data and are better than other numerical solutions.

List of publications

1. **Yali Yang**, Seok Jae Chu*,Wei song Huang, Hao Chen. Crack growth and energy release rate for an angled crack under mixed mode loading. Applied Science.2020.10,4227.
2. **Yali Yang**, Seokjae Chu*, Hao Chen. Prediction of shape change for fatigue crack in a round bar using three-parameter growth circles. Applied Science.2019.9, 1751.
3. Meiling Geng, Hao Chen*, **Yali Yang**. Prediction of crack shape in a cylindrical bar under combined fatigue tension and torsion loading. Theoretical and Applied Fracture Mechanics.2020.7.
4. Seokjae Chu*, **Yali Yang**, Hao Chen. Prediction of shape change of a surface crack in a round bar using a three-parameter ellipse and fatigue crack growth circles. 2019 Annual Conference of Korean Society of Mechanical Engineers, 2019, 11.
5. Yuquan Bao, **Yali Yang***. Multiscale damage evolution analysis of aluminum alloy based on defect visualization. Applied Science.2020.9, 5251.
6. **Ya li Yang***, Hao Chen, Jie Shen, Yongfang Li. Study on fatigue damage of automotive aluminum alloy sheet based on CT scanning. Proceedings of the Second World Congress on Condition Monitoring (WCCM). 2019.12:550-555.

References

[1] Irwin, G.R. Onset of fast crack propagation in high strength steel and aluminum alloys. Sagamore Research Conference Proceedings. 1956, 2, 289-305.

[2] Ueda, Y.; Ikeda, K.; Yao, T.; Aoki, M. Characteristics of brittle fracture under general combined modes including those under bi-axial tensile loads. Engineering Fracture Mechanics. 1983, 18, 1131-1158.

[3] Melin, S. Fracture from a straight crack subjected to mixed mode loading. International Journal of Fracture. 1987, 32, 257-263.

[4] He, M.Y.; Bartlett, A.; Evans, A.G.; Hutchinson, J.W. Kink of a crack out of an interface: Role of in-plane stress. Journal of the American Ceramic Society. 1991, 74, 767-771.

[5] Hammouda, M.M.; Fayed, A.S.; Sallam, H.E. Simulation of mixed mode I/II cyclic deformation at the tip of a short kinked inclined crack with frictional surfaces. International Journal of Fatigue. 2003, 25, 743-753.

[6] Xie,Y.J.; Hu, X.Z.; Wang, X. H.; Chen, J.; Lee, K.Y. A theoretical note on mode-I crack branching and kink. Engineering Fracture Mechanics. 2011, 78, 919-929.

[7] Chatterjee, S.N. The stress field in the neighborhood of a branched crack in an infinite elastic sheet. International Journal of Solids and Structures. 1975, 11, 521-538.

[8] Amestoy, M.; Leblond, J.B. Crack path in plane situations-II. Detailed form of the expansion of the stress intensity factors. International Journal of Solids and Structures. 1992, 29, 465-501.

[9] Kishen, J.M.C.; Singh, K.D. Stress intensity factors based fracture criteria for kink and branching of interface crack: application to dams. Engineering Fracture Mechanics. 2001, 68, 201-219.

[10] Meggiolaro, M.A.; Miranda, A.C.O.; Castro, J.T.P.; Martha, L.F. Stress intensity factor equations for branched crack growth. Engineering Fracture Mechanics. 2005, 72, 2647-2671.

[11] Berto, F.; Lazzarin, P. On higher order terms in the crack tip stress field. International Journal of Fracture. 2010, 161, 221-226.

[12] Sih, G.C. Strain-energy-density factor applied to mixed mode crack problems. International Journal of Fracture. 1974, 10(3), 305-320.

[13] Cornetti, P.; Sapora, A.; Carpinteri, A. T-stress effects on crack kink in finite fracture mechanics. Engineering Fracture Mechanics. 2014, 132, 169-176.

[14] Li, X.F.; Lee, K.Y.; Tang, G.J. Kink angle and fracture load for an angled crack subjected to far-field compressive loading. Engineering Fracture Mechanics. 2012, 82, 172-184.

[15] Fajdiga, G.; Zafošnik, B. Determining a kink angle of a crack in mixed mode fracture using maximum energy release rate, SED and MTS criteria. Journal of Multidisciplinary Engineering Science and Technology. 2015, 2, 356-362.

[16] Guo, B.K.; Yan, H.H.; Zhang, L. Cracking angle of an arbitrary oriented crack embedded in a strip under I-II mixed mode loading. International Journal of Material Science. 2016, 6, 52-57.

[17] Hussain, M.A.; Pu, S.L.; Underwood, J. Strain energy release rate for a crack under combined Mode I and Mode II. In Fracture Analysis: Proceedings of the 1973 National Symposium on Fracture Mechanics, Part II; Irwin, G., Ed.; ASTM International: West Conshohocken, PA, USA, 1974, 2-28.

[18] Andersson, H. Stress-intensity factors at the tips of a star-shaped contour in an infinite tensile sheet. Journal of the Mechanics and Physics of Solids. 1969, 17, 405-417.

[19] Muskhelishvili, N.I. Some basic problems of the mathematical theory of elasticity; Springer Dordrecht: Groningen, Netherlands, 1977.

[20] Knowles, J. K.; Sternberg, E. On a class of conservation laws in linearized and finite elastostatics. Archive for Rational Mechanics and Analysis. 1972, 44, 187-211.

[21] Williams, M.L. On the stress distribution at the base of a stationary crack. Journal of Applied Mechanics. 1956, 24, 109-114.

[22] Erdogan, F.; Sih, G.C. On the crack extension in plates under plane loading and transverse shear. Journal of Basic Engineering. 1963, 85, 519-527.
[23] Williams, J.G.; Ewing, P.D. Fracture under complex stress-the angled crack problem. International Journal of Fracture Mechanics. 1972, 8, 441-446.
[24] Cotterell, B.; Rice, J. R. Slightly curved or kinked cracks. International Journal of Fracture. 1980, 16, 155-169.
[25] Anderson, T.L. Fracture mechanics fundamentals and applications; CRC Press: Boca Raton, FL, USA, 2005.
[26] Wu, C.H. Fracture under combined loads by maximum-energy-release-rate criterion. Journal of Applied Mechanics. 1978, 45, 553-558.
[27] Hayashi, K.; Nemat-Nasser, S. Energy-release rate and crack kink under combined loading. Transactions of ASME. 1981, 48, 520-524.
[28] Chambolle, A.; Francfort, G.A.; Marigo, J.J. Revisiting energy release rates in brittle fracture. Nonlinear Science. 2010, 20, 395-424.
[29] Azhdari, A.; Nemat-Nasser, S. Energy-release rate and crack kink in anisotropic brittle solids. Journal of the Mechanics and Physics of Solids. 1996, 44, 929-951.
[30] Sih G.C.; Paris, P.C.; Erdogan, F. Crack-Tip, Stress-Intensity Factors for Plane Extension and Plate Bending Problems. Journal of Applied Mechanics, 1962, 29(2), 306-312.
[31] Nezu, K.; Machida, S.; Nakamura, H. Stress intensity factor of surface cracks and fatigue crack propagation behavior in a cylindrical bar. In Proceedings of the 25th Japan Congress on Material Research, Metallic Metals, Kyoto, Japan, 25-28 March 1982; pp. 87–92.
[32] Forman, R.G.; Shivakumar, V. Growth behavior of surface cracks in the circumferential plane of solid and hollow cylinders. In Fracture Mechanics: Seventeen Volume; American Society of Testing and Materials: Conshohocken, PA, USA , 1986; pp. 59–74.

[33] Bush, A.J. Experimentally determined stress-intensity factors for single-edge-crack round bars loaded in bending. Experimental Mechanics. 1976, 16, 249-257.

[34] Mattheck, C.; Morawietz, P.; Munz, D. Stress intensity factors of sickle-shaped cracks in cylindrical bars. International Journal of Fatigue. 1985, 7(1), 45-47.

[35] Caspers, M.; Mattheck, C.; Munz, D. Propagation of surface cracks in notched and unnotched rods. In Surface-Crack Growth: Models, Experiments, and Structures; American Society of Testing and Materials: Conshohocken, PA, USA, 1990; pp. 365-389.

[36] Hobbs, J.; Burguete, R.; Heyes, P.; Patterson, E. A photoelastic analysis of crescent-shaped cracks in bolts. The Journal of Strain Analysis for Engineering Design. 2001, 36(1), 93-100.

[37] Carpinteri, A.; Brighenti, R.; Vantadori, S.; Viappiani, D. Sickle-shaped crack in a round bar under complex mode I loading. Fatigue & Fracture of Engineering Materials & Structures. 2007, 524-534.

[38] Carpinteri, A.; Vantadori, S.; Sickle-shaped surface crack in a notched round bar under cyclic tension and bending. Fatigue & Fracture of Engineering Materials & Structures. 2009, 32, 223–232.

[39] Mackay, T.L.; Alperin, B.J. Stress intensity factors for fatigue cracking in high-strength bolts. Engineering Fracture Mechanics. 1985, 21, 391–297.

[40] Caspers, M.; Mattheck, C. Weighted averaged stress intensity factors of circular-fronted cracks in cylindrical bars. Fatigue & Fracture of Engineering Materials & Structures. 1987, 9, 329–341.

[41] Ael din, S.S.; Lovegrove, J.M. Stress intensity factors for fatigue cracking of round bars. International Journal of Fatigue. 1981, 3, 117–123.

[42] Daoud, O.E.K.; Cartwright, D.J. Strain energy release rate for a circular-arc edge crack in a bar under tension or bending. The Journal of Strain Analysis for Engineering Design. 1985, 20(1), 53-58.

[43] Athanassiadis, A.; Boissenot, J.M.; Brevet, P.; Francois, D.; Raharinaivo, A. Linear elastic fracture mechanics computations of cracked cylindrical tensioned bodies. International Journal of Fatigue. 1981, 17, 553–566.

[44] Levan, A.; Royer, J. Part-circular surface cracks in round bars under tension, bending and twisting. International Journal of Fracture. 1993, 61, 71-99.

[45] Lorentzen, T.; Kjaer, N.E.; Henriksen, T.K. The application of fracture mechanics to surface cracks in shafts. Engineering Fracture Mechanics. 1986, 23, 1005–1014.

[46] Lin, X.B.; Smith, R.A. Shape growth simulation of surface cracks intension fatigued round bars. International Journal of fatigue. 1997, 19(6), 461-469.

[47] Lin, X.B.; Smith, R.A. Shape evolution of surface cracks in fatigued round bar with a semicircular circumferential notch. International Journal of Fatigue. 1999, 21, 965-973.

[48] Toribio, J.; Matos, J.C.; González, B.; Escuadra, J. Compliance evolution in round cracked bars under tensile fatigue. Engineering Fracture Mechanics. 2011, 78, 3243-3253.

[49] Branco, R.; Costa, J.D.; Antunes, F.V. Fatigue behavior and life prediction of lateral notched round bars under bending-torsion loading. Engineering Fracture Mechanics. 2014,119, 66-84.

[50] Carpinteri, A.; Ronchei, C.; Vantadori, S. Stress intensity factors and fatigue growth of surface cracks in notched shell and round bars: Two decades of research work. Fatigue & Fracture of Engineering Materials & Structures. 2013, 36, 1–13.

[51] Carpinteri, A. Elliptical-arc surface cracks in round bars. Fatigue & Fracture of Engineering Materials & Structures. 1992, 15, 1141–1153.

[52] Carpinteri, A. Shape change of surface cracks in round bars under cyclic axial loading. International Journal of Fatigue. 1993, 15, 21–26.

[53] Carpinteri, A. Part-through cracked round bars under cyclic bending. Transactions on Engineering Sciences. 1994, 6, 1743-3533.

[54] Carpinteri, A.; Brighenti, R. Part-through cracks in round bars under cyclic combined axial and bending loading. International Journal of Fatigue. 1996, 18(1), 33-39.

[55] Carpinteri, A.; Brighenti, R.; Vantadori, S. Surface cracks in notched round bars under cyclic tension and bending. International Journal of Fatigue. 2006, 28, 251–260.

[56] Carpinteri, A.; Vantadori, S. Surface crack in round bars under cyclic tension or bending. Key Engineering Materials. 2008, 378–379, 341–254.

[57] Carpinteri, A.; Brighenti, R. Fatigue propagation of surface flaws in round bars: A three-parameter theoretical model. Fatigue & Fracture of Engineering Materials & Structures. 1996, 19, 1471–1480.

[58] Couroneau, N.; Royer, J. Simplified model for the fatigue growth analysis of surface cracks in round bars under mode I. International Journal of Fatigue. 1998, 20, 711–718.

[59] Paris, P.; Erdogan, F. A critical analysis of crack propagation laws. Journal of Basic Engineering. 1963, 85(4), 528-533.

[60] Ayhan, A.O. Simulation of three-dimensional fatigue crack propagation using enriched finite elements. Computers and Structures. 2011, 89, 801–812.

[61] Shin, C.S.; Cai, C.Q. Experimental and finite element analyses on stress intensity factors of an elliptical surface crack in a circular shaft under tension and bending. International Journal of Fatigue. 2004, 129, 239–264.

[62] Yang, F.P.; Kuang, Z.B.; Shlyannikov, V.N. Fatigue crack growth for straight-fronted edge crack in a round bar. International Journal of Fatigue. 2006, 28, 431–437.

[63] Cai, C.Q.; Shin, C.S. A normalized area-compliance method for monitoring surface crack development in a cylindrical rod. International Journal of Fatigue. 2005, 27, 801–809.

[64] Ismail, A.E.; Ariffin, A.K.; Abdullah, S.; Ghazali, M.J.; Daud, R. Elastic-plastic analysis of surface crack in round bars under torsion. Key Engineering Materials. 462-463, 2011:651-656.

[65] Ismail, A.E.; Noor, F.M.; Mohamad, Z. et al. A model for predicting J-integral of surface cracks in round bars under combined mode I loading. IOP Conference Series: Materials Science and Engineering. 2017, 226,1-8.

[66] Irwin, G.R.; Washington, D.C. Analysis of stresses and strains near the end of a crack traversing a plate. Journal of Applied Mechanics, 1957, 24,361–364.

[67] Hetnarski, R.B. Encyclopedia of thermal stresses; Springer Netherlands: Berlin, Germany, 2014.

[68] Wu, C.H. Elasticity problems of a slender Z-crack. Journal of Elasticity. 1978, 8, 183-205.

[69] Cherepanov, G.P. Mechanics of brittle fracture; McGraw-Hill: New York, 1979.

[70] Liu, C.H.; Chu, S.J. Physical interpretation of the J_2 integral by identifying the crack translation associated with it. Journal of Mechanical Science and Technology. 2016, 30, 3079-3084.

[71] Cornetti, P.; Sapora, A.; Carpinteri, A. T-stress effects on crack kink in finite fracture mechanics. Engineering Fracture Mechanics. 2014, 132, 169-176.

[72] Richard, H.A. Specimens for investigating biaxial fracture and fatigue process. In Biaxial and Multiaxial Fatigue; Brown, M.W.; Miller, K.J.; Eds.; Mechanical Engineering Publications: London, UK, 1989; pp. 217–229.

[73] Ayatollahi, M.R.; Zakeri, M. An improved definition for mode I and mode II crack problems. Engineering Fracture Mechanics. 2017, 175, 235-246

[74] Henshell, R.D.; Shaw, K.G. Crack tip finite elements are unnecessary. International Journal for Numerical Methods in Engineering. 1975, 9, 495 – 507.

[75] Barsoum, R.S. On the use of isoparametric finite elements in linear fracture mechanics. International Journal for Numerical Methods in Engineering. 1976, 10, 25 – 37.

[76] Luca, S.; John, Y.; Alfredo, N.; Thierry, P.L. Fracture and structural integrity: Annals 2014; Italy: Gruppo Italiano Frattura: 2014.

[77] Pantano, A.; Averill, R.C. A penalty-based interface technology for coupling independently modeled three-dimensional finite element meshes. Finite Elements in Analysis and Design. 2007, 43, 271–286.

[78] ASTM E 647-88 Standard Test Method for Measurement of Fatigue Crack Growth Rates. American Society for Testing and Materials Standards, 1988, 3(1), 636.

[79] Liu, C.H; Chu, S.J. Prediction of shape change of corner crack by fatigue crack growth circles. International Journal of Fatigue. 2015, 75, 80–88.